COMPARISON OF EKF, EKF2 AND UKF IN A LOOSELY COUPLED INS/GPS INTEGRATION

A THESIS SUBMITTED TO
THE GRADUATED SCHOOL OF NATURAL AND APPLIED SCIENCES
OF
MIDDLE EAST TECHNICAL UNIVERSITY

BY

HANDE JANE

IN PARTIAL FULFILLMENT OF THE REQUIREMENTS
FOR
THE DEGREE OF MASTER OF SCIENCE
IN
ELECTRICAL AND ELECTRONICS ENGINEERING

JANUARY 2018

Approval of the the thesis:

COMPARISON OF EKF, EKF2 AND UKF IN A LOOSELY COUPLED INS/GPS INTEGRATION

submitted by **HANDE JANE** in partial fulfillment of the requirements for the degree of **Master of Science in Electrical and Electronics Engineering Department, Middle East Technical University** by,

Prof. Dr. Gülbin Dural Ünver _____
Dean, Graduate School of **Natural and Applied Sciences**

Prof. Dr. Tolga Çiloğlu _____
Head of Department, **Electrical and Electronics Engineering**

Prof. Dr. Buyurman Baykal _____
Supervisor, **Electrical and Electronics Engineering Dept., METU**

Examining Committee Members:

Prof. Dr. Tolga Çiloğlu _____
Electrical and Electronics Engineering Dept., METU

Prof. Dr. Buyurman Baykal _____
Electrical and Electronics Engineering Dept., METU

Prof. Dr. Temel Engin Tuncer _____
Electrical and Electronics Engineering Dept., METU

Assoc. Prof. Dr. Umut Orguner _____
Electrical and Electronics Engineering Dept., METU

Assoc. Prof. Dr. Özgül Salor Durna _____
Electrical and Electronics Engineering Dept., Gazi University

Date: 23/01/2018

I hereby declare that all information in this document has been obtained and presented in accordance with academic rules and ethical conduct. I also declare that, as required by these rules and conduct, I have fully cited and referenced all material and results that are not original to this work.

Name, Last Name : Hande JANE

Signature :

ABSTRACT

COMPARISON OF EKF, EKF2 AND UKF IN A LOOSELY COUPLED INS/GPS INTEGRATION

Jane, Hande
M. Sc., Department of Electrical and Electronics Engineering
Supervisor: Prof. Dr. Buyurman Baykal

January 2018, 92 pages

Developing effective navigation solutions in land, sea, air, and space travels is an ever increasing necessity maintaining its validity. Nowadays, although a navigation aid called satellite based Global Positioning System (GPS) is used to develop a navigation solution, standalone GPS cannot achieve the desired accuracy in some applications. For this reason, GPS measurements are integrated with the Inertial Navigation System (INS) to develop an enhanced accurate integrated navigation solution. Extended Kalman Filter (EKF) is used widely as an estimation algorithm in the INS/GPS integrated systems. In this thesis, instead of EKF, unscented Kalman Filter (UKF) and Second Order Extended Kalman Filter (EKF2) shall be used and comparison is made between the results in terms of the accuracy of the navigation systems, sensitivity to Inertial Measurement Unit (IMU) noise, effect of changing process noise covariance matrix and complexity for GPS available situation.

According to experimental results, it is observed that UKF increased the accuracy of the navigation system with respect to EKF and EKF2, as mentioned in the literature, EKF2 has better accuracy performance than EKF. In addition to this, EKF is more sensitive to additive noise on IMU measurements with respect to UKF. Also, increasing the noise on IMU measurements forces the EKF2 to diverge quickly. UKF can work with wide range of noise levels with respect to the other algorithms. EKF, UKF and EKF2 complexity is rising, respectively.

Also, accuracy of estimation algorithms are compared for GPS interference (outage or outlier). UKF has the best performance with respect to EKF and EKF2 when GPS signal is lost and although EKF2 introduces an increase in the performance according to EKF without GPS interruption, it is not robust to GPS outages and/or GPS outlier. For nonlinear problems, EKF is a good solution for GPS outlier situation as a result of poor robustness of UKF.

Keywords: Extended Kalman Filter (EKF), Inertial Navigation System/Global Positioning System (INS/GPS), Second Order Extended Kalman Filter (EKF2), Unscented Kalman Filter (UKF), Unscented Transformation (UT)

ÖZ

GEVŞEK BAĞLI ANS/KKS TÜMLEŞTİRMESİNDE GKF, GKF2 VE KKF KARŞILAŞTIRMASI

Jane, Hande
Yüksek Lisans, Elektrik ve Elektronik Mühendisliği Bölümü
Tez Yöneticisi: Prof. Dr. Buyurman Baykal

Ocak 2018, 92 sayfa

Kara, hava, deniz ve uzay seyahatlerinde etkin navigasyon çözümleri geliştirmek, geçerliliğini her zaman koruyacak olan bir ihtiyaçtır. Günümüzde, uydu tabanlı Küresel Konumlama Sistemi (KKS) kullanılarak navigasyon yapılabiliyor olsa da sadece KKS kullanan navigasyon bazı uygulamalarda yeterli hassasiyet sağlamamaktadır. Bu nedenle KKS ölçümleri Ataletsel Navigasyon Sistemi (ANS) ile entegre edilip navigasyonun hassasiyetinde iyileştirme sağlanmaktadır. Genişletilmiş Kalman Filtresi (GKF) ANS/KKS entegre sistemlerde yaygın kullanılan kestirim algoritmasıdır. Bu tez kapsamında GKF yerine İkinci Dereceden Genişletilmiş Kalman Filtresi (GKF2) ve Kokusuz Kalman Filtresi (KKF) kullanılmış ve sonuçlar konum belirleme hassasiyeti, Ataletsel Ölçüm Birimi (AÖB) üzerindeki gürültüye karşı hassasiyet, süreç gürültüsü kovaryans matrisinin değişiminin etkisi ve karmaşıklık açısından KKS'nin var olduğu durum için karşılaştırılmıştır.

Deneysel sonuçlara göre; KKF'nin GKF ve GKF2'ye göre navigasyon sisteminin hassasiyetini arttırdığı, literatürde belirtildiği gibi GKF2'nin de GKF'ye göre hassasiyet açısından daha iyi performans gösterdiği gözlemlenmiştir. Ek olarak, GKF'nin KKF'ye göre AÖB ölçümleri üzerindeki gürültüye karşı hassasiyeti daha fazladır. Ayrıca AÖB ölçümleri üzerindeki gürültünün artırılması GKF'nin daha çabuk sapmasına neden olmaktadır. KKF diğer iki algoritmaya göre daha geniş

gürültü seviyesi aralığında çalışabilmektedir. Karmaşıklık ise sırasıyla GKF'den KKF'ye, KKF'den GKF2'ye artmaktadır.
Ayrıca, kestirim algoritmalarının hassasiyeti KKS girişimi (kesintisi/aykırılığı) için de karşılaştırılmıştır. KKS sinyali kesintiye uğradığında KKF, GKF ve GKF2'ye göre en iyi performansa sahiptir ve KKS girişimi olmadığında GKF2, GKF'ye göre performansta bir artış sağlamasına rağmen, KKS kesintisi ve/veya KKS aykırılığı durumlarına gürbüz değildir. Doğrusal olmayan problemler için KKS aykırılığı durumunda KKF'nin gürbüz olmayışının sonucu olarak GKF iyi bir çözümdür.

Anahtar Kelimeler: Genişletilmiş Kalman Filtresi (GKF), Ataletsel Navigasyon Sistemi/Küresel Konumlama Sistemi (ANS/KKS), İkinci Dereceden Genişletilmiş Kalman Filtresi (GKF2), Kokusuz Kalman Filtresi (KKF), Kokusuz Dönüşüm (KD)

To My Endless Love Onur JANE and My Little Prince Umut JANE…

ACKNOWLEDGEMENTS

First of all, I would like to express my sincere thanks to my supervisor Prof. Dr. Buyurman BAYKAL for his guidance, advice, criticism and encouragement along the M.Sc. study.

I would like to express my appreciation to Assoc. Dr. Umut ORGUNER for providing me continuous support along this study.

Finally, I would like to express my special thanks to my dear husband Onur JANE, I always feel his support beside me, for his valuable ideas and encouragement and my family for their permanent support and understanding.

TABLE OF CONTENTS

LIST OF TABLES

TABLES

LIST OF FIGURES

FIGURES

LIST OF ABBREVIATIONS

ANS	: Ataletsel Navigasyon Sistemi
AÖB	: Ataletsel Ölçüm Birimi
CKF	: Cubature Kalman Filter
EKF	: Extended Kalman Filter
EKF2	: Second Order Extended Kalman Filter
FOG	: Fiber Optic Gyroscopes
GKF	: Genişletilmiş Kalman Filtresi
GKF2	: İkinci Dereceden Genişletilmiş Kalman Filtresi
GPS	: Global Positioning System
IMU	: Inertial Measurement Unit
INS	: Inertial Navigation System
KD	: Kokusuz Dönüşüm
KF	: Kalman Filter
KKF	: Kokusuz Kalman Filtresi
KKS	: Küresel Konumlama Sistemi
MEMS	: Micro Electromechanical Systems
PF	: Particle Filter
RLG	: Ring Laser Gyroscopes
RMSE	: Root Mean Square Error
SINS	: Strap-down Inertial Navigation System
UKF	: Unscented Kalman Filter
UPF	: Unscented Particle Filter
UT	: Unscented Transform

CHAPTER 1

INTRODUCTION

1.1 Objectives of the Thesis

Various estimation algorithms have been applied in the process of Inertial Navigation Systems (INS)/Global Positioning System (GPS) integration. Extended Kalman Filter (EKF) based on nonlinear system and measurement models is the standart and most widely used algorithm. In this thesis, different methods in INS/GPS integration are proposed and compared in terms of the accuracy of the navigation system, sensitivity to Inertial Measurement Unit (IMU) noise variance, effect of changing process noise covariance matrix and complexity for GPS available situation. Also, accuracy of estimation algorithms is compared for GPS outage and GPS outlier situations. In other words, in the scope of this thesis, a Second Order Extended Kalman Filter (EKF2) is used to increase the performance of EKF and Unscented Kalman Filter (UKF) to improve the accuracy of navigation performance in INS/GPS integrated system. In addition to this, sensitivity to IMU noise variance, effect of changing process noise covariance matrix and complexity of algorithms are investigated for GPS available situation. Moreover, GPS outage and GPS outlier situations are also examined.

1.2 Related Work

INS is designed to obtain the velocity, position, and also attitude of a moving object. INS includes IMU which includes three accelerometers and three gyroscopes. Accelerometers and gyroscopes give the linear acceleration and angular velocity measurements according to Newton’s law of motion, respectively. IMU generates position information of a moving object by using these measurements and the initial position of the system.

GPS is a satellite-based three-dimensional navigation system. The basic working principle of GPS is the calculation of speed and position using radio signals broadcast by GPS satellites.

In some cases, both INS and GPS are incomplete and inadequate. That is, errors in sensor output in IMU unit additively increase and after a while go beyond tolerance. Disadvantages of INS and GPS can be removed with the integration of the two systems. Superior navigation performance than either alone can be obtained by using both of these systems together. Hence, integrating the outputs obtained by each sensor lead to a drift free INS.

Lijun et. al. (2008) worked on a loosely coupled GPS/INS system using EKF. They experimentally showed that GPS/INS hybrid navigation system can effectively improve the whole performance.

Ding et. al. (2010) implemented an algorithm which is based on covariance matching using EKF in a loosely coupled integration using the field data collected from an unmanned air vehicle platform.

Duong and Nguyen (2014) implemented a nine-state EKF to estimate position, velocity, and attitude of an air vehicle.

Studies based on efficiency of loosely coupled GPS/INS are also available in the literature. Yu (2012) employed an adaptive filter estimating measurement noise variance. With the knowledge of large errors of GPS information in position, the experimental results proved that the proposed adaptive filter estimated the position and attitude errors effectively than EKF.

Abdoli et. al. (2016) also studied on adaptive KF for INS/GPS integration. They investigated the selection of initial measurement noise covariance matrix and a new adaptive approach. The results confirmed that tuning the measurement noise

covariance matrix in adaptive KF approach performs better than the conventional KF in INS/GPS integration.

In navigation application, navigation and measurement equations are physically expressed very clearly, that is there is no uncertainty. However, the problem is non-linear equation of state and measurement. Therefore, in order to improve navigation performance even further, UKF can be used instead of EKF. It has been reported that UKF performs better than EKF when there is no high degree of linear equations (Julier and Uhlmann 2004).

Siddiqui (2013) studied on increasing the performance of UKF. UKF has a divergence in Cholesky matrix factorization. Square Root UKF can be a solution for this problem, but it does not applicable to non-Gaussian noises. Siddiqui (2013) examined Central Difference UKF along with Square Root UKF and Square Root Central Difference UKF with large initial attitude errors, GPS outage situations, and higher noise situations. Central Difference UKF gave the best result in terms of computation time, accuracy and it is more stable despite higher noise.

EKF2 has a second order Taylor expansion of a nonlinear system. It is seldom used in applications due to the requirement of Jacobian and Hessian of the system equations, and the high complexity.

Sadeghi and Moshiri (2007) compared EKF2 and UKF for tracking maneuvering targets and experimentally showed that main nonlinear equations in UKF made it more useful than EKF2.

Roth and Gustafsson (2011) proposed an algorithm based on an enlarged set of sigma points. Proposed algorithm does not need either Jacobian or Hessian.

In the literature, there are also studies on algorithms which can be alternative to EKF, EKF2 and UKF.

Zhao (2015) studied on an alternative estimation algorithm to the first order approximated EKF, called Cubature Kalman Filter (CKF) that has cabability for nonlinear systems to get higher order terms. CKF was found best in the GPS outage and large misalignment situations for systems having high nonlinearity.

Zhangsong Shi et. al. (2016) proposed cubature attitude estimation method for micro aerial vehicles due to the linearization error of EKF and high time cost problem of UKF. The estimation accuracy and the stability of CKF were found equivalent to UKF and better than EKF. In terms of time consumption, CKF was found better than UKF.

Moreover, the studies on examining the effect of process covariance matrix are also available in the literature.

Unlike previous methods, Hashlamon and Erbatur (2016) proposed the idea of the recursive estimation of the KF by developing two recursive updating rules for the process and observation covariances. The results show that the adaptive KF estimates are more accurate, have less noise, and are more stable against biased covariances.

Wu and Hung (2017) developed an adaptive UKF that process noise covariance matrix was first estimated at each step and adaptive gain was used to avoid deterioration of filter when process noise changes or sudden disturbance occurs due to the fixed process noise covariance matrix.

GPS is undefended to jamming and signal interference. When the GPS outage and/or GPS outlier are considered, accuracy of the state estimate is decreasing. In recent years, there are also studies on those issues.

Bistrovs and Kluga (2013) investigated the estimation performance of linear KF, EKF and UKF during GPS signal outage and UKF gave the lowest velocity error than EKF.

Rhudy et. al. (2013) also compared the robustness of EKF and UKF during GPS outage situation and the experimental results of Rhudy et. al. (2013) showed that UKF and EKF were found more robust and computationally efficient respectively. In GPS outages cases, there were not significant differences between the algorithm results.

Liu et. al. (2014) studied on outlier rejection algorithm in Integrated Navigation for UKF to solve the nonlinearity. The algorithm first detects the outliers and fixes outliers observed by Newton interpolation, suppresses effect of outliers to algorithm and gets more accurate estimation result.

Baiqiang Zhang et. al. (2015) used a method that when GPS worked well, Strap-down Inertial Navigation System (SINS) and GPS integrated with KF.

Graham et. al. (2015) presented a robust recursive filtering algorithm that can provide estimates in the presence of both measurement and state prediction outliers. Proposed algorithm improved the performance of state estimation over existing robust filtering approaches.

Abd Rabbou and El-Rabbany (2015) worked on an improvement to Particle Filter (PF), the Unscented Particle Filter (UPF), which consists of the UKF and PF. Working principle of UPF is based on decreasing the number of samples. Abd Rabbou and El-Rabbany (2015) showed that the advantage of UPF is both processing time and increased position accuracy during GPS outage situation.

Also, Ko et. al. (2016) developed a method to detect the outlier and interference of GPS. When GPS outlier and interference were detected using the error covariance of estimated location, the method excluded GPS data from navigation process and fused available sensor measurements through EKF. It was proved that method detected GPS outlier and interference as well as the GPS recovery, which freed the navigation from the GPS abnormality problem.

Zheng Jingsen et. al. (2016) proposed a method based on the combination of EKF and neural network in order to improve tha accuracy performance for both GPS available and GPS outages situations.

Aftatah et. al. (2016) studied on hybridization of GPS with INS and odometer. GPS and odometer was integrated with INS where GPS was available or not respectively to improve the accuracy of filtering in degraded GPS enviroments.

Zhao et. al. (2017) developed a robust iterated EKF based on the generalized maximum likelihood approach for dynamic state estimation that can effectively suppresses observation and innovation outliers.

1.3 Outline of the Thesis

Chapter 2 provides necessary background into INS and GPS. Inertial sensors and their design technologies are all included in this chapter. Also fundamental characteristics, advantages and disadvantages of GPS are presented.

Chapter 3 provides background information about estimation algorithms, EKF, EKF2 and UKF. Pseudo codes for each algorithm are presented in sections of this chapter. Also this chapter presents INS/GPS integration architectures; loosely coupled, tightly coupled and ultra tightly coupled discussing their benefits and drawbacks. Last part of this chapter provides the state space model and the measurement model used in the INS/GPS integration process in this thesis.

Chapter 4 presents overall results of the simulations about the proposed methods for GPS available situation and algorithms are compared in terms of sensitivity to IMU noise variance and complexity. Also, effect of changing process noise matrix on EKF, EKF2 and UKF result are examined. EKF, EKF2 and UKF results for GPS outage and GPS outlier situations are also studied.

Chapter 5 provides a brief summary and conclusions of this study. The comparison of the results and the future work of the thesis are also mentioned in this chapter.

CHAPTER 2

INERTIAL NAVIGATION SYSTEMS (INS) AND GLOBAL POSITIONING SYSTEMS (GPS)

This chapter gives background information about INS and GPS. After making an introduction to INS, inertial sensors and their technologies of design / production are explained. Last part of this chapter briefly includes GPS.

2.1 Introduction to Inertial Navigation Systems (INS)

An INS is a very popular system due to its self-contained, non-jammable and nonradiating means for navigation. Also, it is commonly used because of their accuracy, long mean time between failure and self-reliance (Bar-shalom et. al. 2001, Bekir 2007). It can be used as a stand-alone system anywhere on the world, however it must be updated by an independent navigation sources (Bar-shalom et. al. 2001, Grewal et. al. 2001).

Three basic functions of the INS are sensing, computing, and generating. Inertial sensors comprise accelerometers and gyroscopes (measuring rotational rate), both without an external reference (Bar-shalom et. al. 2001, Groves 2008).

An INS system is worked as follows: Supposing the initial position and attitude of the vehicle is known, the velocity is obtained by single integration of the linear accelerations. One more integration of the velocity gives the position of the vehicle and the integrating rotational rates from gyroscope measurements give the attitude (Bar-shalom et. al. 2001).

INS is examined in two categories, either gimbaled or strapdown (Grewal et. al. 2001).

In a gimbaled system, sensor cluster comprises three accelerometers and three gyroscopes is attached to stabilized physical platform. This reduces the requirements on the inertial sensors and simplifies the navigation computation. Gimbaled system is more complicated and expensive than strapdown system because a stabilized platform is needed (Bar-shalom et. al. 2001).

In a strapdown system, stabilized platform is not used. The sensor cluster is attached to axis of the moving object. Due to higher rotation rates, the sensor outputs are less correct than gimbaled systems. Strapdown systems are preferred in many applications because of its smaller size, lower weight, reduced cost, complexity and power consumption (Bar-shalom et. al. 2001).

The internal structure of these two systems is shown in Figure 2.1.

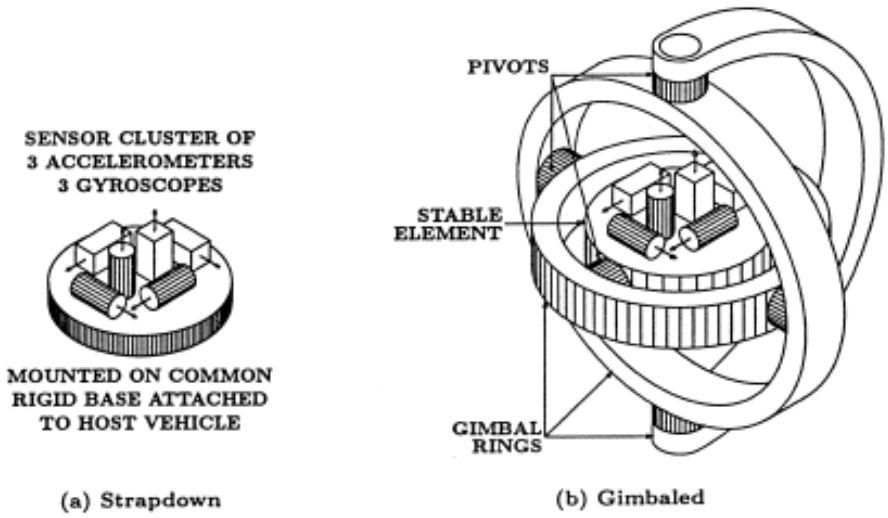

Figure 2.1 Internal structures of (a) strapdown and (b) gimbaled systems
[Figure is adapted from Grewal et. al. (2001).]

2.2 Inertial Measurement Unit (IMU) Technology

Most accelerometers use either pendulous or vibrating beams. They have same working principle of measuring the force on a proof mass.

2.2.1 Vibrating beam accelerometer

Proof mass and pendulous arm structure are used in vibrating beam accelerometer (NATO RTO-SET-054/RTG-30, 2003). This type of accelerometer is also called resonant beam or quartz resonator. When acceleration is applied along the sensitive axis, the beam pulls or pushes the proof mass and that results compressed or tensed beam, which causes frequency to decrease or increase respectively as seen in Figure 2.2. As a result, measuring of the resonant frequency gives the acceleration of the system (Groves 2008).

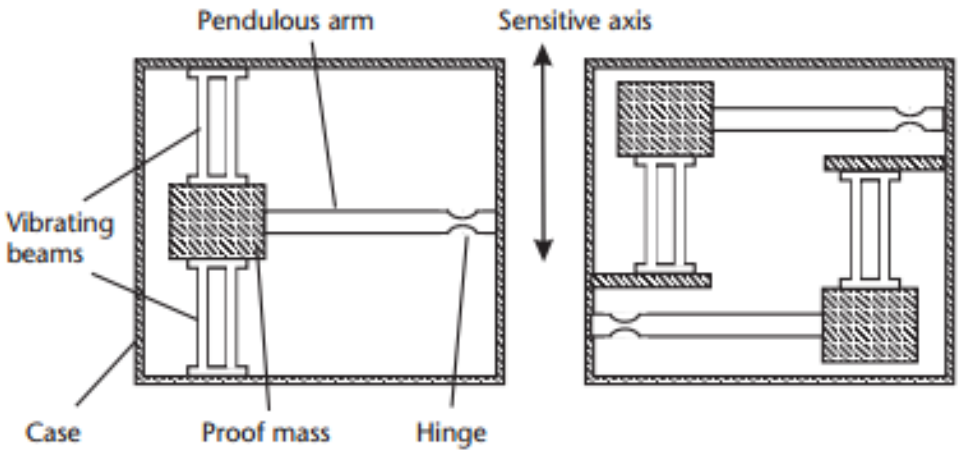

Figure 2.2 Internal structure of vibrating beam accelerometer
[Figure is adapted from Groves (2008).]

2.2.2 Force feedback accelerometer

Applied acceleration causes a deflection in the movement of the proof mass which is detected by the pick-off system. The detected signal is used in the torquer system for moving the proof mass back to its initial position. The force required to do this in the torquer system is a measure of the applied acceleration (NATO RTO-SET-054/RTG-30, 2003).

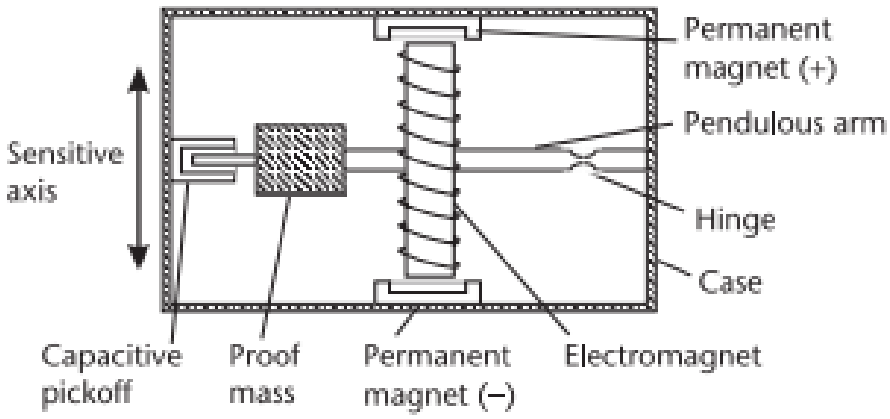

Figure 2.3 Internal structure of force feedback accelerometer
[Figure is adapted from Groves (2008).]

The design of the internal structure elements of force feedback accelerometer in Figure 2.3 are the main components affecting the performance (Groves 2008).

2.3 Gyroscope Technology

Gyroscope technology is not simple or cheap as the other technologies (INS and IMU). There are many different solutions for design of the gyroscopes (NATO RTO-SET-054/RTG-30, 2003).

Gyroscope technology can be examined as spinning mass, coriolis, optical and Micro Electromechanical Systems (MEMS) gyroscopes. Ring Laser Gyroscopes (RLG) and Fiber Optic Gyroscopes (FOG) are two types of optical gyroscopes.

2.3.1 Spinning mass gyroscope

In spinning mass gyroscopes, a measure of the amount of applied rotation is found by the response of rotation action in perpendicular to its spin axis. For all mechanical gyroscopes, this principle is the basis without external references (NATO RTO-SET-054/RTG-30, 2003).

2.3.2 Coriolis gyroscope

Coriolis gyroscopes use the fundamental idea in vibrating gyroscopes nevertheless the shapes can be very different from each other.

When there is a sinusoidally vibrated mass in a plane, and the plane is rotated, that mass is caused to vibrate sinusoidally perpendicular to the plane by Corolis force. The rotation rate is proportional to that amount of vibration. Tuning fork gyroscopes and hemispherical resonating gyroscopes are some of the more common Coriolis gyroscopes (NATO RTO-SET-054/RTG-30, 2003).

2.3.3 Optical gyroscopes

The principle of optical gyroscopes is based on the light travelling at a fixed speed in an inertial frame. Groves (2008) explains that "When a light is sent in both directions around a non-rotating waveguide, the path lenght will be the same for both beams. However, rotating the waveguide in the same direction with the light path increases the path lenght and rotating it in the opposite direction decreases the path length from the perpective of an inertial frame. This is called as sagnac effect. The changes in path length are measure of the angular rate of the waveguide with respect to inertial frame.".

2.3.3.1 Ring Laser Gyroscopes (RLG)

The sagnac effect is the basic principle behind optical gyroscopes.
The drawback of this technology is the lock-in problem, that is, at low rotation rates, RLG does not measure anything. One of the methods to solve this problem is using a mechanical vibration technique called "dithering". Alternatively, there are non-dithered, non-locking laser gyroscopes where more than one laser beam of different frequency is used to overcome the lock-in problem.

High reliability, high accuracy, technological matureness, high dynamic range, and digital output are the advantages of this technology (NATO RTO-SET-054/RTG-30, 2003).

2.3.3.2 Fiber Optic Gyroscopes (FOG)

As in RLG, the sagnac effect is the fundamental idea in FOG. In RLG, the loop is traversed once in either direction. However in this technology, the light beam travelling in fiber optic cable traverses the loop many times.

In FOG systems, the light beam travelling in one direction can be shifted electrically to overcome any possible “lock in” problems and that increases the sensitivity.

In this technology, there are fewer and simpler parts which are no moving. Also, FOG systems are smaller and cheaper than RLG and provide better reliability. Unlike RLG, high voltage is not used in FOG systems (NATO RTO-SET-054/RTG-30, 2003).

Internal structures of RLG and FOG systems are shown in Figure 2.4.

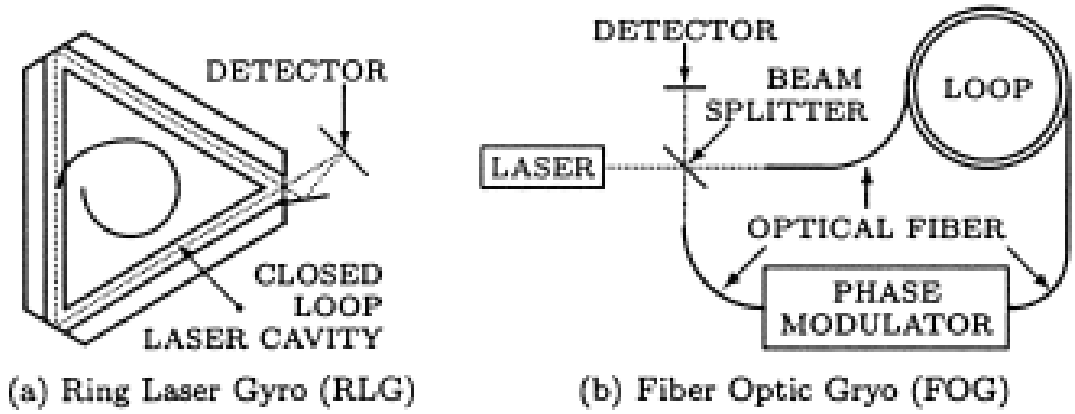

Figure 2.4 Internal structure of (a) ring laser gyro and (b) fiber optic gyro
[Figure is adapted from Grewal et. al. (2001).]

2.3.4 MEMS gyroscopes

Production technique of MEMS gyroscopes differs from the others. MEMS gyroscopes are micromachined directly on silicon or similar substrates by using chip electronics technology and minimum power requirements.

Costs of MEMS gyroscopes are very low with a very small size. Micromachined production of MEMS gyroscopes causes mass production capability (NATO RTO-SET-054/RTG-30, 2003).

2.4 Global Positioning Systems (GPS)

Passive radio signals provide 3D position and velocity to the users of GPS.

Measurement of range to at least four satellites is necessary to specify latitude, longitude, altitude and time information.

Radio signals consist of the position and velocity of each satellite and transmission time of it from the satellite. Considering that signal travels with the speed of light, the range between satellites and the GPS receiver antenna is obtained by evaluating the time taken for a radio signal transmitted from the satellite to the receiver (NATO RTO-SET-054/RTG-30, 2003).

The advantages of GPS are global coverage, absolute reference frame, accuracy, no error growth with time, and low cost receiver. However, GPS is not self-contained, that is, it is dependent on external signals. Also, GPS may have discontinuities. In other words, positionshifts can occur because of changing satellite geometry. Tall buildings can prevent the GPS signal. Received satellite signals are not strong and undefended to interference or jamming (NATO RTO-SET-054/RTG-30, 2003).

Space, control and user segments are the three main segments of GPS.

The constellation of satellites forms the space segment. The satellite constellation consists of the set of satellites in orbit and it ensures the ranging signals and data messages to the user (Kaplan and Hegarty 2006). Constellation contains 24 satellites in six orbital planes around the earth. (NATO RTO-SET-054/RTG-30, 2003).

Antenna stations tracks and monitors the health of GPS satellites and these forms the ground control segment (NATO RTO-SET-054/RTG-30, 2003). Additionaly, the control segment updates satellite's clock corrections and other parameters at least once a day (Kaplan and Hegarty 2006).

The user segment consists of a GPS receiver and a receiver antenna. L-band radio frequency signals are converted to the electronic signals and receiver ensures position, velocity, and time information (Kaplan and Hegarty 2006).

CHAPTER 3

ESTIMATION TECHNIQUES AND INTEGRATION ARCHITECTURES

This chapter provides background information about estimation algorithms, integration architectures in INS/GPS integration and nonlinear process model used in this thesis.

3.1 Estimation Techniques in Navigation

Short review of standart KF is given with mathematical models. Then, Extended, Second Order Extended, and Unscented Kalman Filters are explained in detail.

3.1.1 Kalman Filter (KF)

KF is an estimator ensures optimal state estimate by prediction and update steps. It is recursive because the previous estimate and the new input data is used to derivation of each state estimate. There is no need to store the whole past measurement data, only the previous estimate is required (Haykin 2001, Angrisano 2010).

Discrete time process and measurement model of a linear dynamic system is shown in Equation (3.1) and Equation (3.2),

$$x_{k+1}=F_k x_{k+} w_k \tag{3.1}$$

$$y_k=H_k x_k+v_k \tag{3.2}$$

where

x_k: the state vector,

F_k: the transition matrix,

w_k: the process noise,

y_k: the measurement vector at time k,

H_k: the measurement matrix, and

v_k is the measurement noise.

w_k and v_k are assumed to be zero-mean and additive Gaussian processes that is $w_k \sim N(0, Q_k)$ and $v_k \sim N(0, R_k)$ where

Q_k: covariance matrices of the process noise and

R_k: covariance matrices of the measurement noise.

Moreover, v_k is not correlated with w_k (Haykin 2001).

The standart KF algorithm is given in Table 3.1.

Table 3.1 Summary of the Kalman filter
[Table is adapted from Haykin (2001).]

State-space model	x_{k+1}=$F_{k+1,k}x_k$+w_k y_k=$H_k x_k$+v_k where w_k and v_k are independent, zero-mean, Gaussian noise processes of covariance matrices Q_k and R_k, respectively.
Initialization: For k=0, set	$\hat{x}_0$=$E[x_0]$ P_0=$E[(x_0 - E[x_0])][(x_0 - E[x_0])^T]$
Computation: For k=1, 2, ….., compute	
State estimation propagation	$\hat{x}_k^-$= $F_{k,k-1}\hat{x}_{k-1}^-$
Error covariance propagation	$\hat{P}_k^-$= $F_{k,k-1}P_{k-1}F_{k,k-1}^T$+$Q_{k-1}$
Kalman gain matrix	G_k=$P_k^- H_k^T[H_k P_k^- H_k^T + R_k]^{-1}$
State estimate update	$\hat{x}_k$=$\hat{x}_k^-$+$G_k(y_k - H_k\hat{x}_k^-)$
Error covariance update	$P_k = (I - G_k H_k)P_k^-$

3.1.2 Extended Kalman Filter (EKF)

Standart KF problem focuses on the estimation of a state vector in a linear model of a dynamical system. KF can be extended to estimation of nonlinear model of nonlinear systems by a linearization procedure. That filter is called as Extended Kalman Filter (Haykin 2001).

Equation (3.3) and Equation (3.4) shows the state-space model of a nonlinear system,

$$x_{k+1} = f(k, x_k) + w_k \tag{3.3}$$

$$y_k = h(k, x_k) + v_k \tag{3.4}$$

Where
$f(k, x_k)$: the nonlinear transition function and
$h(k, x_k)$: the nonlinear measurement function.

The main principle of EKF is linearizing the nonlinear functions $f(k, x_k)$ and $h(k, x_k)$ at each time step (Haykin 2001). Linearization procedure provides "first order" approximations to the optimal terms. Second order errors are caused by these approximations in the mean and covariance of the state estimate and sometimes filter divergence is resulted (Wan and Merwe 2000). After linear model is obtained, KF equations are implemented.

EKF algorithm is given in Table 3.2.

Table 3.2 Extended Kalman filter
[Table is adapted from Haykin (2001).]

State-space model	$x_{k+1}=f(k,x_k)+w_k$, $y_k=h(k,x_k)+v_k$, where w_k and v_k are independent, zero-mean, Gaussian noise processes of covariance matrices Q_k and R_k, respectively.
Definitions	$F_{k+1,k}=\frac{\partial f(k,x)}{\partial x}\|_{x=x_k}$, $H_k=\frac{\partial h(k,x)}{\partial x}\|_{x=x_k^-}$ where the Jacobian of the vector f and h.
Initialization: For k=0, set	$\hat{x}_0=E[x_0]$ $P_0=E[(x_0-E[x_0])(x_0-E[x_0])^T]$.
Computation: For k=1, 2,…., compute:	
State estimate propagation	$\hat{x}_k^-=f(k,\hat{x}_{k-1})$
Error covariance propagation	$P_k^-=F_{k,k-1}P_{k-1}F_{k,k-1}^T+Q_{k-1}$
Kalman gain matrix	$G_k=P_k^-H_k^T[H_kP_k^-H_k^T+R_k]^{-1}$
State estimate update	$\hat{x}_k=\hat{x}_k^-+G_ky_k-h(k,\hat{x}_k^-)$
Error covariance update	$P_k=(I-G_kH_k)P_k^-$.

3.1.3 Second Order Extended Kalman Filter (EKF2)

EKF2 is based on a second order Taylor expansion, that is, it includes second-order correction terms (Roth and Gustafsson 2011).

The algorithm of EKF2 is shown in Table 3.3.

Table 3.3 Second order extended Kalman filter algorithm
[Algorithm is adapted from Bar-Shalom et. al. (2001)]

State-space model

x_{k+1}=$f(k, x_k)$+w_k,

y_k=$h(k, x_k)$+v_k,

where w_k and v_k are independent, zero-mean, Gaussian noise processes of covariance matrices Q_k and R_k, respectively.

Definitions

$f_x(k) \triangleq [\nabla_x f(k,x)']'|_{x=\hat{x}_{k|k}} \triangleq \frac{\partial f}{\partial x}$ and

$f_{xx}(k) \triangleq [\nabla_x \nabla'_x f(k,x)]|_{x=\hat{x}_{k|k}} \triangleq \dfrac{\partial^2 f}{\partial x^2}$

are the Jacobian and Hessian of the vector f evaluated at the latest estimate of the state, respectively. e_i is the ith n_x-dimensional Cartesian basis vector (ith component unity, the rest zero).

State prediction

$\hat{x}_{k+1|k}$=$f\left(k, \hat{x}_{k|k}\right) + \frac{1}{2}\sum_{i=1}^{n_x} e_i tr[f_{xx}^i(k) P_{k|k}]$

State prediction covariance

$P_{k+1|k} = f_x(k) P_{k|k} f_x(k)' + \frac{1}{2}\sum_{i=1}^{n_x}\sum_{j=1}^{n_x} e_i e'_j \, tr\left[f_{xx}^i(k) P_{k|k} f_{xx}^j(k) P_{k|k}\right] + Q_k$

Measurement prediction

$\hat{z}_{k+1|k} = h\left(k+1, \hat{x}_{k+1|k}\right) + \frac{1}{2}\sum_{i=1}^{n_x} e_i \, tr[h_{xx}^i(k+1) P_{k+1|k}]$

Measurement prediction covariance

$$S(k+1) = h_x(k+1) P_{k+1|k} h_x(k+1)' + \frac{1}{2}\sum_{i=1}^{n_x}\sum_{j=1}^{n_x} e_i e'_j \, tr\left[h^i{}_{xx}(k+1) P_{k+1|k} h^j{}_{xx}(k+1) P_{k+1|k}\right] + R_{k+1}$$

Filter Gain

$W(k+1) \triangleq P_{k+1|k} H(k+1)' S(k+1)^{-1}$

State Estimate

$\hat{x}_{k+1|k+1} = \hat{x}_{k+1|k} + W(k+1) v(k+1)$

where $v(k+1) \triangleq z(k+1) - \hat{z}_{k+1|k}$ is called innovation.

State Estimate Covariance

$P_{k+1|k+1} = P_{k+1|k} - W(k+1) S(k+1) W(k+1)'$

3.1.4 Unscented Kalman Filter (UKF)

The distribution of the state is again represented as a Gaussian random variable. UKF approaches the approximation problem of EKF by carefully selecting deterministic sigma points. These sigma points represent the mean and covariance vector. In the literature, there are various methods for the sigma point selection one of which is Unscented Transformation (UT).

Although EKF is used widely, a lot of difficulties arise from the need of linearization. To overcome this limitation, UT is a basic operation of UKF (Wan and Merwe 2000, Julier and Uhlmann 2003).

Set of sigma points are selected and nonlinear function is implemented to each point and transformed points are obtained. Transformed covariance and mean estimation is calculated by using the statistics of the transformed points (Wan and Merwe 2000, Julier and Uhlmann 2003).

The approach is illustrated in Figure 3.1.

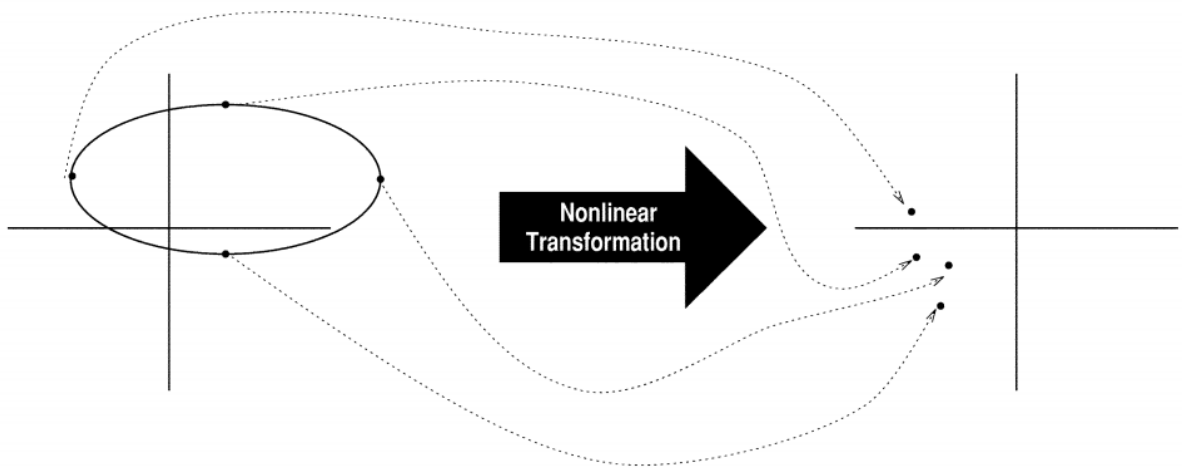

Figure 3.1 Nonlinear transformation in UKF
[Figure is adapted from Julier and Uhlmann (2003)]

UT and UKF algorithms are given in Table 3.4 and Table 3.5 respectively.

Table 3.4 Unscented transform

(Table is adapted from Julier and Uhlmann (2003).)

Finding the sigma points

We set the sigma points and their weights for $\emptyset \sim N\left(\emptyset, \overline{\emptyset}, \Phi\right)$ as

$\emptyset^{(0)}=\overline{\emptyset}$

$\emptyset^{(i)}=\overline{\emptyset}+\left[\sqrt{\frac{n_\emptyset}{1-\pi^{(0)}}\Phi}\right]_{:,i}$

$\emptyset^{(i+n_\emptyset)}=\overline{\emptyset}-\left[\sqrt{\frac{n_\emptyset}{1-\pi^{(0)}}\Phi}\right]_{:,i}$ for $i = 1, \ldots., n_\emptyset$

$\pi^{(0)} = \pi^{(0)}$

$\pi^{(i)} = \dfrac{1-\pi^{(0)}}{2n_\emptyset}$

$\pi^{(i+n_\emptyset)} = \dfrac{1-\pi^{(0)}}{2n_\emptyset}$

Note that there are $2n_\emptyset + 1$ sigma points and we have $\sum_{i=0}^{2n_\emptyset} \pi^{(i)} = 1$

$\sum_{i=0}^{2n_\emptyset} \pi^{(i)} \emptyset^{(i)} = \overline{\emptyset}$

$\sum_{i=0}^{2n_\emptyset} \pi^{(i)} \left(\emptyset^{(i)} - \overline{\emptyset}\right)\left(\emptyset^{(i)} - \overline{\emptyset}\right)^T = \overline{\emptyset}$

Find the sigma points and their weights $\pi^{(i)}$, $\emptyset^{(i)}$ for $i = 0\ to\ 2n_\emptyset$

Transform the sigma points with transformation $g(\emptyset)$ as

$\varphi^{(i)} = g(\emptyset^{(i)})$ for $i = 0\ to\ 2n_\emptyset$

Find the transformed mean and covariance as

$\bar{\varphi} = \sum_{i=0}^{2n_\emptyset} \pi^{(i)} \varphi^{(i)}$

$\varphi = \sum_{i=0}^{2n_\emptyset} \pi^{(i)} \left(\varphi^{(i)} - \bar{\varphi}\right)\left(\varphi^{(i)} - \bar{\varphi}\right)^T$

Table 3.5 Unscented Kalman filter algorithm
(Table is adapted from Julier and Uhlmann (2003).)

Start with $\hat{x}_{0|0}$, $\hat{P}_{0|0}$, set $k = 1$

For each k

Prediction update

Generate sigma points and their weights $\pi^{(i)}$, ${x_{k-1|k-1}}^{(i)}$ from $i = 0$ to $2n_x$ for $N(x_{k-1}; \hat{x}_{k-1|k-1}, P_{k-1|k-1})$

Transform the sigma points

${x_{k|k-1}}^{(i)} = f({x_{k-1|k-1}}^{(i)})$ from $i = 0$ to $2n_x$

Obtain the predicted state estimate $\hat{x}_{k|k-1}$ and its covariance $P_{k|k-1}$ as

$\hat{x}_{k|k-1} = \sum_{i=0}^{2n_x} \pi^{(i)} {x_{k|k-1}}^{(i)}$

$P_{k|k-1} = \sum_{i=0}^{2n_x} \pi^{(i)} \left[\left({x_{k|k-1}}^{(i)} - \hat{x}_{k|k-1}\right)\left({x_{k|k-1}}^{(i)} - \hat{x}_{k|k-1}\right)^T\right] + Q$

Measurement Update

Generate sigma points and their weights $\pi^{(i)}$, ${x_{k|k-1}}^{(i)}$ from $i = 0$ to $2n_x$ for $N(x_k; \hat{x}_{k|k}, P_{k|k-1})$

Transform the sigma points

${y_{k|k-1}}^{(i)} = h({x_{k|k-1}}^{(i)})$ from $i = 0$ to $2n_x$

Obtain the state estimate $\hat{x}_{k|k}$ and its covariance $P_{k|k}$ as

$\hat{x}_{k|k} = \hat{x}_{k|k-1} + K_k\left(y_k - \hat{y}_{k|k-1}\right)$

$P_{k|k} = P_{k|k-1} - K_k S_{k|k-1} K_k^T$

where

$\hat{y}_{k|k-1} = \sum_{i=0}^{2n_x} \pi^{(i)} {y_{k|k-1}}^{(i)}$

$S_{k|k-1} = \sum_{i=0}^{2n_x} \pi^{(i)} ({y_{k|k-1}}^{(i)} - \hat{y}_{k|k-1})({y_{k|k-1}}^{(i)} - \hat{y}_{k|k-1})^T + R$

$\sum_{xy} = \sum_{i=0}^{2n_x} \pi^{(i)} ({x_{k|k-1}}^{(i)} - \hat{x}_{k|k-1})({x_{k|k-1}}^{(i)} - \hat{x}_{k|k-1})^T$

$K_k = \sum_{xy} {S_{k|k-1}}^{-1}$

Unlike EKF and EKF2, UT used in UKF plays an important role in updating its sigma points, $\pi^{(i)}$, and their weights, $\emptyset^{(i)}$ in every step of run by minimizing the error in state estimate. Therefore, optimal accuracy can be adaptively obtained.

The value of $\pi^{(0)}$ controls how the other positions will be repositioned (Julier and Uhlmann 2003).

3.2 Integration Architectures in Navigation

Loosely coupled, tightly coupled, and ultra tightly coupled are mentioned as integration architectures.

3.2.1 Loosely coupled integration

Loosely coupled architecture is used widely as the simplest method of all. In this architecture, GPS and the inertial sensors produce their position, velocity, and attitude independently (Alban et. al. 2003).

The difference between INS and GPS position and velocity are used as input measurements to KF. INS errors are estimated by KF and independent INS solution is corrected using the estimated INS errors and integrated navigation solution is achieved (Grewal et. al. 2001).

This architecture ensures higher bandwidth and better noise characteristics with respect to independent GPS solution (Alban et. al. 2003).

3.2.2 Tightly coupled integration

KF uses pseudo-range rates and Doppler data to correct the INS data and this causes nonlinearity to the measurement model.

In this architecture, there is no need to track four satellites because there is no separate GPS solution. KF estimator estimates the INS errors and standalone INS solution is corrected using the estimated errors.

Tightly coupled integration is significantly more accurate and robust but tends to be more complex than loosely coupled integration (Grewal et. al. 2001).

3.2.3 Ultra tightly coupled

Ultra tightly coupled integration is more complicated according to other architectures.

Measurements are in-phase and quadrature samples of the GPS correlators used to update the filter states.

Ultra-tight integration can improve acquisition time and tracking performance, so, Doppler and phase measurements are produced properly.

Robustness to radio frequency interference or multipath are the improvements as regards to independent GPS solution (Alban et. al. 2003).

3.3 Nonlinear INS Process Model

The process model used in this thesis is nonlinear process model with Euler angles. The trigonometric operations in the updates and rotation matrices to transform INS measurements from the body frame to the navigation frame results the system model to be nonlinear.

In the scope of this thesis, a state space model which contains fifteen elements, namely 3D position, velocity and attitude, accelerometer biases and gyroscope biases, is examined. The simplified mechanization model in discrete time is shown as in Equation (3.5)-Equation (3.11) (Zhou et. al. 2010).

$$p_{n,k+1} = p_{n,k} + v_{n,k}\Delta t \tag{3.5}$$

$$v_{n,k+1} = v_{n,k} + [R_{b2n,k}(\tilde{f}_{b,k} - \tilde{f}_{b,k}^{bias}) + g_n]\Delta t \tag{3.6}$$

$$\psi_{k+1} = \psi_k + E_{b2n,k}(\widetilde{w}_{b,k} - \widetilde{w}_{b,k}^{bias})\Delta t \tag{3.7}$$

$$f_{k+1} = \tilde{f}_{b,k}^{bias} \tag{3.8}$$

$$w_{k+1} = \widetilde{w}_{b,k}^{bias} \tag{3.9}$$

$$R_{b2n} = \begin{pmatrix} C\varphi C\phi & C\varphi S\phi S\theta - S\varphi C\theta & C\varphi S\phi C\theta + S\varphi S\theta \\ S\varphi C\phi & S\varphi S\phi S\theta + C\varphi C\theta & S\varphi S\phi C\theta - C\varphi S\theta \\ -S\phi & C\phi S\theta & C\phi C\theta \end{pmatrix} \tag{3.10}$$

$$E_{b2n} = \begin{pmatrix} 1 & S\theta T\phi & C\theta T\phi \\ 0 & C\theta & -S\theta \\ 0 & S\theta/C\phi & C\theta/C\phi \end{pmatrix} \tag{3.11}$$

where

k: the time instant,

$\tilde{f}_b$: the measurement vector of the specific force,

$\widetilde{w}_b$: the measurement vector of angular rate,

g_n: the local gravity vector,

ψ: the Euler angles,

R_{b2n}: the frame rotation matrix from body frame to north east and down navigation frame,

E_{b2n}: the rotation rate transformation matrix between body and navigation frame,

CX: the trigonometric operation of cosine,

SX: the trigonometric operation of sine,

TX: the trigonometric operation of tangent,

θ: roll,

ϕ: pitch, and

φ: yaw.

In this thesis, the measurement model is linear although the process model is nonlinear. Because loosely coupled architecture is used in this study. Therefore, there is no need to use pseudo-range rates and Doppler datas. The difference between INS and GPS position and velocity are used as input measurements to KF so there is no nonlinearity in measurement model.

CHAPTER 4

RESULTS AND DISCUSSIONS

In this chapter, MATLAB simulation results of the INS/GPS integration process are given. In the first part, a 3D flight trajectory, which is generated by pathgen.m open source code from www.instk.org website, is used as the main navigation scenario. This code generates the accelerometer and gyroscope datas at 400 Hz and GPS navigation datas at 4 Hz. Therefore, prediction update of KF is done 100 times, and then measurement update is done only once, and so on. In this study, results of the standart EKF, UKF and EKF2 techniques are compared. In the second part, a different 3D flight trajectory is generated and those techniques are applied again.

4.1 Case 1 Simulation Results

Experimental results in this thesis will be investigated case by case. Cases are classified according to generated paths. Generated path as true navigation data in Case 1 is shown in Figure 4.1.

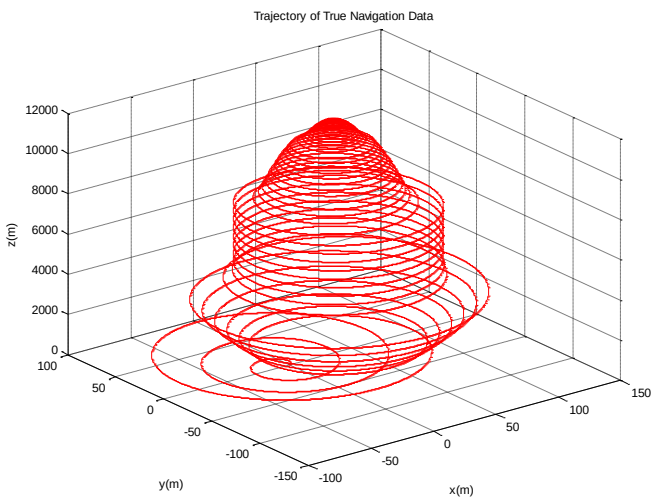

Figure 4.1 Trajectory of true navigation data in case 1

4.1.1 True navigation, standalone inertial and GPS results

In this section, true navigation, standalone inertial (INS) and GPS results will be investigated comparatively.

3D flight trajectory of true navigation data in Figure 4.1 is split into its Cartesian coordinates as x, y, and z as seen in Figure 4.2.

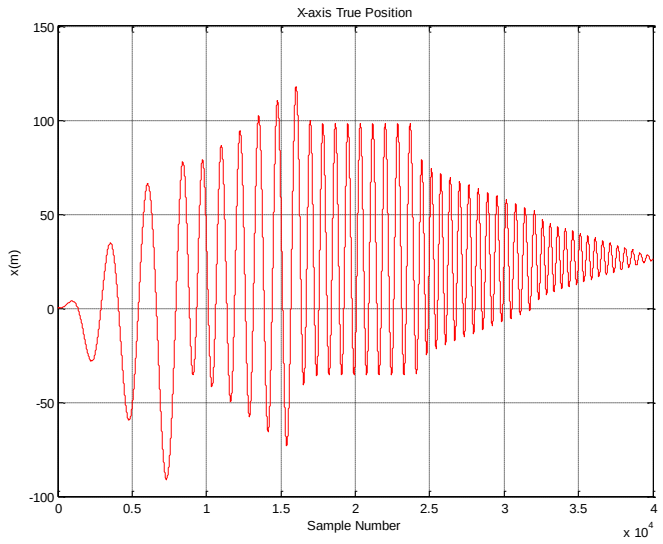

a.

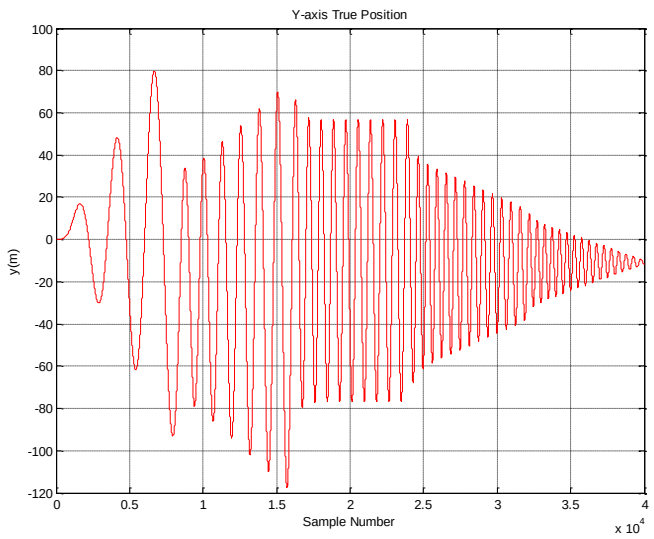

b.

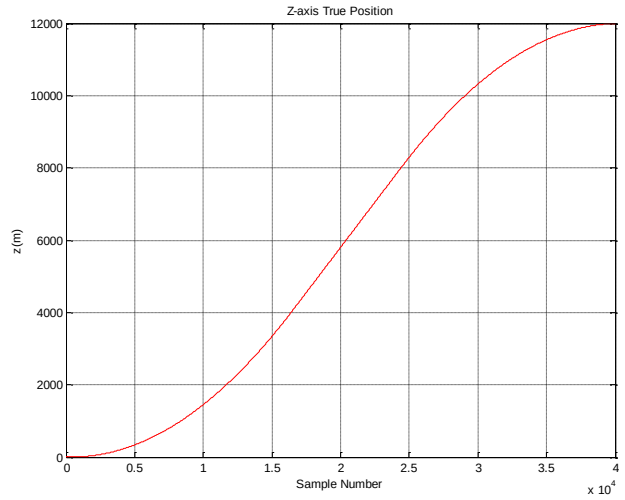

c.

Figure 4.2 Split coordinates of true navigation data into its Cartesian coordinates, (a) x-axis, (b) y-axis, and (c) z-axis for case 1

After generating true navigation data, pathgen.m open source code generates GPS data as shown in Figure 4.3.

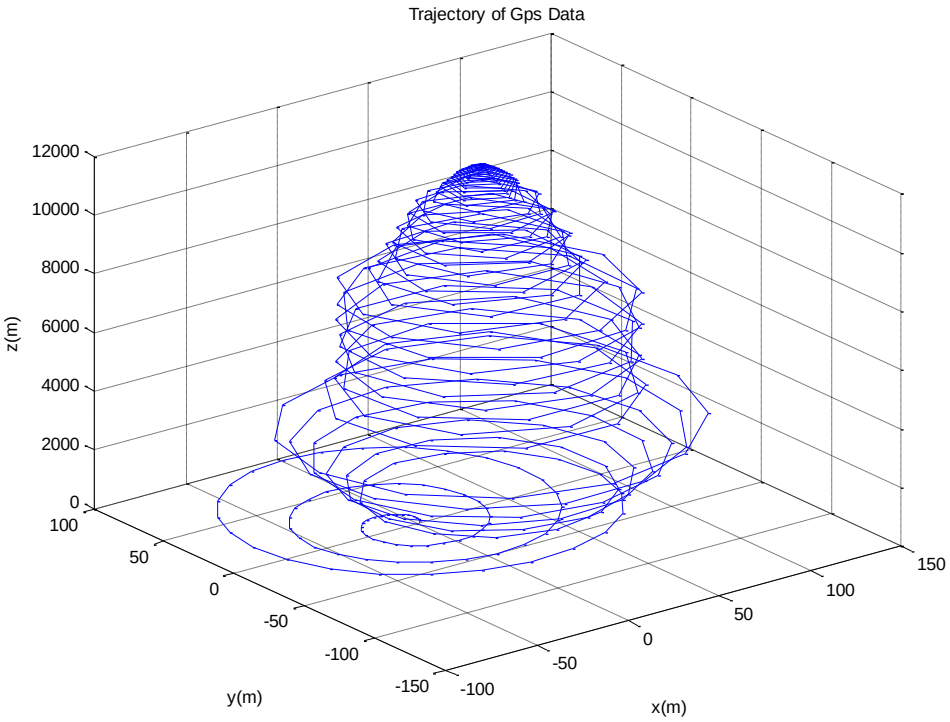

Figure 4.3 Trajectory of GPS data in case 1

3D flight trajectory of GPS data in Figure 4.3 is split into its Cartesian coordinates as x, y, and z as seen in Figure 4.4.

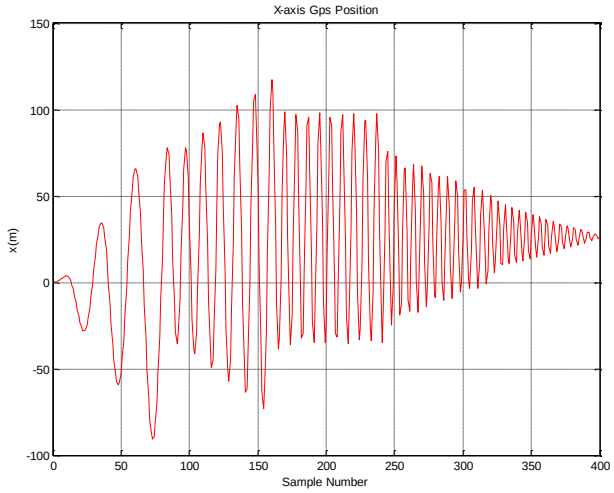

a.

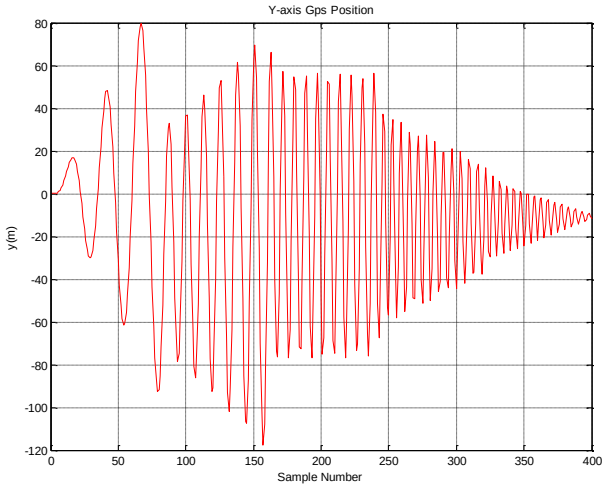

b.

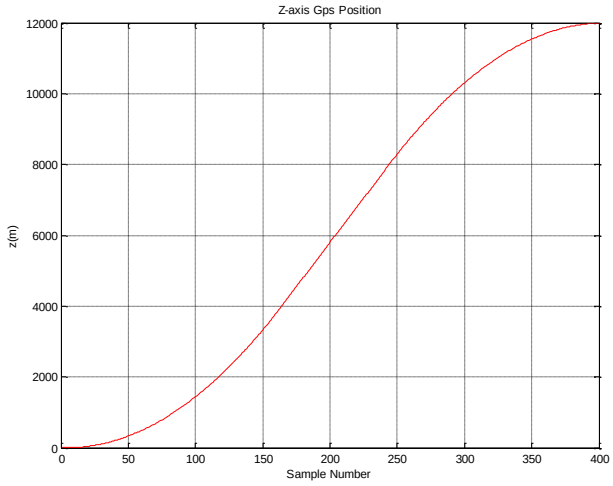

c.

Figure 4.4 Split coordinates of GPS data into its Cartesian coordinates, (a) x-axis, (b) y-axis, and (c) z-axis for case 1

True navigation data in Figure 4.2 and GPS data in Figure 4.4 are comparatively shown in Figure 4.5.

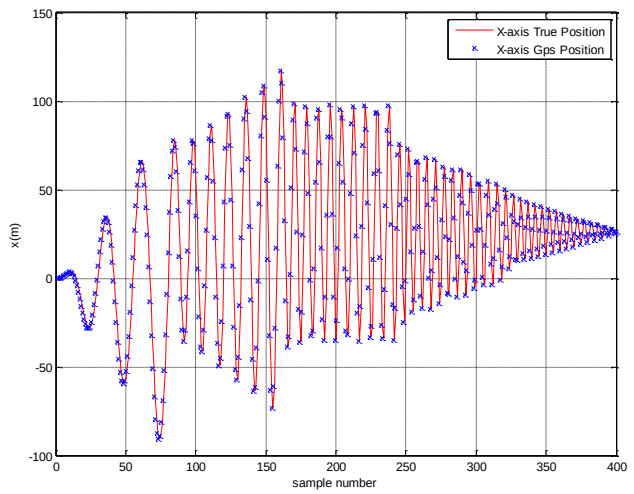

a.

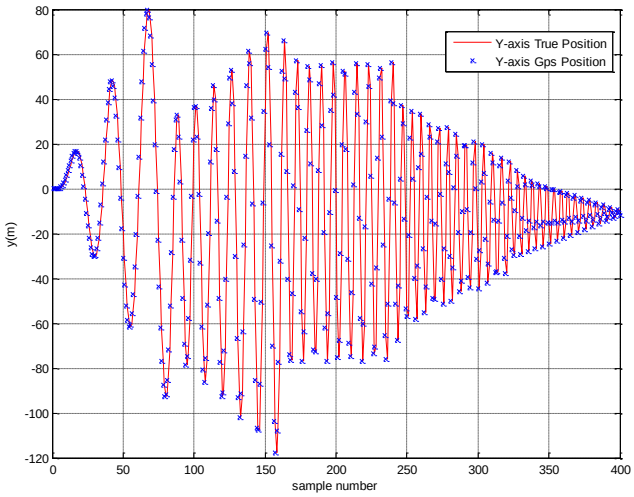

b.

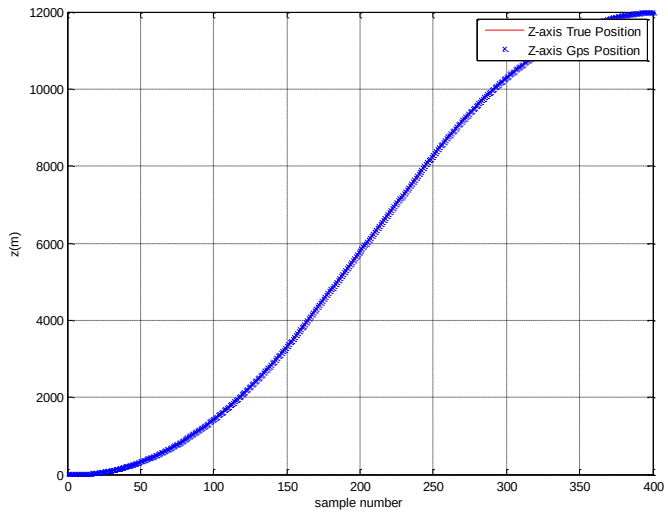

c.

Figure 4.5 Comparison of true navigation data and GPS data in (a) x-axis, (b) y-axis, and (c) z-axis for case 1

Other outputs of pathgen.m open source code are also linear accelerations and rotational rates which are accelerometer and gyroscope datas, respectively. As explained in Chapter 2, the velocity of the vehicle is obtained by single integration of the linear accelerations and one more integration of the velocity gives the position of the vehicle in three Cartesian coordinates as shown in Figure 4.6.

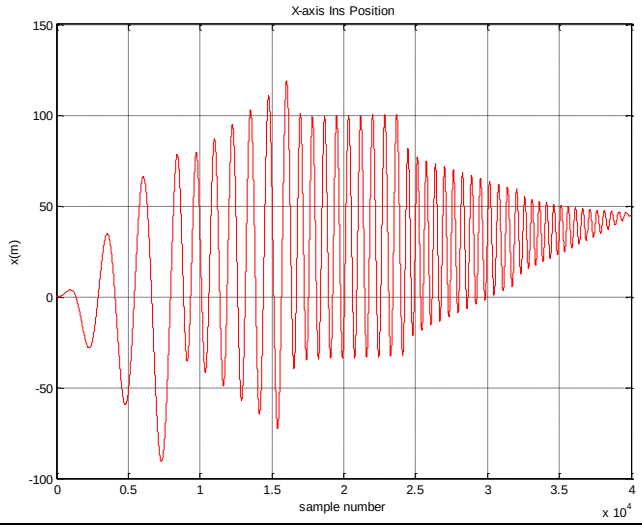

a.

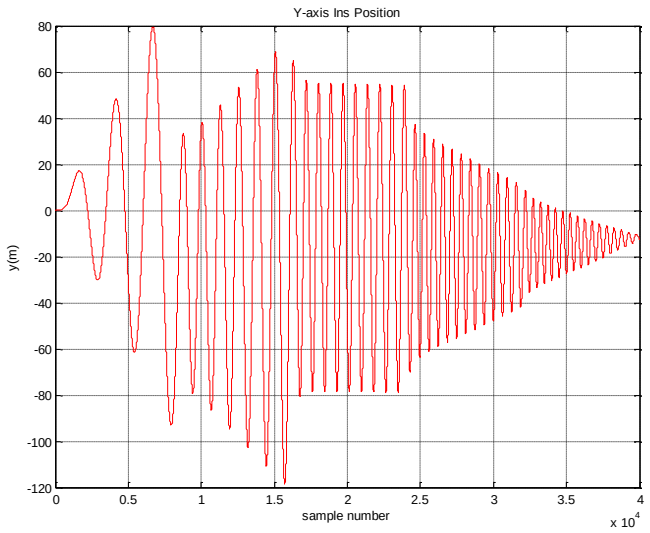

b.

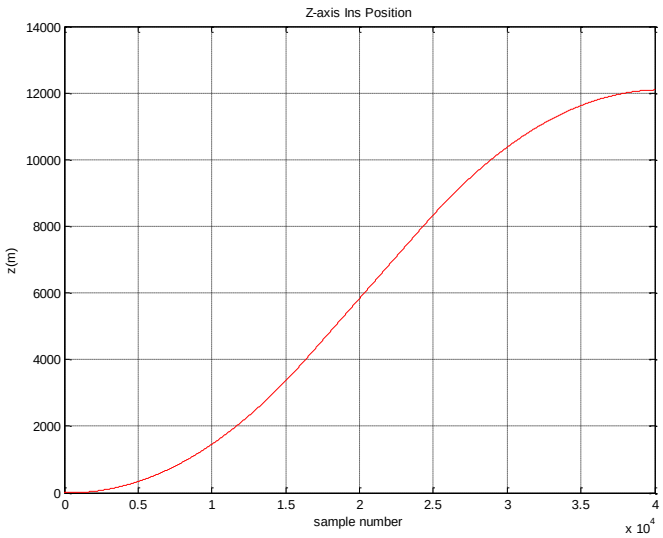

c.

Figure 4.6 Split coordinates of INS data into its Cartesian coordinates, (a) x-axis, (b) y-axis, and (c) z-axis for case 1

As in Figure 4.5, true navigation data in Figure 4.2 and INS data in Figure 4.6 are comparatively shown in Figure 4.7.

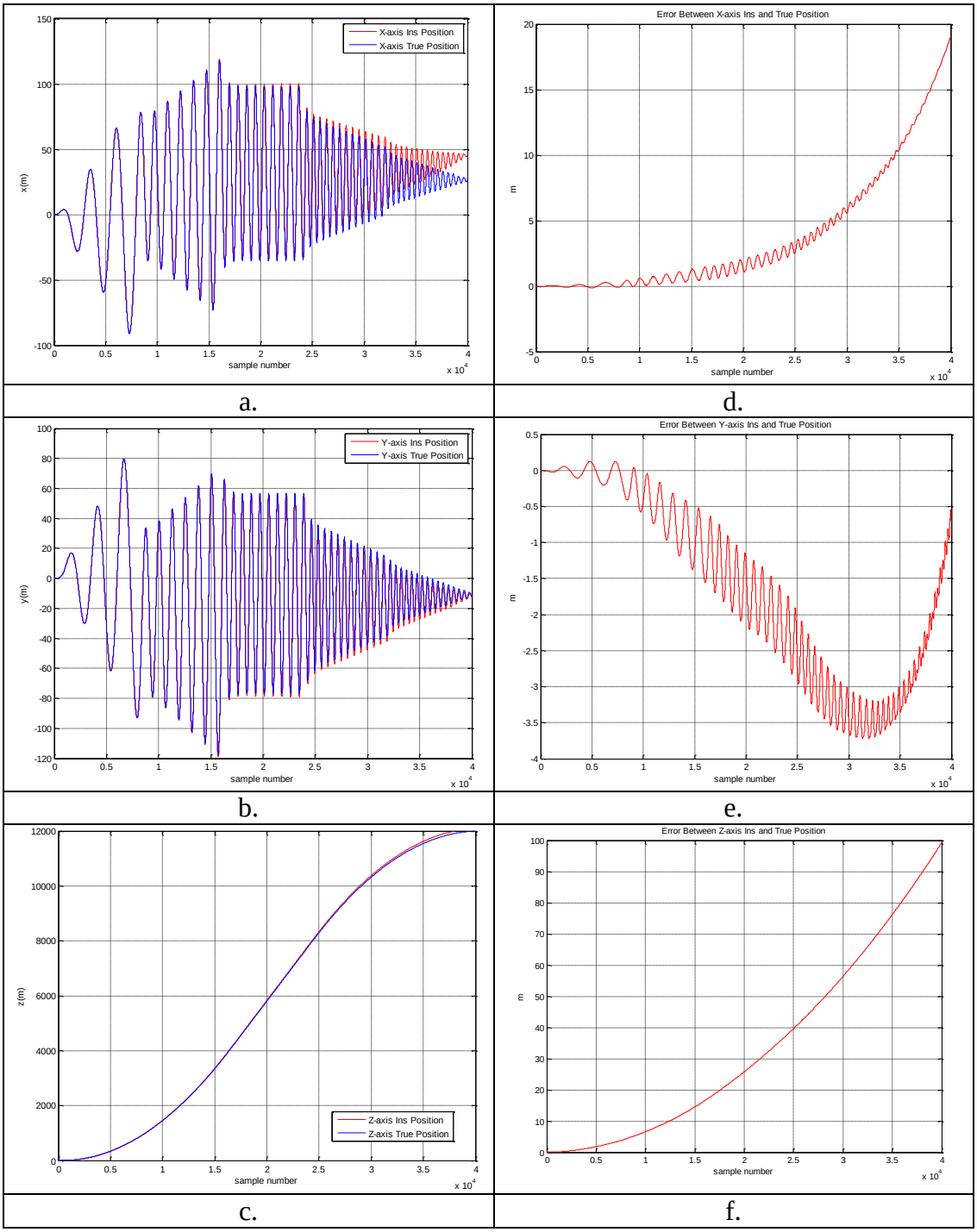

Figure 4.7 Comparison of true navigation data and INS data in (a) x-axis, (b) y-axis, and (c) z-axis, and errors for (d) x-axis, (e) y-axis, and (f) z-axis for case 1

4.1.2 EKF, EKF2 and UKF results for GPS available situation

In this section, EKF, EKF2, and UKF results for GPS available situation will be investigated comparatively.

Identical system and measurement models are employed in all of the estimation algorithms. The same initial state covariance matrix, process noise and measurement noise matrices are used for a significant comparison of the performances.

True navigation data in Figure 4.2 and EKF results for three Cartesian coordinates are comparatively shown in Figure 4.8. Figure 4.8 (d-f) also show the zoomed versions of Figure 4.8 (a-c).

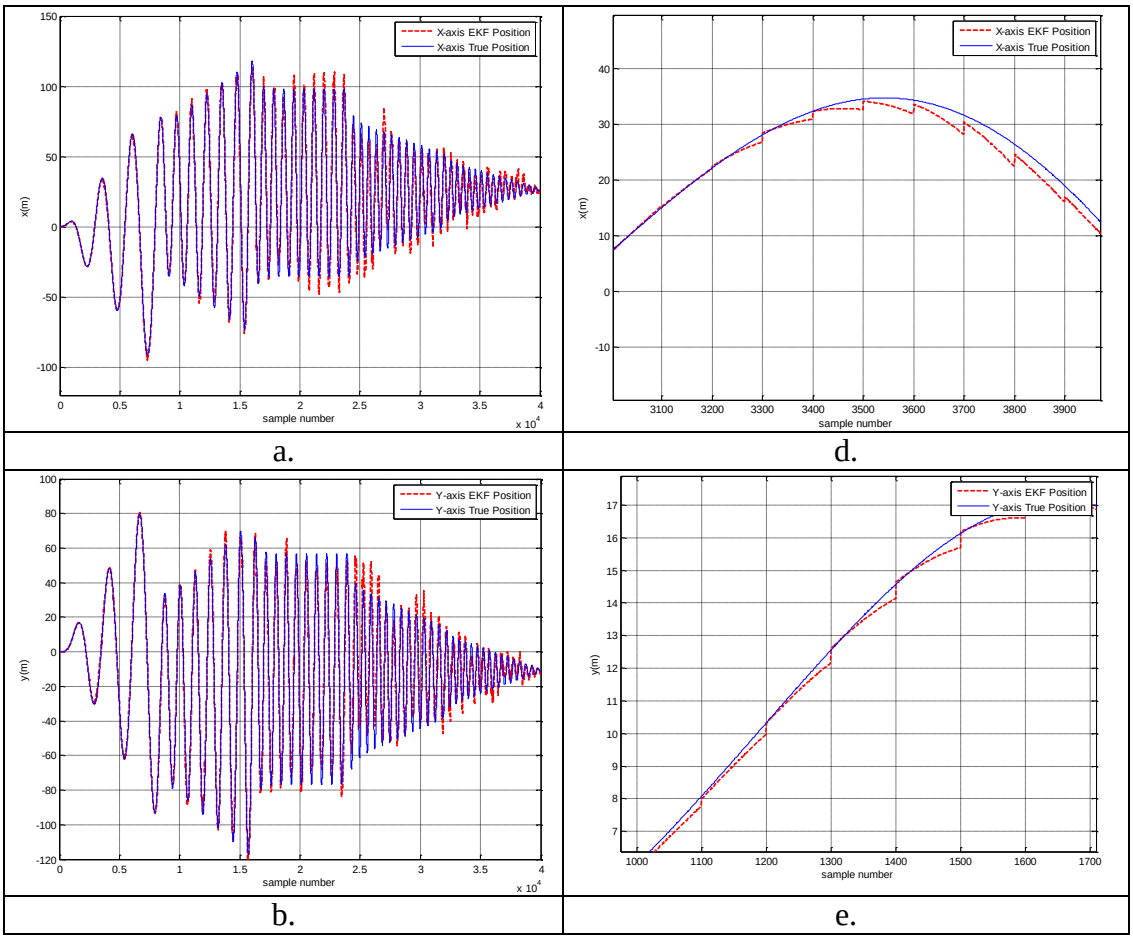

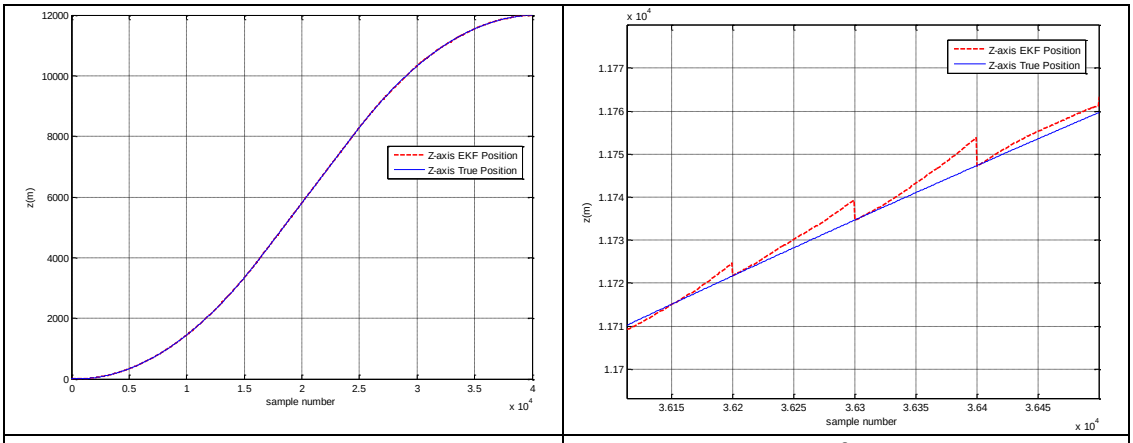

c. f.

Figure 4.8 Comparison of true navigation data and EKF results in (a) x-axis, (b) y-axis, and (c) z-axis and zoomed versions for (d) x-axis, (e) y-axis, and (f) z-axis for case 1

The accelerometer and gyroscope datas are generated at 400 Hz and GPS navigation datas at 4 Hz. Hence, as expected, there will be 1 measurement update after every 100 prediction update. As can be seen from filter outputs in Figure 4.8, filter output is separated from true navigation position along the prediction update process due to accumulation of inertial sensor errors, then gets closer to true navigation position when the GPS data is updated.

Performance of the filters is compared in terms of the Root Mean Square Error (RMSE) metric. RMSE of the results is calculated as in Equation (4.1),

$$RMSE = \sqrt{\frac{1}{K}\sum_{k=1}^{K}((x_k - x_k^{true})^2 + (y_k - y_k^{true})^2 + (z_k - z_k^{true})^2)} \qquad (4.1)$$

where K is the number of samples in the scenario, $(x_k^{true}, y_k^{true}, z_k^{true})$ are the true navigation data, and (x_k, y_k, z_k) are the state estimates of the filter at time k.

Table 4.1 comparatively shows RMSE results for EKF in terms of three Cartesian coordinates.

Table 4.1 RMSE results for EKF in case 1

EKF	x-axis	y-axis	z-axis
RMSE (m)	5.0254	5.376024057975308	4.751929880242610

True navigation data in Figure 4.2 and second order EKF results for three Cartesian coordinates are comparatively shown in Figure 4.9. Figure 4.9 (d-f) show the zoomed versions of Figure 4.9 (a-c).

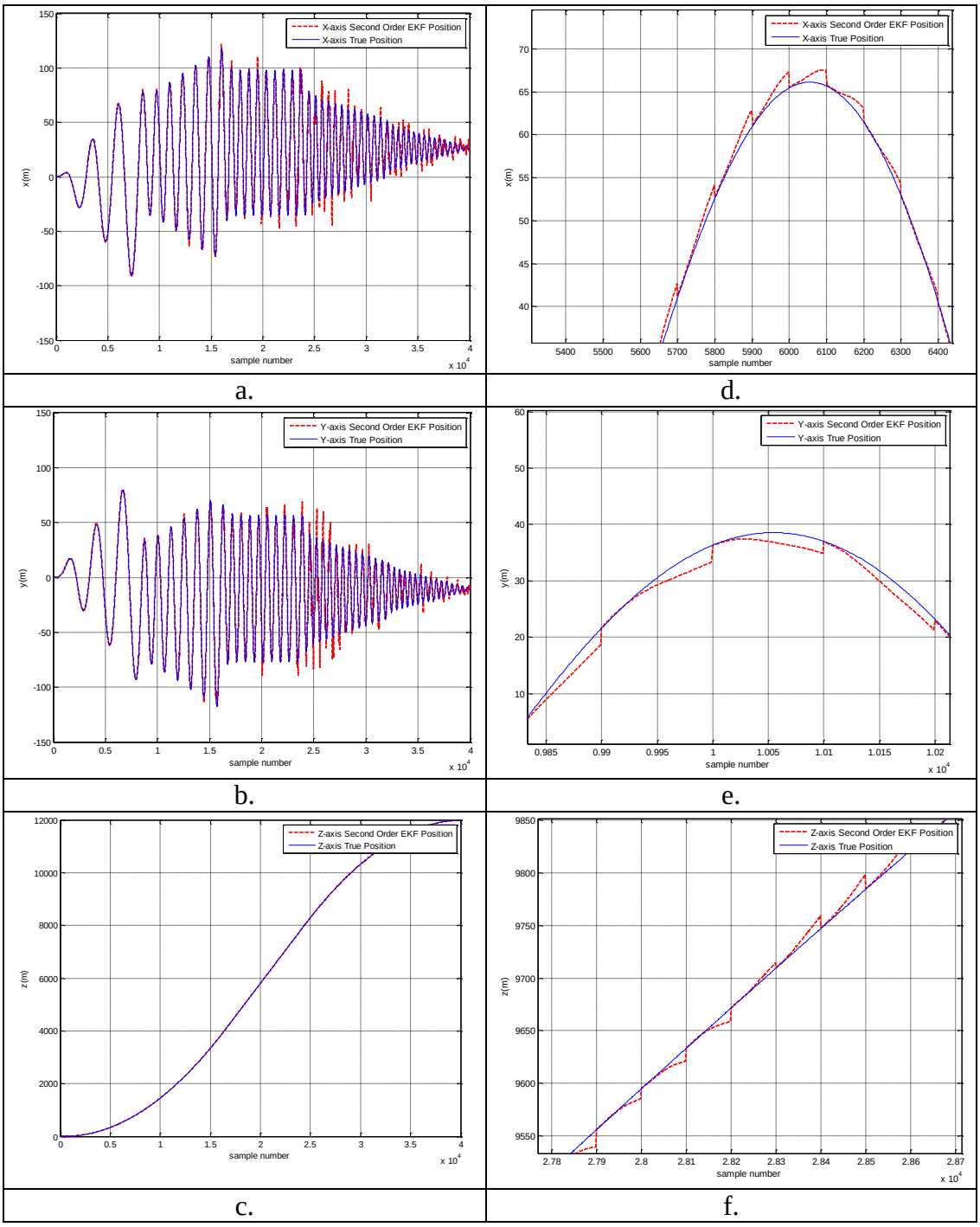

Figure 4.9 Comparison of true navigation data and second order EKF results in (a) x-axis, (b) y-axis, and (c) z-axis and zoomed versions for (d) x-axis, (e) y-axis, and (f) z-axis for case 1

Table 4.2 comparatively shows RMSE results for second order EKF in terms of three Cartesian coordinates.

Table 4.2 RMSE results for EKF2 in case 1

EKF2	x-axis	y-axis	z-axis
RMSE (m)	3.4533	3.6407	3.0736

Finally, true navigation data in Figure 4.2 and UKF results for three Cartesian coordinates are comparatively shown in Figure 4.10. Figure 4.10 (d-f) show the zoomed versions of Figure 4.10 (a-c).

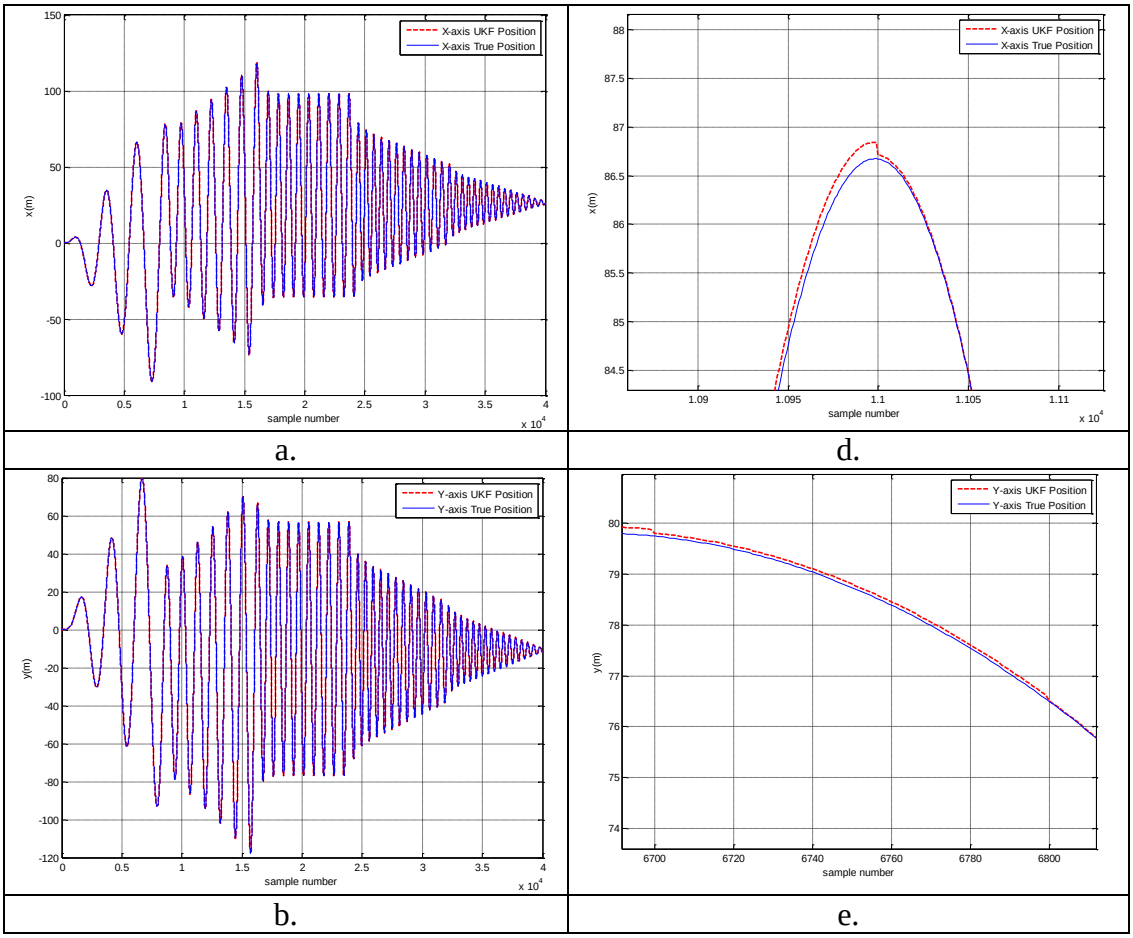

a. d.

b. e.

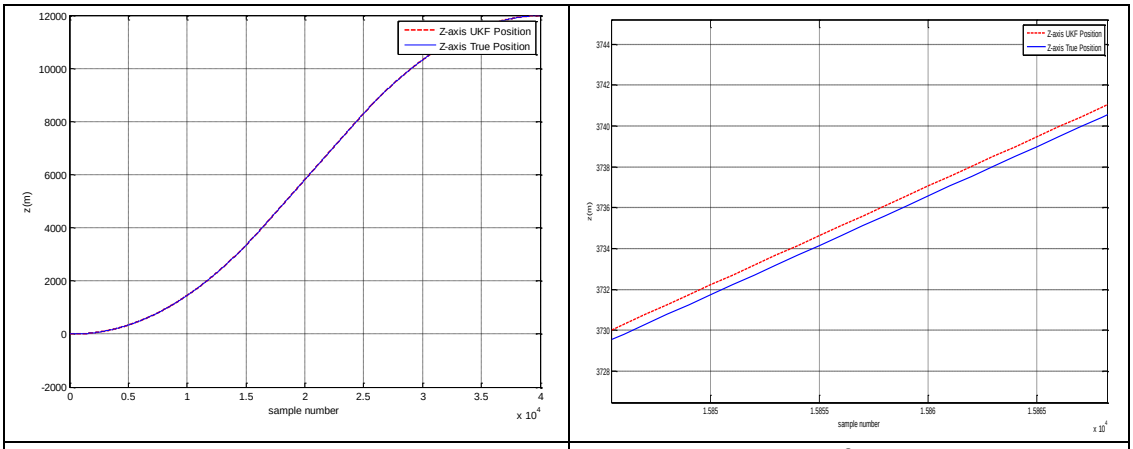

c. f.

Figure 4.10 Comparison of true navigation data and UKF results in (a) x-axis, (b) y-axis, and (c) z-axis and zoomed versions for (d) x-axis, (e) y-axis, and (f) z-axis for case 1

Table 4.3 comparatively shows RMSE results for UKF in terms of three Cartesian coordinates.

Table 4.3 RMSE results for UKF in case 1

UKF	x-axis	y-axis	z-axis
RMSE (m)	0.2532	0.2531	0.3432

As a summary, total error between estimation algorithm results and true navigation data ($\sqrt{\left((x_k - x_k^{true})^2 + \left(y_k - y_k^{true}\right)^2 + (z_k - z_k^{true})^2\right)}$) are shown in Figure 4.11.

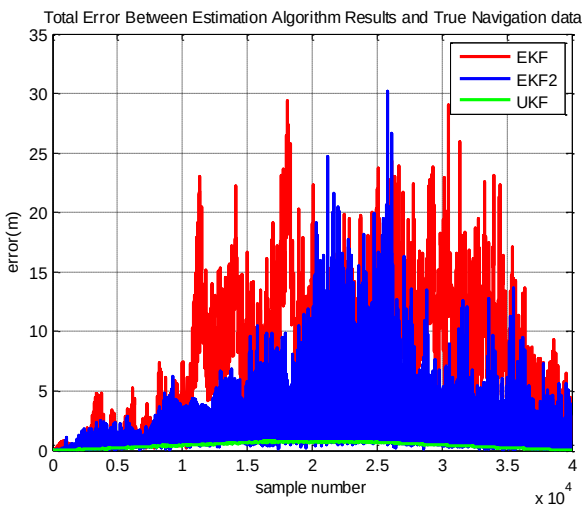

Figure 4.11 Total error between estimation algorithms and true navigation data for GPS available case

After the comparison of true navigation data and EKF, EKF2 and UKF algorithm results, the effect of changing process covariance matrix, Q_k, on each algorithm will be investigated.

4.1.3 Effect of changing process noise covariance matrix (Q_k) on EKF, EKF2, and UKF results for GPS available situation

Kalman Gain Matrix in EKF equations is $G_k = P_k^- H_k^T [H_k P_k^- H_k^T + R_k]^{-1}$ where $P_k^- = F_{k,k-1} P_{k-1} F_{k,k-1}^T + Q_{k-1}$ (Haykin 2001). Kalman gain simply means how much "updating" needs to be done at each recursive computation of the state estimate (Iyad et. al. 2016). As can be seen in that equation, the Kalman gain G_k decreases with R_k and increases with Q_k.

Indeed, the selection of Q_k and R_k effects the accuracy of UKF. If Q_k and/or R_k are too small, a biased solution might appear. On the other hand, too large Q_k and/or R_k will probably force the filter to diverge.

After the elements of Q_k are increased and decreased, the algorithms are runned again as shown in Table 4.4 (R_k is kept at the original value.). The effect of process covariance matrix Q_k on estimation results is examined and the filter divergence points are seen.

Table 4.4 The effect of changing process covariance matrix on each algorithm

Algorithms	Process Noise Covariance Matrix	RMSE Values (m)		
		x-axis	y-axis	z-axis
EKF	$0.01 \times Q$	14.0347	15.1096	5.7103
	$0.02 \times Q$	7.3112	6.3247	4.3132
	$0.3 \times Q$	5.5899	6.5039	7.7336
	Q (as used in Section 4.1.2)	5.0254	5.3760	4.7519
	$5 \times Q$	3.6744	3.5614	3.7453
	$15 \times Q$	2.5308	2.5683	2.4777
	$50 \times Q$	1.6593	1.6340	1.7787
	$75 \times Q$	2.1684	1.9627	1.5907
	$90 \times Q$	137.6562	123.6231	18.7284
	$100 \times Q$	DIVERGED		
EKF2	$0.002 \times Q$	4.1969	4.1900	3.5757
	$0.01 \times Q$	3.5608	3.8962	3.4328
	Q (as used in Section 4.1.2)	3.4533	3.6407	3.0736
	$5 \times Q$	2.1824	2.2635	1.8156
	$10 \times Q$	2.0126	2.1269	1.3258
	$15 \times Q$	27.26	13.4942	11.9818
	$20 \times Q$	DIVERGED		
UKF	$0.002 \times Q$	0.2392	0.2394	0.3463
	$0.01 \times Q$	0.2400	0.2400	0.3449
	Q (as used in Section 4.1.2)	0.2532	0.2531	0.3432
	$5 \times Q$	0.4280	0.4278	0.3449
	$15 \times Q$	0.7644	0.7640	0.3499
	$50 \times Q$	1.0206	1.0212	0.6128
	$75 \times Q$	17.4900	22.5495	16.9865
	$150 \times Q$	19.5032	23.7452	18.6314
	$200 \times Q$	42.4761	36.7382	33.8085
	$500 \times Q$	DIVERGED		

It is clear from the Table 4.4 that the effect of increasing Q_k is that the estimates follow the measurements more closely in both EKF and EKF2 for a while then

estimates begin to deviate with too large Q_k as expected and UKF starts to bias when there is an increase in Q_k.

The adaptive UKF adjusting the process noise covariance Q_k can be used to improve the performance of standart UKF for such a case.

After the effect of changing process covariance matrix is investigated, the effect of GPS outage on each algorithm will also be investigated.

4.1.4 EKF, EKF2, and UKF results for GPS outage situation

GPS is undefended to jamming and signal interference. When the GPS outage is considered, accuracy of the state estimate is decreasing with time, depending on the duration of measurement outage.

Two different scenarios for the INS/GPS integration process in GPS outage situation are constituted as follows:

Scenario 1: Comparison of the algorithm results among 2, 5 and 10 seconds of GPS outage.

As shown from Table 4.5, UKF has the best performance with respect to EKF and EKF2 when GPS signal is lost. If the duration of GPS outage is extended, UKF goes on estimating the positions after a while with lower error than EKF. Also, RMSE values of EKF2 in longer GPS outage duration become higher than the other algorithms. EKF2 can not work good in harsh environment condition.

Table 4.5 The effect of increasing GPS outage duration on each algorithm

Algorithms	GPS Outage Duration	RMSE Values (m)		
		x-axis	y-axis	z-axis
EKF	2 sec.	4.7860	3.8489	4.1882
	5 sec.	5.9590	5.0765	7.0669
	10 sec.	7.7220	7.3070	37.2618
EKF2	2 sec.	1.2732	1.2508	1.6261
	5 sec.	14.1835	14.8741	18.9284
	10 sec.	341.0404	273.4587	191.9014
UKF	2 sec.	0.2538	0.2539	0.3455
	5 sec.	0.2861	0.2597	0.3969
	10 sec.	0.6755	0.7516	1.1165

Error between true navigation data and EKF, EKF2 and UKF results for three Cartesian coordinates are comparatively shown in Figure 4.12-4.14 respectively.

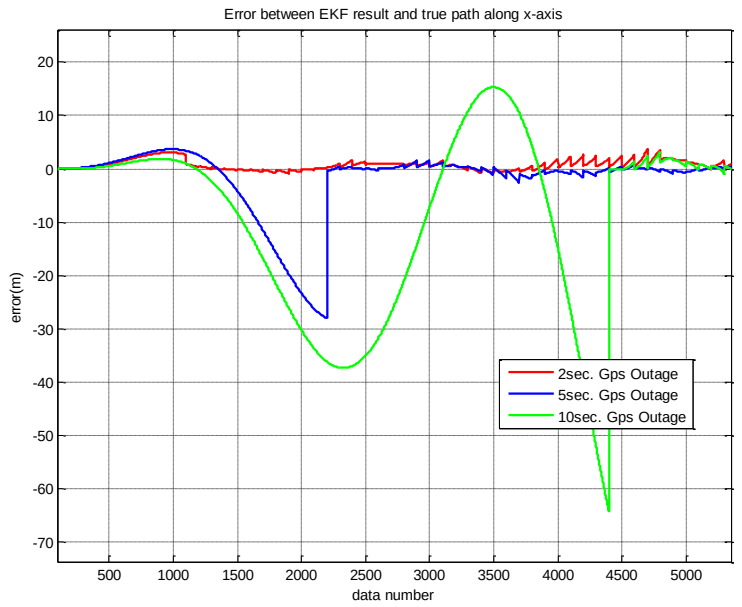

a.

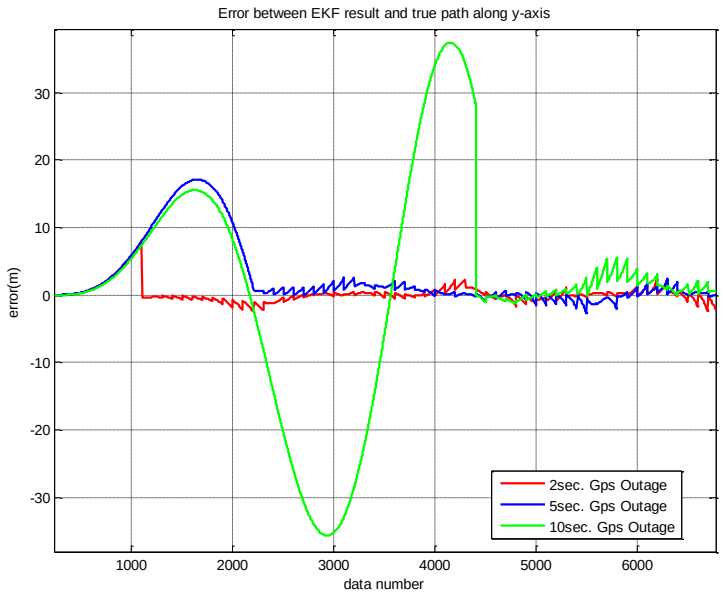

b.

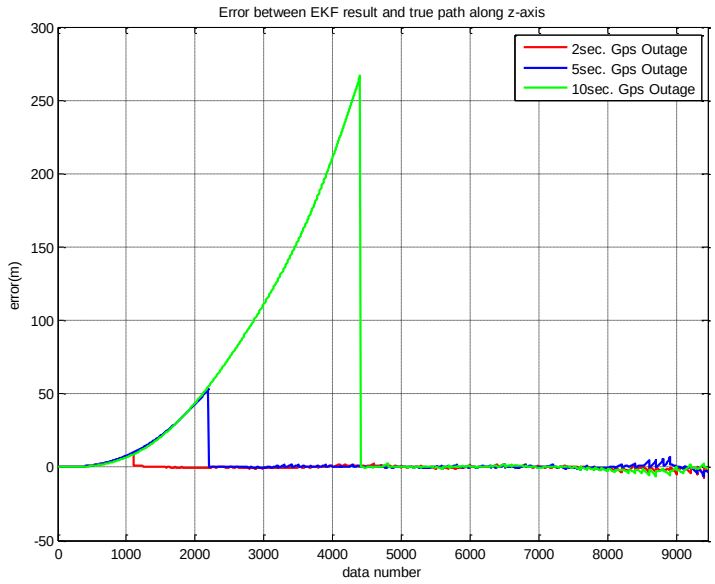

c.

Figure 4.12 Error between true navigation data and EKF results in (a) x-axis, (b) y-axis, and (c) z-axis for 2, 5 and 10 seconds GPS outage

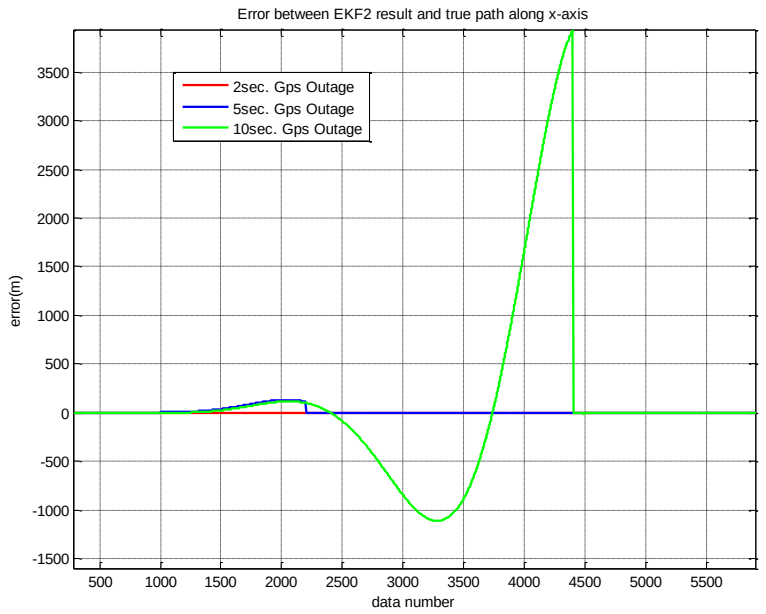
Error between EKF2 result and true path along x-axis
2sec. Gps Outage
5sec. Gps Outage
10sec. Gps Outage
error(m)
data number
3500
3000
2500
2000
1500
1000
500
0
-500
-1000
-1500
500
1000
1500
2000
2500
3000
3500
4000
4500
5000
5500

a.

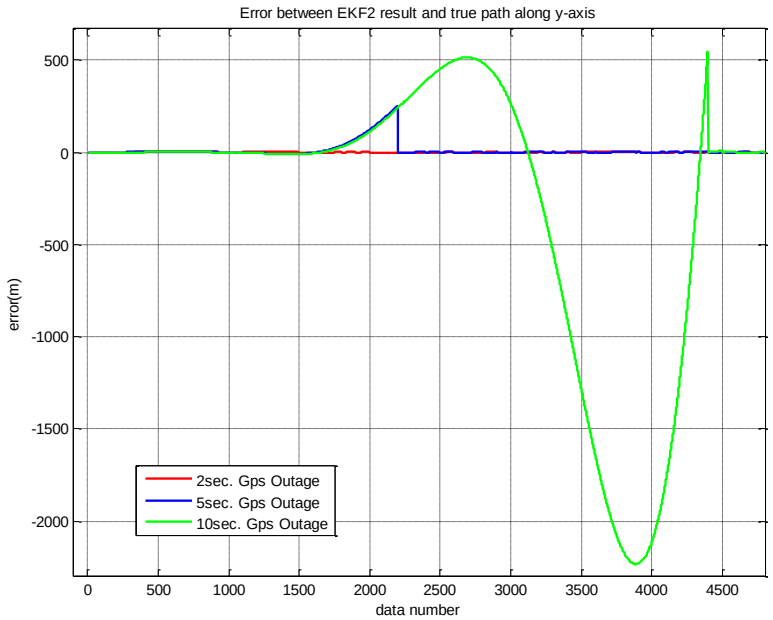
Error between EKF2 result and true path along y-axis
2sec. Gps Outage
5sec. Gps Outage
10sec. Gps Outage
error(m)
data number
500
0
-500
-1000
-1500
-2000
0
500
1000
1500
2000
2500
3000
3500
4000
4500

b.

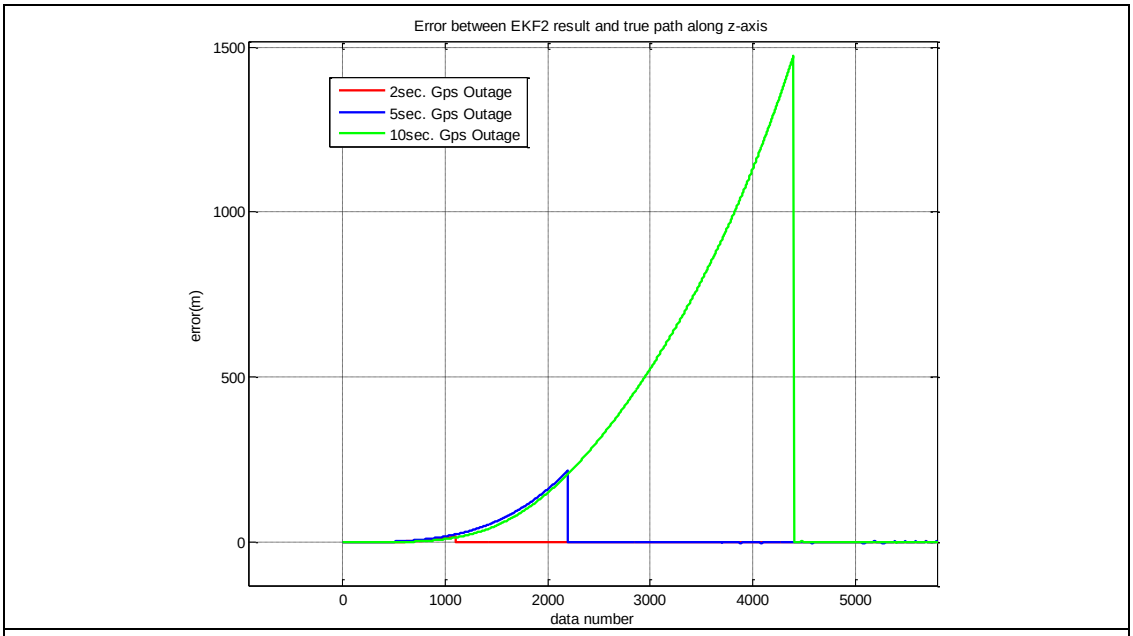

c.

Figure 4.13 Error between true navigation data and EKF2 results in (a) x-axis, (b) y-axis, and (c) z-axis for 2, 5 and 10 seconds GPS outage

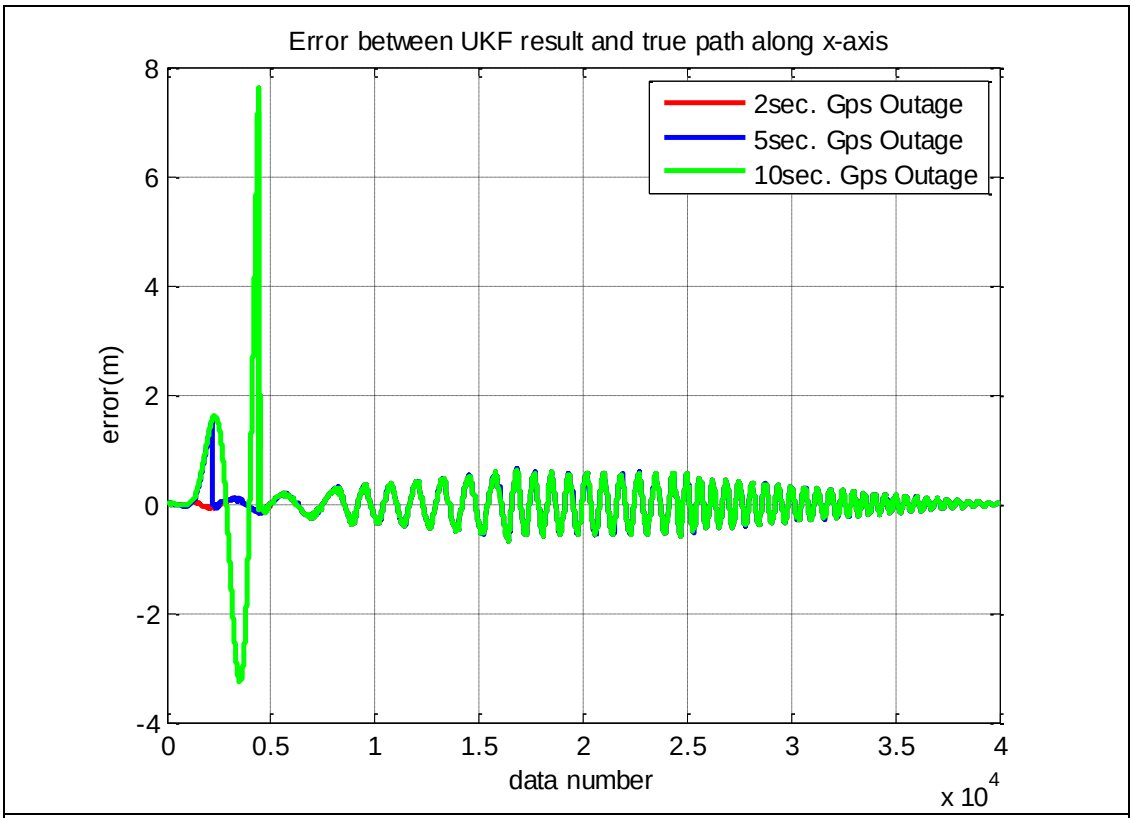

a.

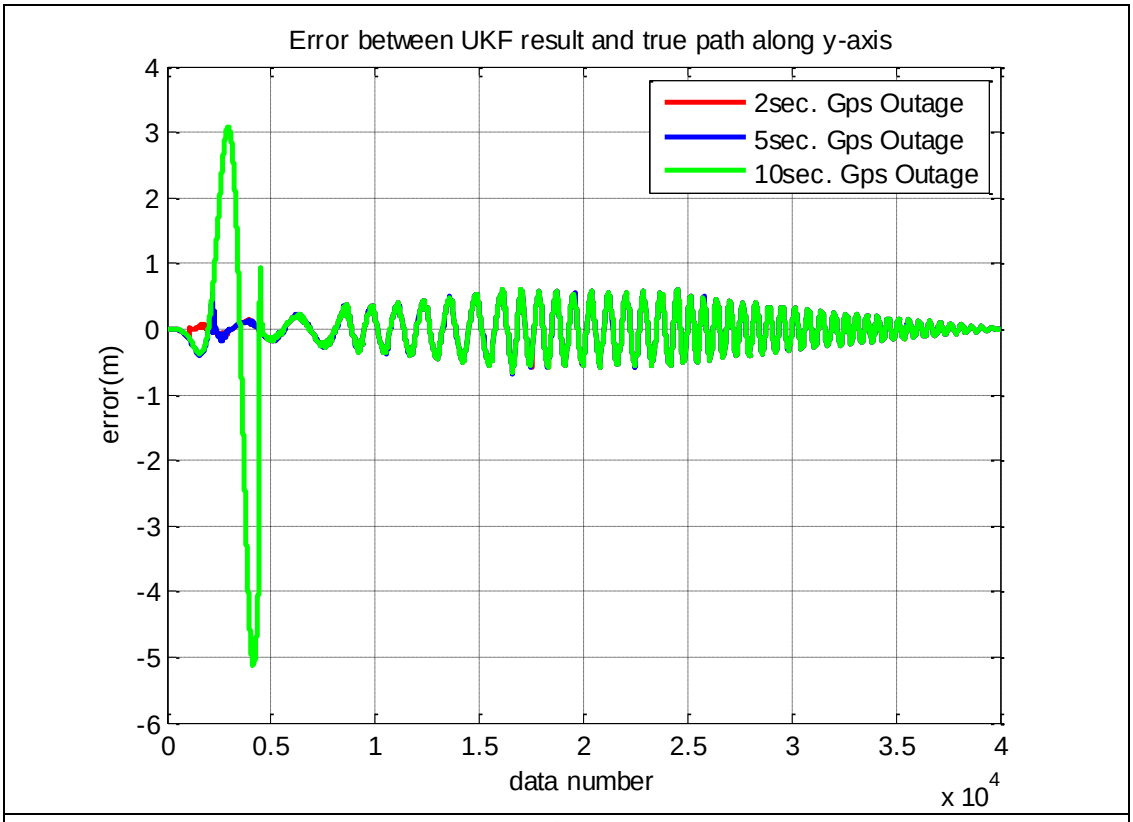

b.

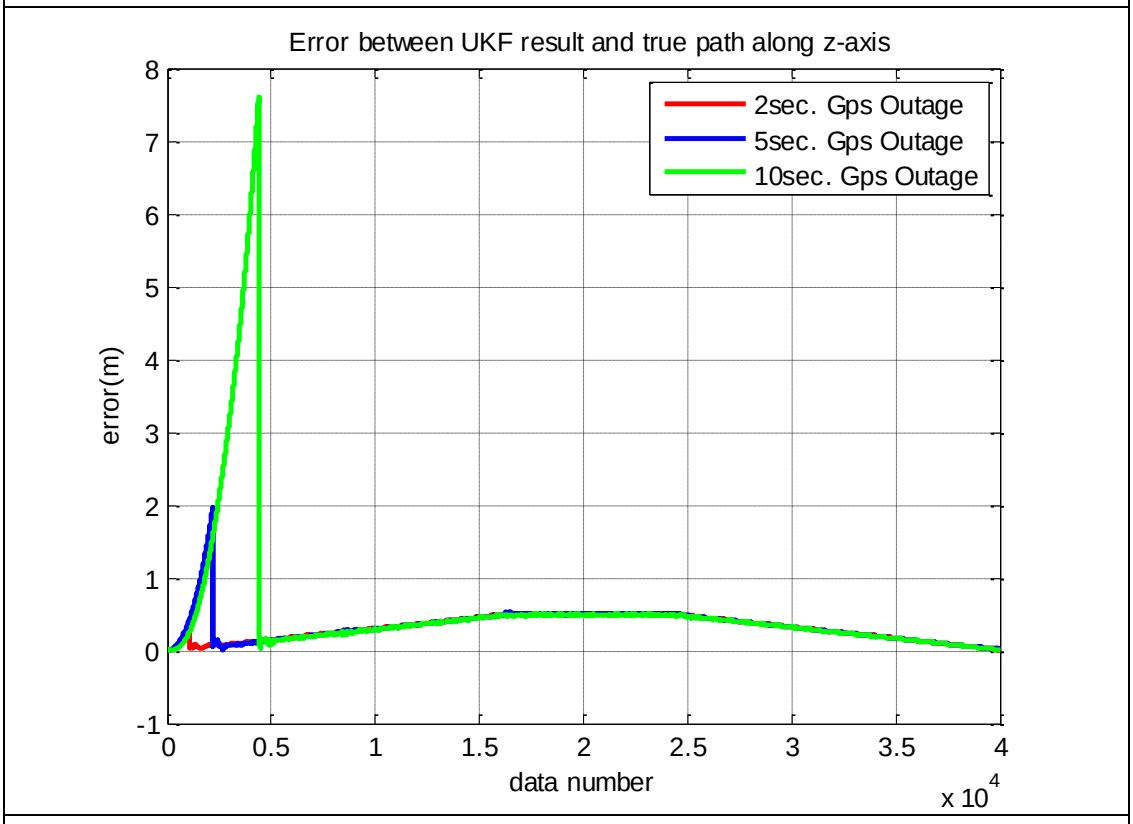

c.

Figure 4.14 Error between true navigation data and UKF results in (a) x-axis, (b) y-axis, and (c) z-axis for 2, 5 and 10 seconds GPS outage

As seen from Figure 4.12-4.14, error between true navigation data and estimates are increasing as the duration of GPS outage extends. By looking at the error levels, it can be said that UKF makes the best estimation in GPS outage situation with respect to EKF and EKF2. Moreover, although EKF2 introduces an increase in the performance according to standart EKF without GPS interruption, it is not robust to GPS outages.

Also, total errors between true navigation data and estimation algorithm results ($\sqrt{\left((x_k - x_k^{true})^2 + \left(y_k - y_k^{true}\right)^2 + (z_k - z_k^{true})^2\right)}$) for 2, 5 and 10 seconds GPS outage are shown in Figure 4.15 (a-c).

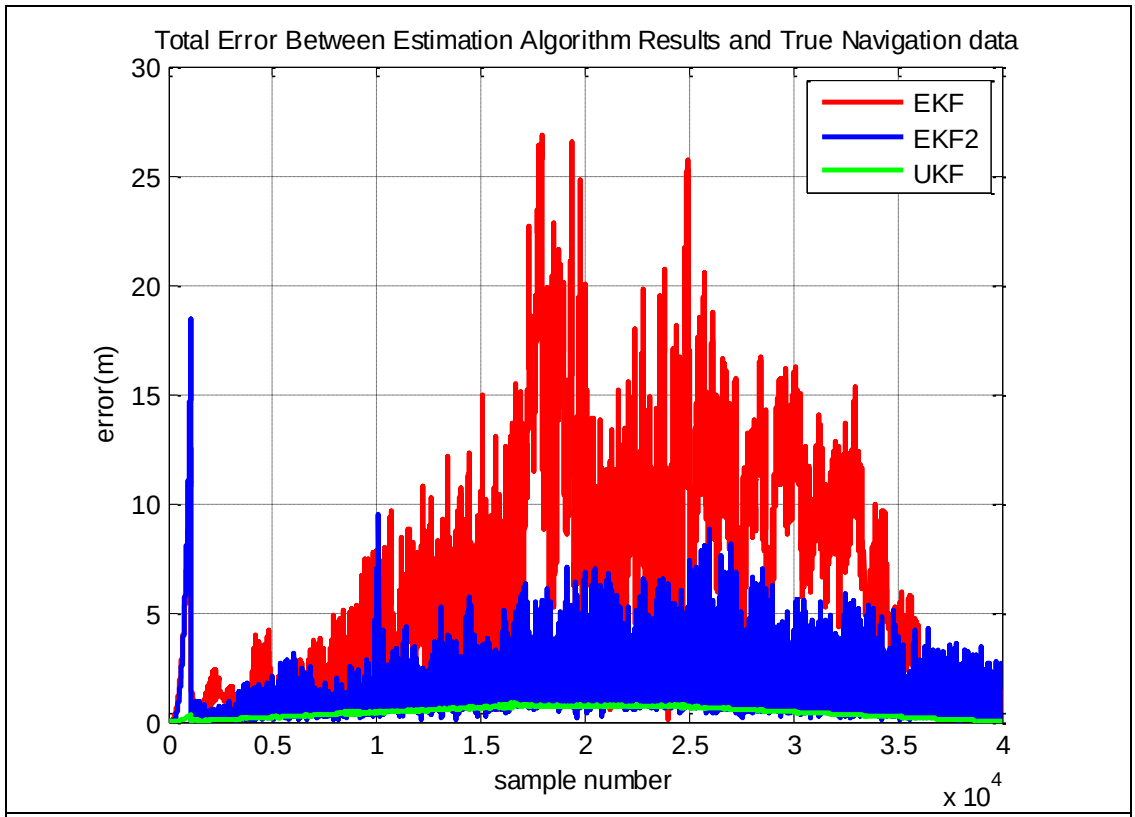

a.

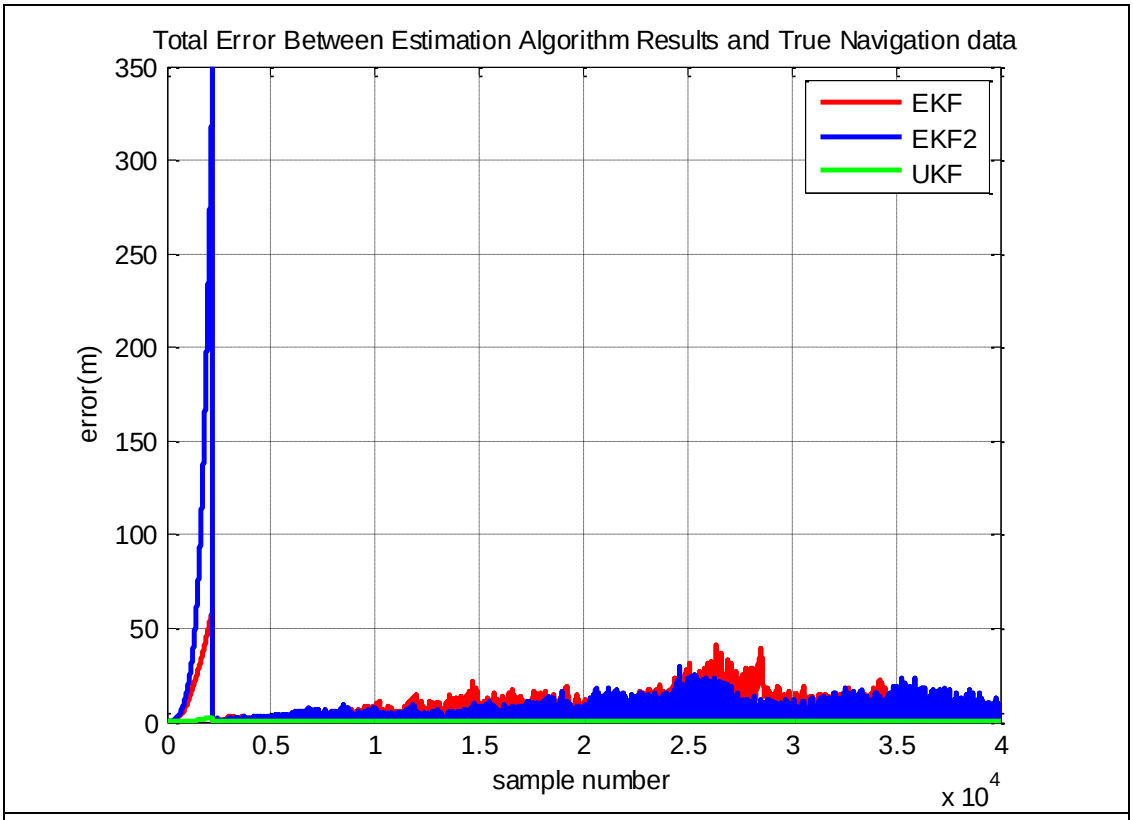

b.

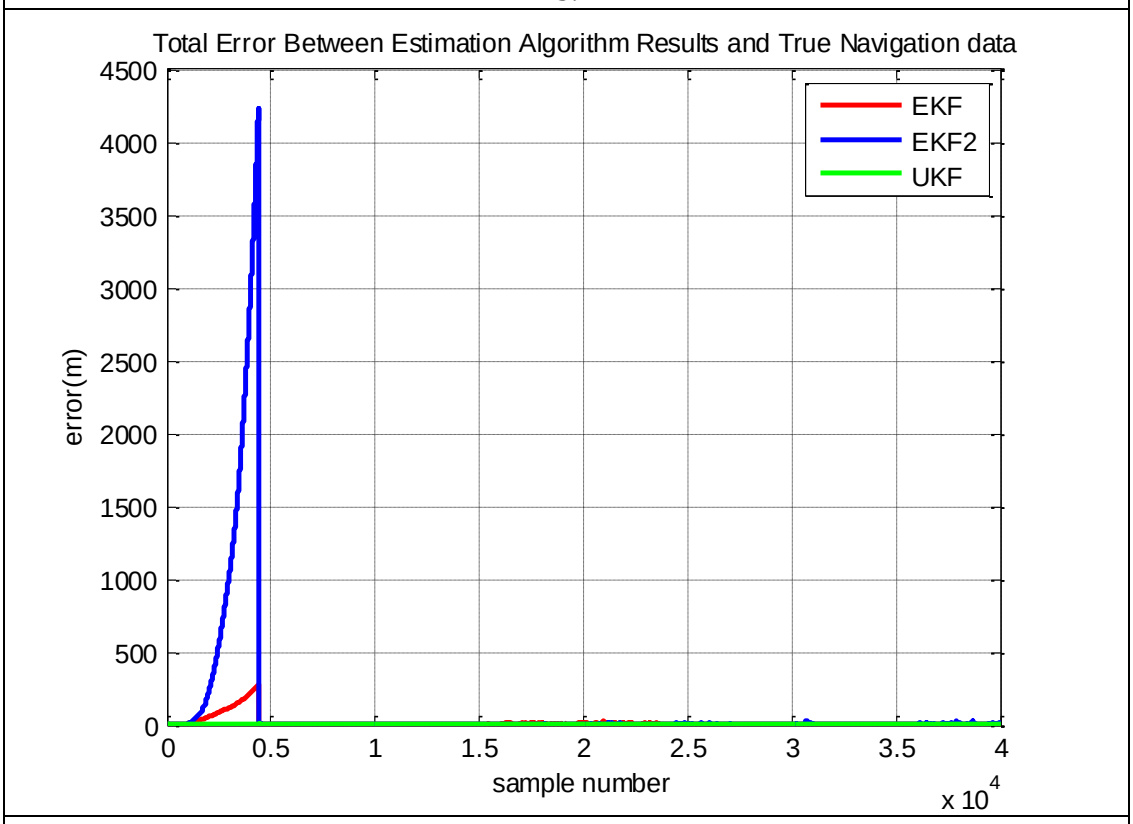

c.

Figure 4.15 Total error between true navigation data and estimation algorithm results for GPS outage durations (a) 2 seconds, (b) 5 seconds, and (c) 10 seconds

Scenario 2: Investigation of effect of GPS outage for different time intervals that GPS is available or not (ON or OFF).

The time intervals that GPS is available in Table 4.6 and Table 4.8 causes RMSE values for each algorithm as shown in Table 4.7 and Table 4.9 respectively. Sample numbers of navigation data corresponding to moments when the GPS signal is interrupted are also shown in Table 4.6 and Table 4.8.

Table 4.6 GPS outage periods in the trajectory

	GPS Availability					
	OFF	**ON**	**OFF**	**ON**	**OFF**	**ON**
Time Periods (seconds)	0-10	10-35	35-40	40-65	65-70	70-100
Sample Number	0-4000	4000-14000	14000-16000	16000-26000	26000-28000	28000-40000

Table 4.7 RMSE results for each algorithm

Algorithms	**RMSE Values (m)**		
	x-axis	**y-axis**	**z-axis**
EKF	384.0592	345.5416	60.6752
EKF2	1306.4	699.7230	432.0053
UKF	0.6689	1.0000	1.3550

Error between true navigation data and EKF, EKF2 and UKF results for three Cartesian coordinates are comparatively shown in Figure 4.16, Figure 4.17 and Figure 4.18 respectively.

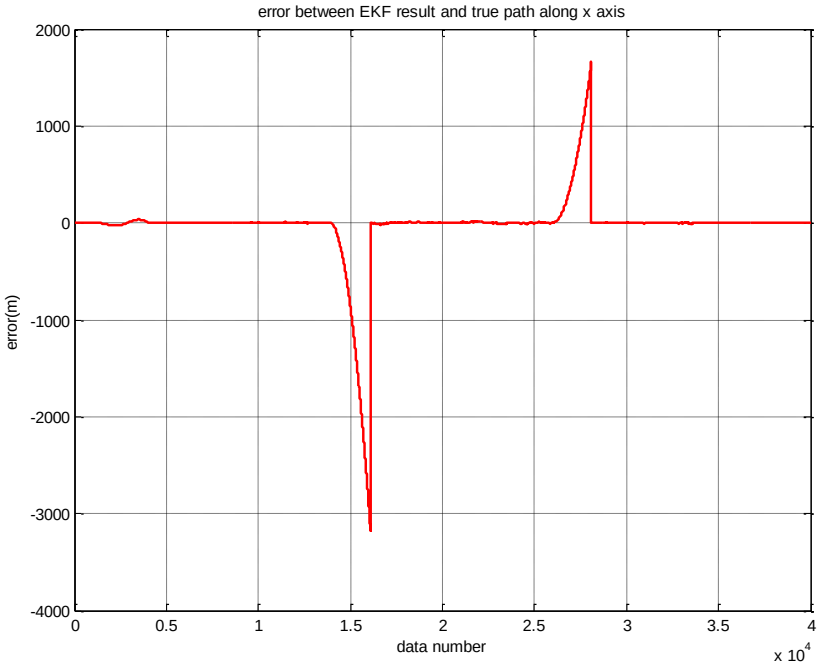
error between EKF result and true path along x axis
2000
1000
0
-1000
-2000
-3000
-4000
error(m)
0
0.5
1
1.5
2
2.5
3
3.5
4
data number
x 10^4

a.

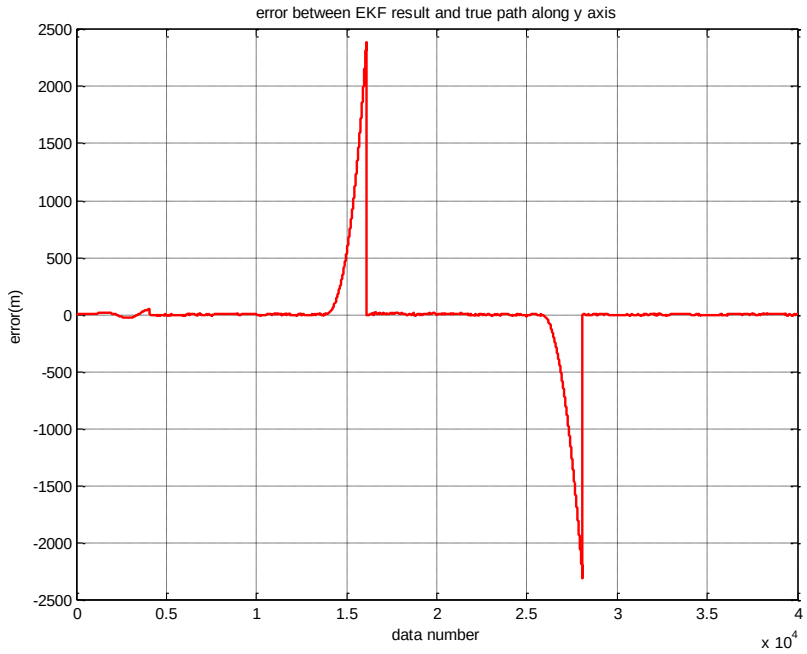
error between EKF result and true path along y axis
2500
2000
1500
1000
500
0
-500
-1000
-1500
-2000
-2500
error(m)
0
0.5
1
1.5
2
2.5
3
3.5
4
data number
x 10^4

b.

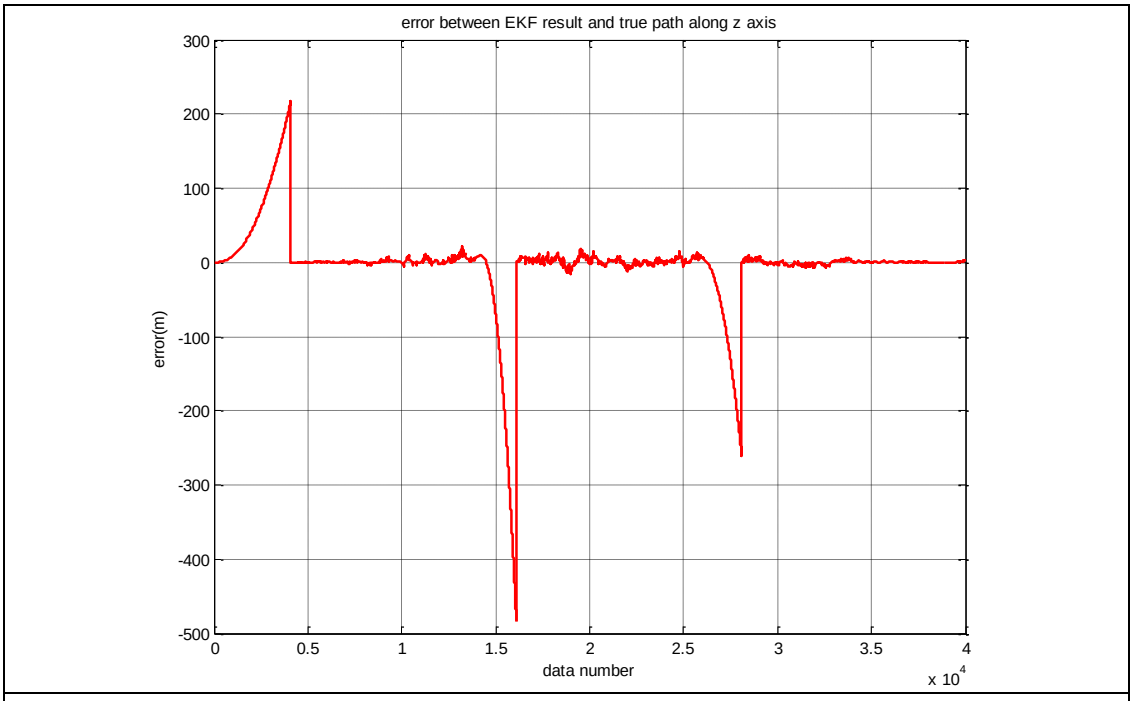

c.

Figure 4.16 Error between EKF results and true navigation data along (a) x-axis, (b) y-axis, and (c) z-axis while GPS outage periods in the trajectory in Table 4.6 are applied

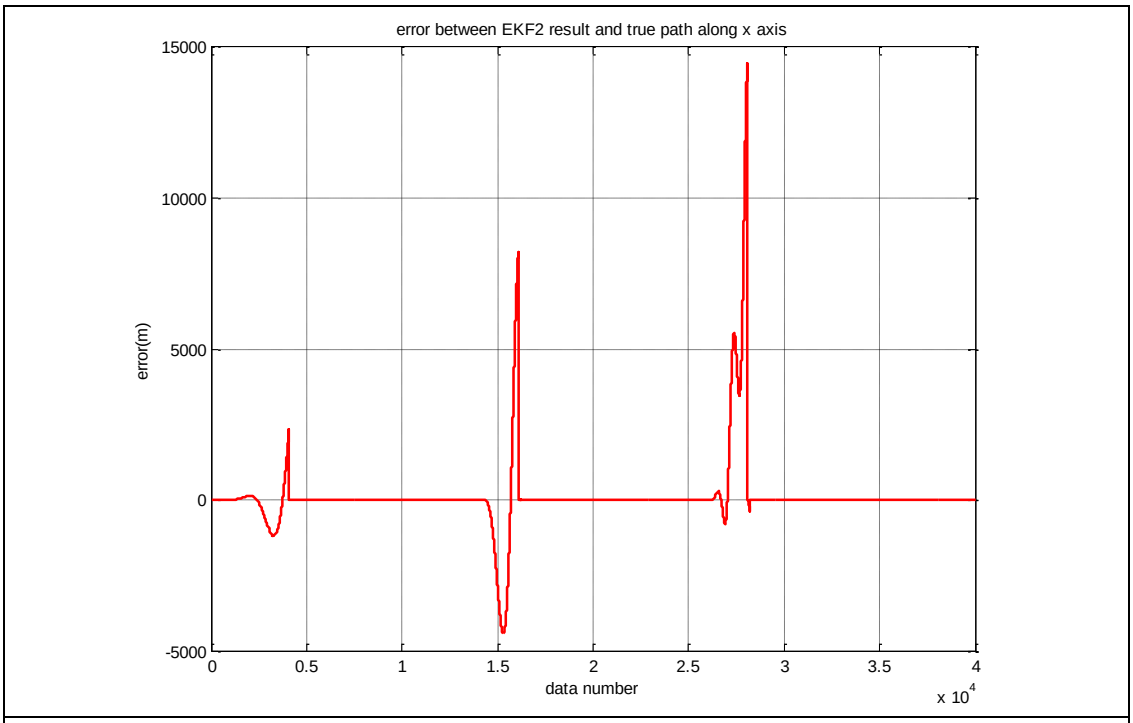

a.

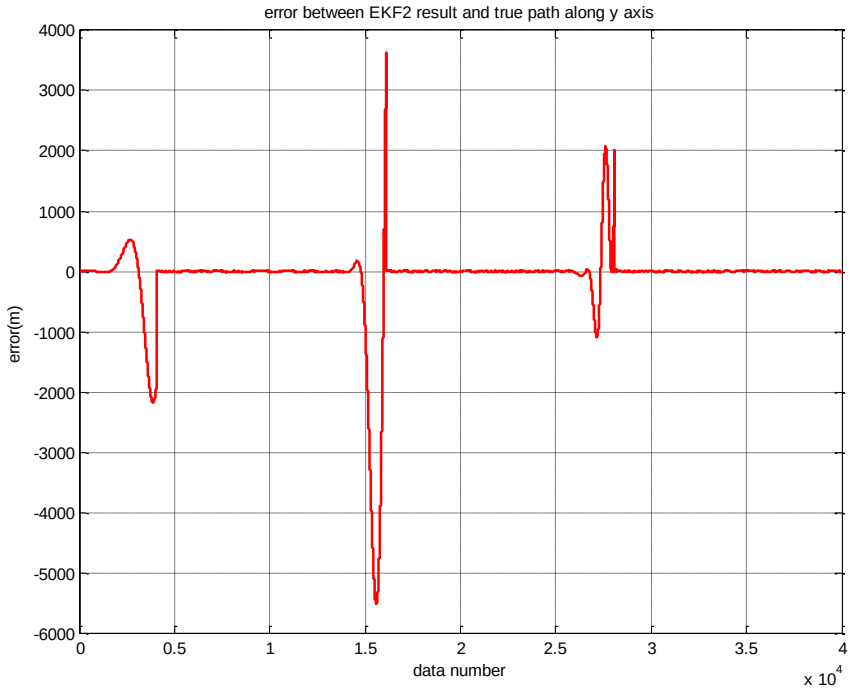

b.

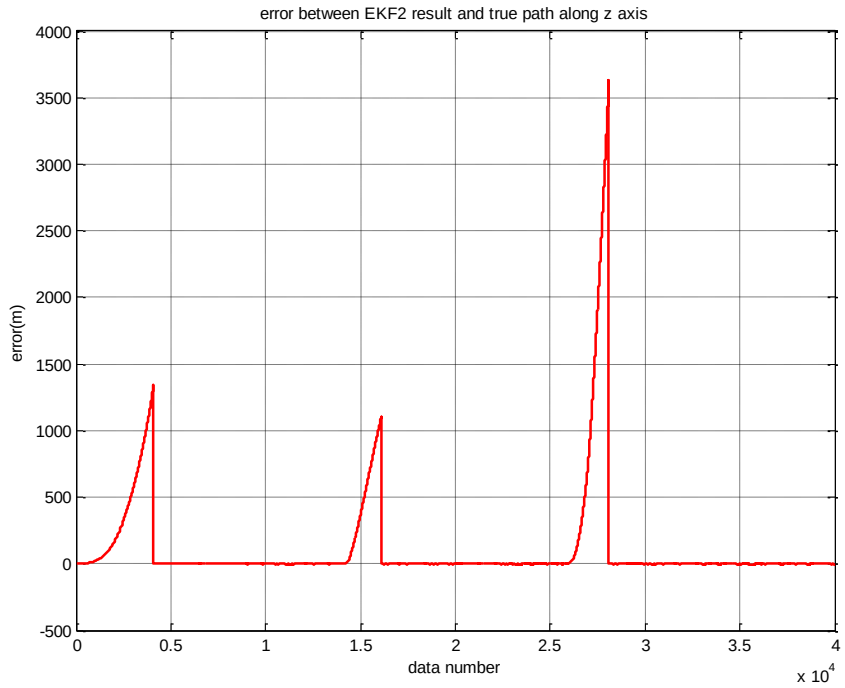

c.

Figure 4.17 Error between EKF2 results and true navigation data along (a) x-axis, (b) y-axis, and (c) z-axis while GPS outage periods in the trajectory in Table 4.6 are applied

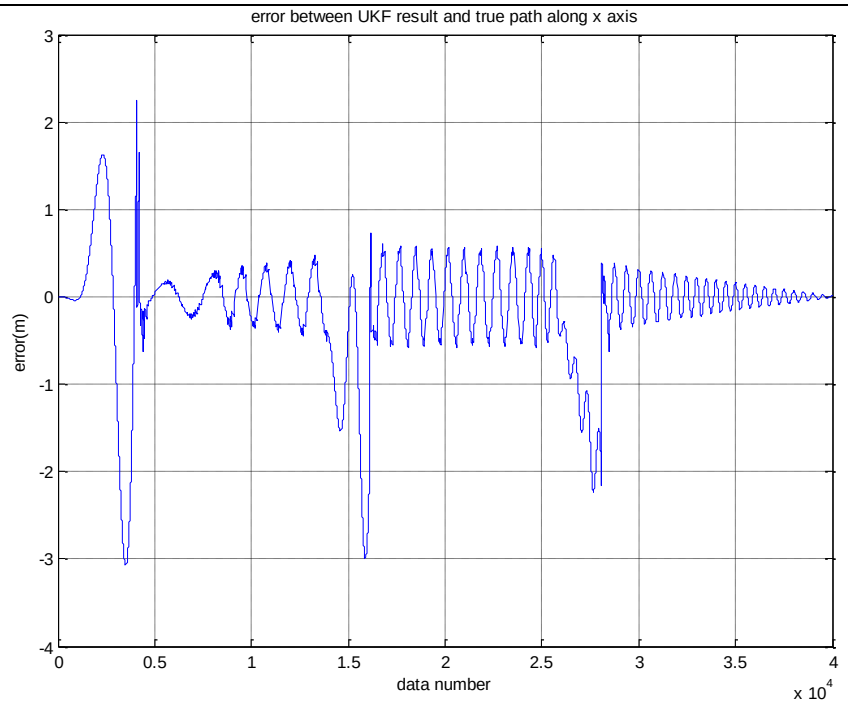
error between UKF result and true path along x axis
error(m)
data number
x 10^4
3
2
1
0
-1
-2
-3
-4
0
0.5
1
1.5
2
2.5
3
3.5
4

a.

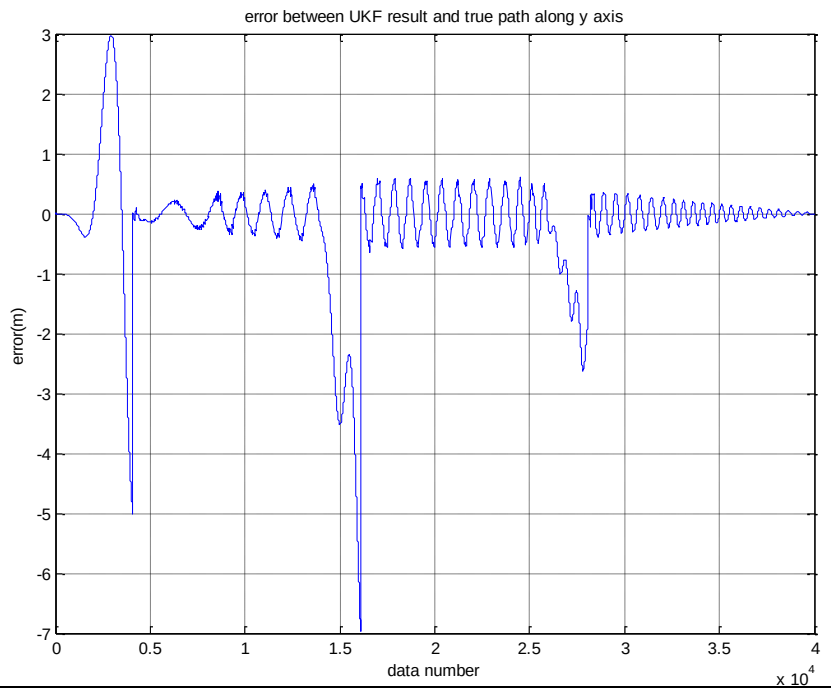
error between UKF result and true path along y axis
error(m)
data number
x 10^4
3
2
1
0
-1
-2
-3
-4
-5
-6
-7
0
0.5
1
1.5
2
2.5
3
3.5
4

b.

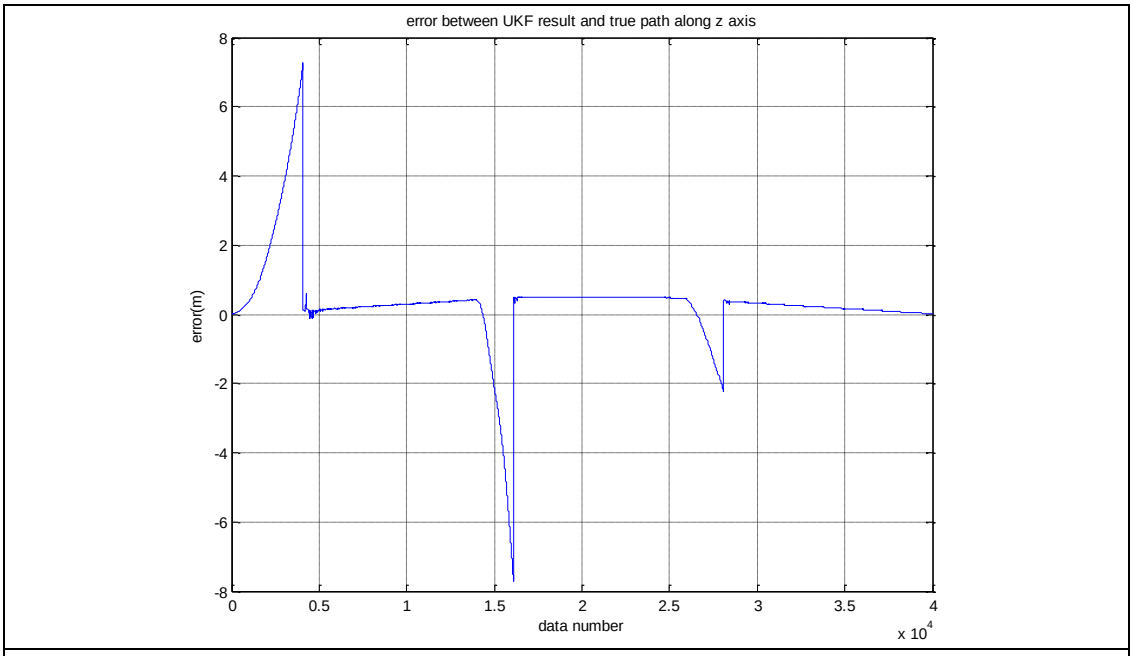

c.

Figure 4.18 Error between UKF results and true navigation data along (a) x-axis, (b) y-axis, and (c) z-axis while GPS outage periods in the trajectory in Table 4.6 are applied

Table 4.8 GPS outage periods in the trajectory

	GPS Availability					
	OFF	**ON**	**OFF**	**ON**	**OFF**	**ON**
Time Periods (seconds)	0-10	10-20	20-50	50-60	60-80	80-100
Sample Number	0-4000	4000-8000	8000-20000	20000-24000	24000-32000	32000-40000

Table 4.9 RMSE results for each algorithm

Algorithms	**RMSE Values (m)**		
	x-axis	**y-axis**	**z-axis**
EKF	24947	8462.2	6147.2
EKF2	DIVERGED		
UKF	16.1370	8.6851	80.8991

Error between true navigation data and EKF and UKF results for three Cartesian coordinates are comparatively shown in Figure 4.19 and Figure 4.20 respectively.

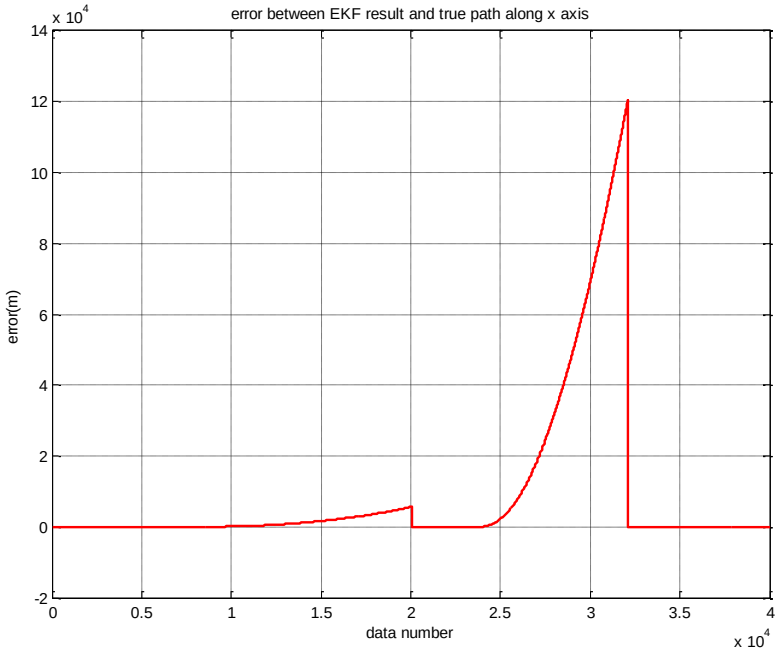

a.

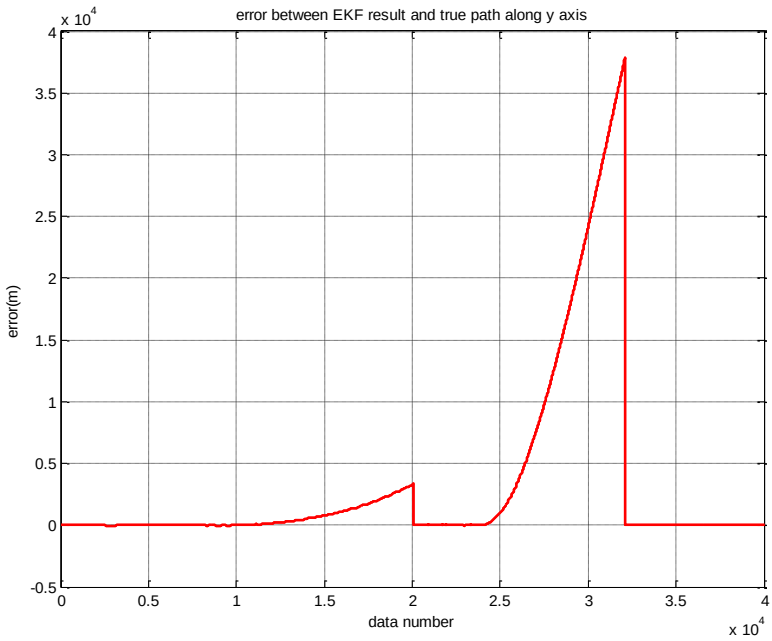

b.

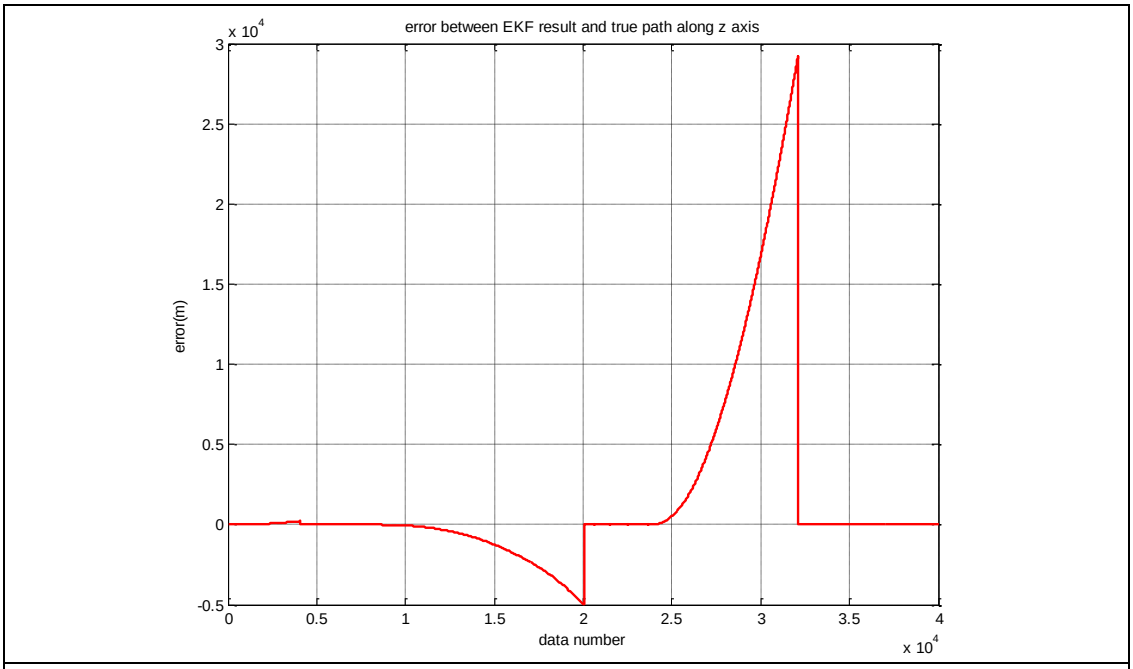

c.

Figure 4.19 Error between EKF results and true navigation data along (a) x-axis, (b) y-axis, and (c) z-axis while GPS outage periods in the trajectory in Table 4.8 are applied

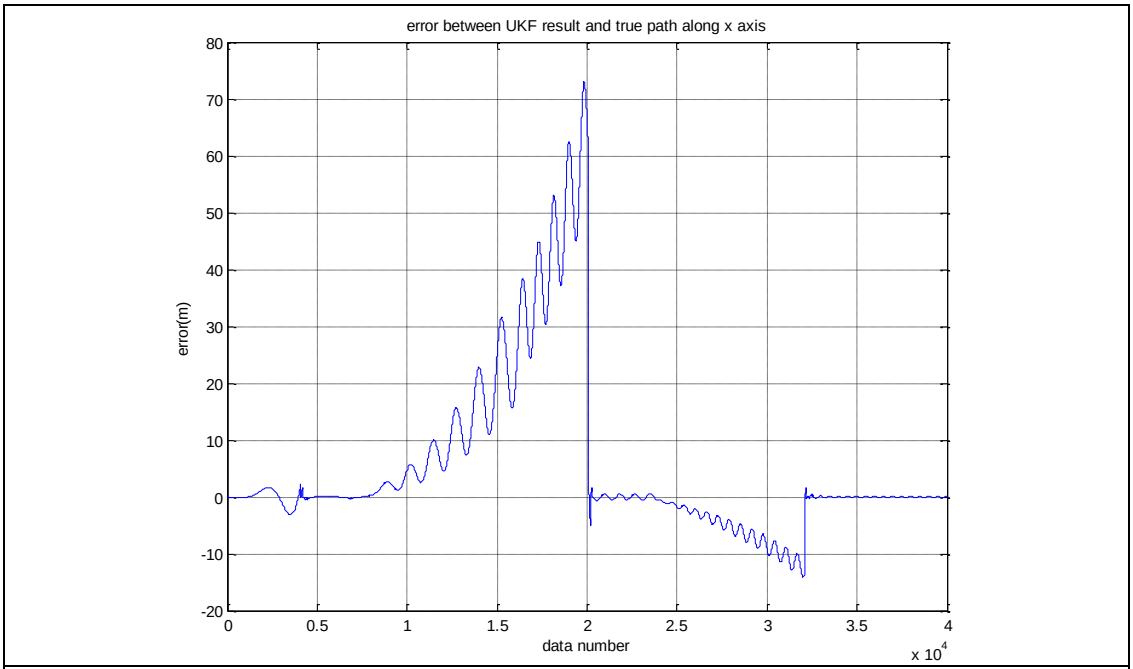

a.

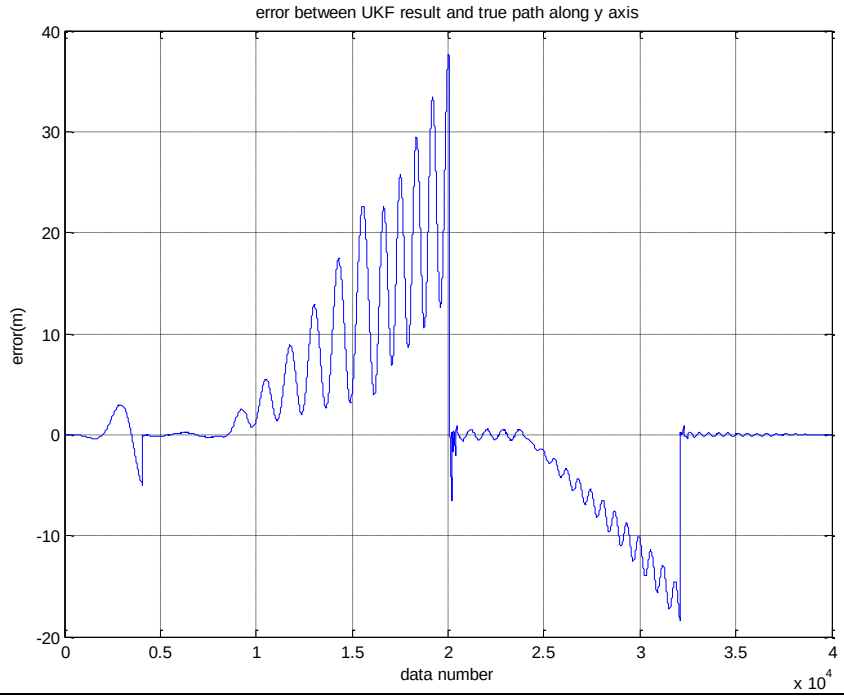

b.

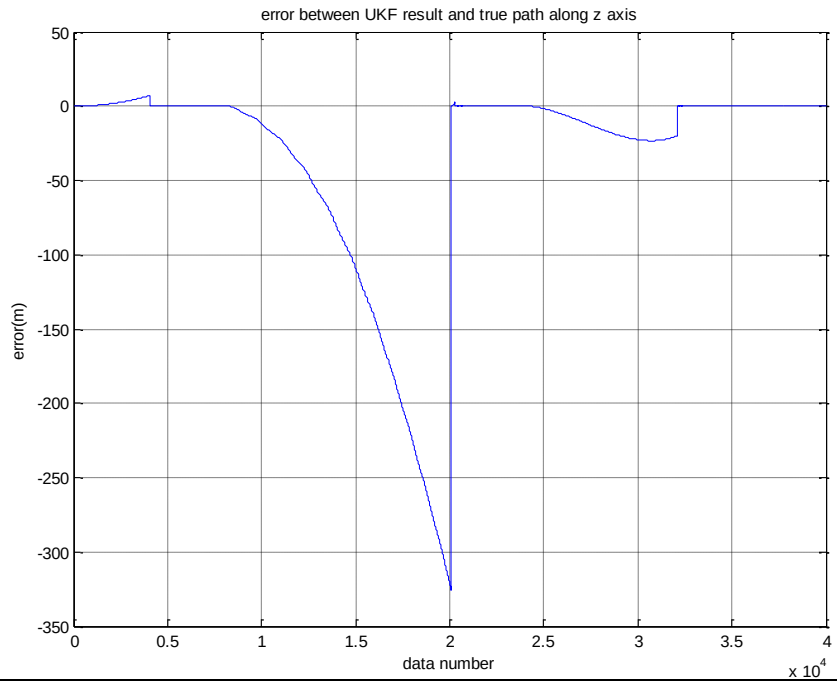

c.

Figure 4.20 Error between UKF results and true navigation data along (a) x-axis, (b) y-axis, and (c) z-axis while GPS outage periods in the trajectory in Table 4.8 are applied

When there are multiple GPS outages, the performance of the filters depends on the time interval of GPS outages. As shown from the Table 4.7 and Table 4.9, increasing

the length of the GPS outages (as in Table 4.8) forces EKF2 to diverge while RMSE values in EKF and UKF increases. However, UKF has the best performance in all cases.

Also, when Figure 4.16-4.20 are examined, it is clearly seen that the points at which the erroneous points correspond to the range where the GPS signal is off. When the GPS signal is on again, UKF can continue to make estimations by correcting the error more quickly than EKF and EKF2.

Another situation can be the one that GPS signal can be corrupted by noise or another interference, which is called “outlier”.

4.1.5 EKF, EKF2, and UKF results for GPS outlier situation

In this section, the effect of GPS outlier on EKF, EKF2, and UKF will be examined by using trajectory of navigation data in Section 4.1.1. The time in seconds belong to GPS outlier data and related noise standart deviations are shown in Table 4.10.

True navigation data and EKF, EKF2 and UKF results for three Cartesian coordinates are comparatively shown in Figure 4.21 (a-c)-4.23 (a-c) respectively. Figure 4.21 (d-f)-4.23 (d-f) also show zoomed versions of Figure 4.21 (a-c)-4.23 (a-c) respectively when standart deviation of GPS outlier is 31.62 m.

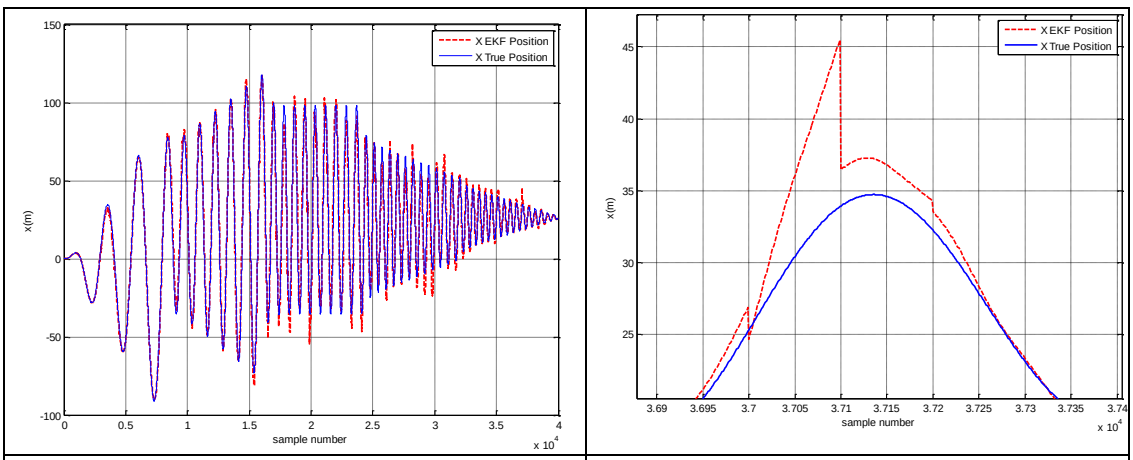

a.	d.

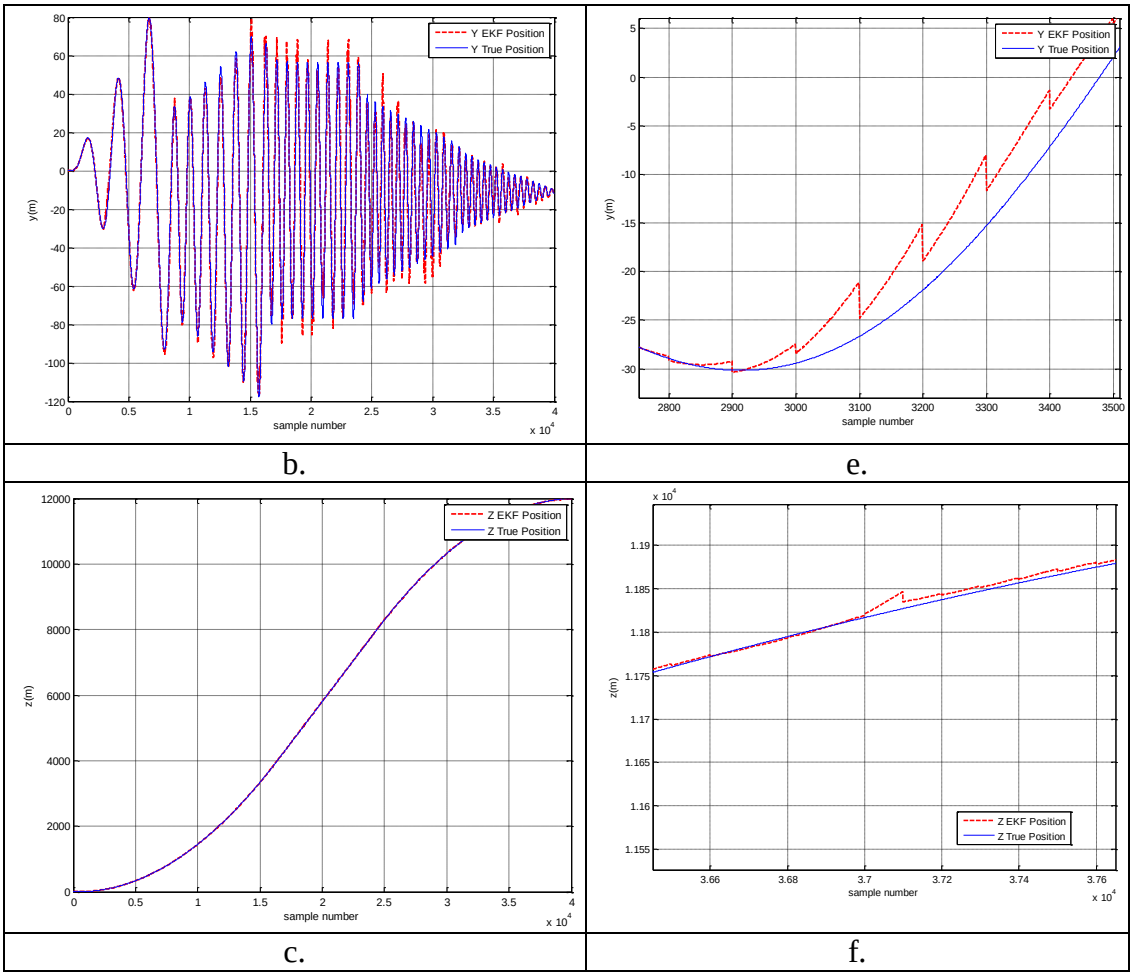

Figure 4.21 Comparison of true navigation data and EKF results in (a) x-axis, (b) y-axis, and (c) z-axis and zoomed versions for (d) x-axis, (e) y-axis, and (f) z-axis

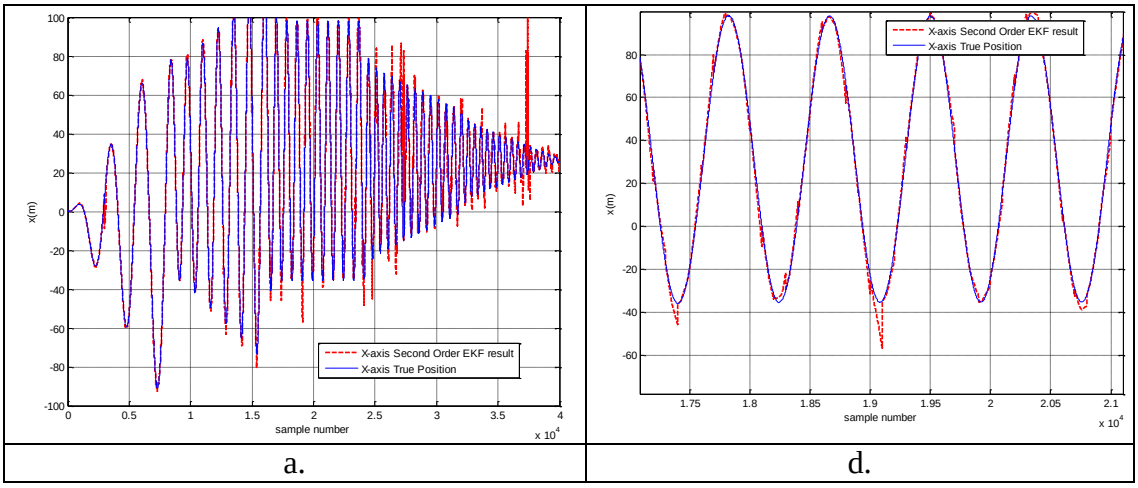

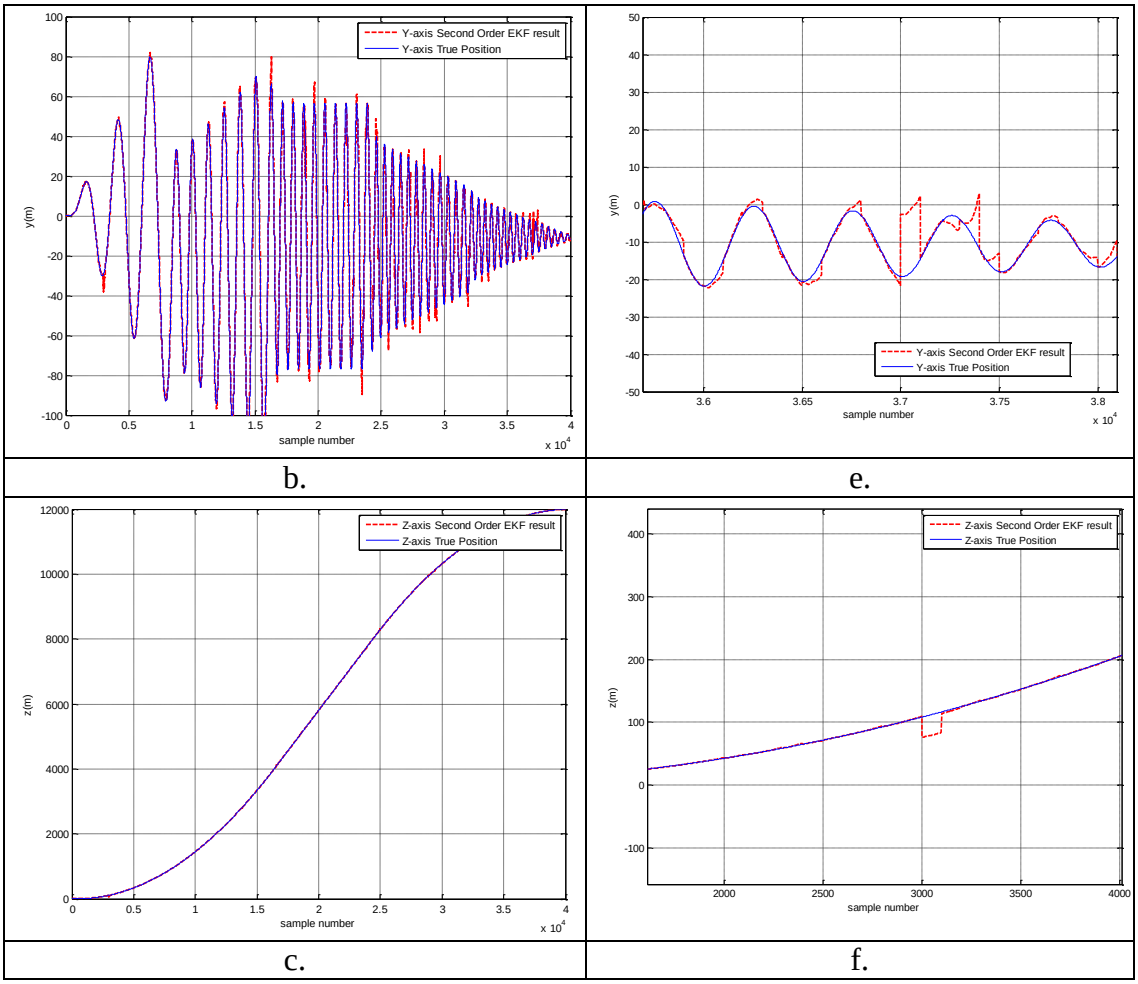

Figure 4.22 Comparison of true navigation data and EKF2 results in (a) x-axis, (b) y-axis, and (c) z-axis and zoomed versions for (d) x-axis, (e) y-axis, and (f) z-axis

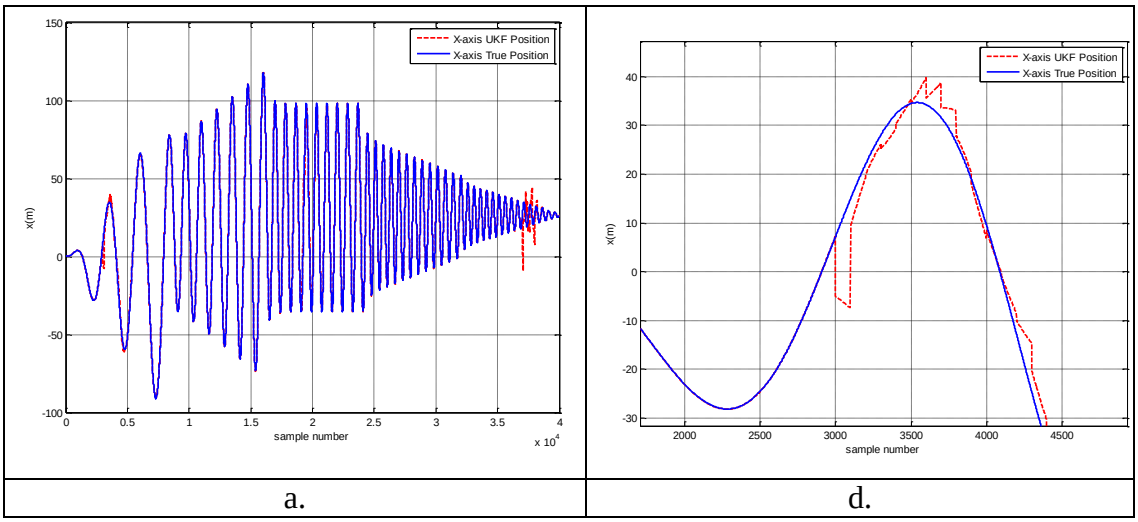

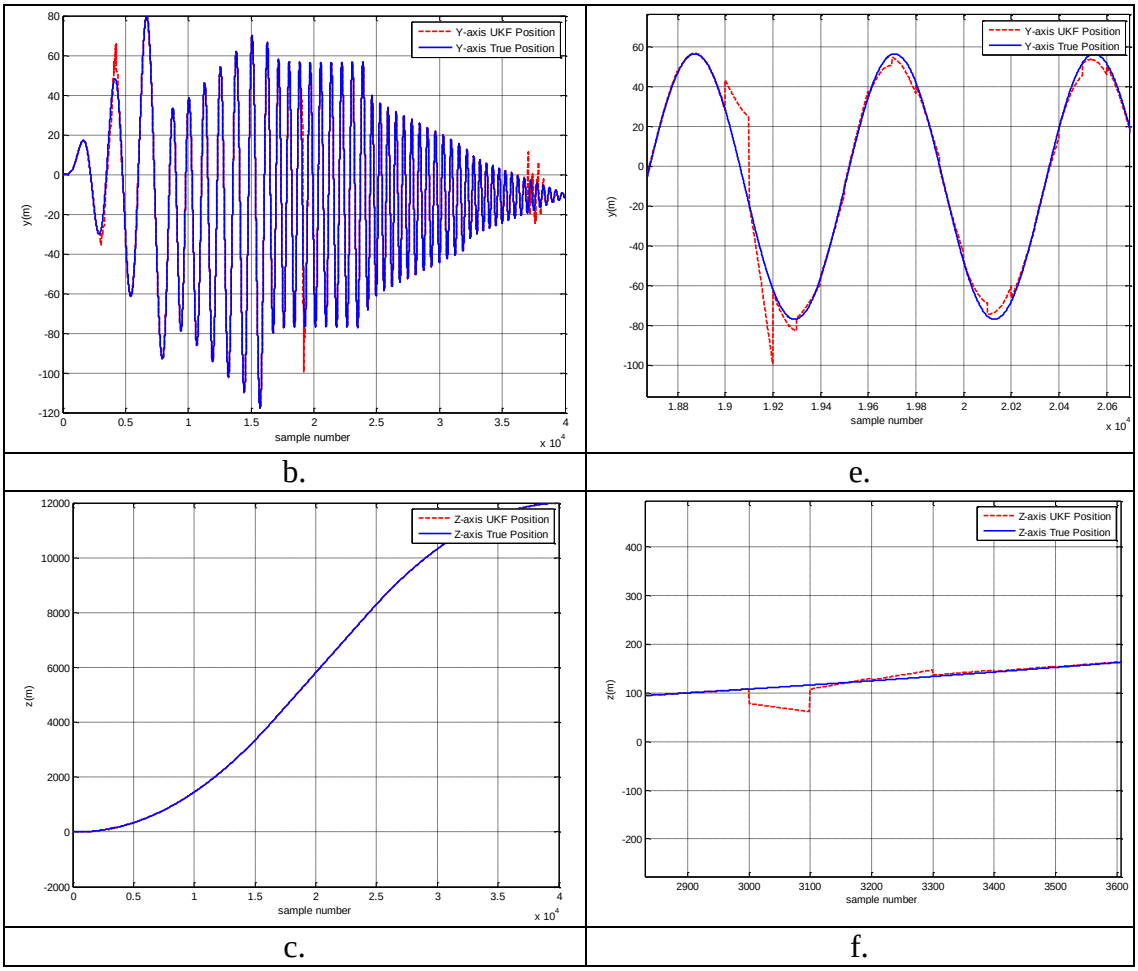

Figure 4.23 Comparison of true navigation data and UKF results in (a) x-axis, (b) y-axis, and (c) z-axis and zoomed versions for (d) x-axis, (e) y-axis, and (f) z-axis

Total error between estimation algorithm results and true navigation data ($\sqrt{\left(\left(x_k - x_k^{true}\right)^2 + \left(y_k - y_k^{true}\right)^2 + \left(z_k - z_k^{true}\right)^2\right)}$) when standart deviation of GPS outlier is 31.62 m is shown in Figure 4.24

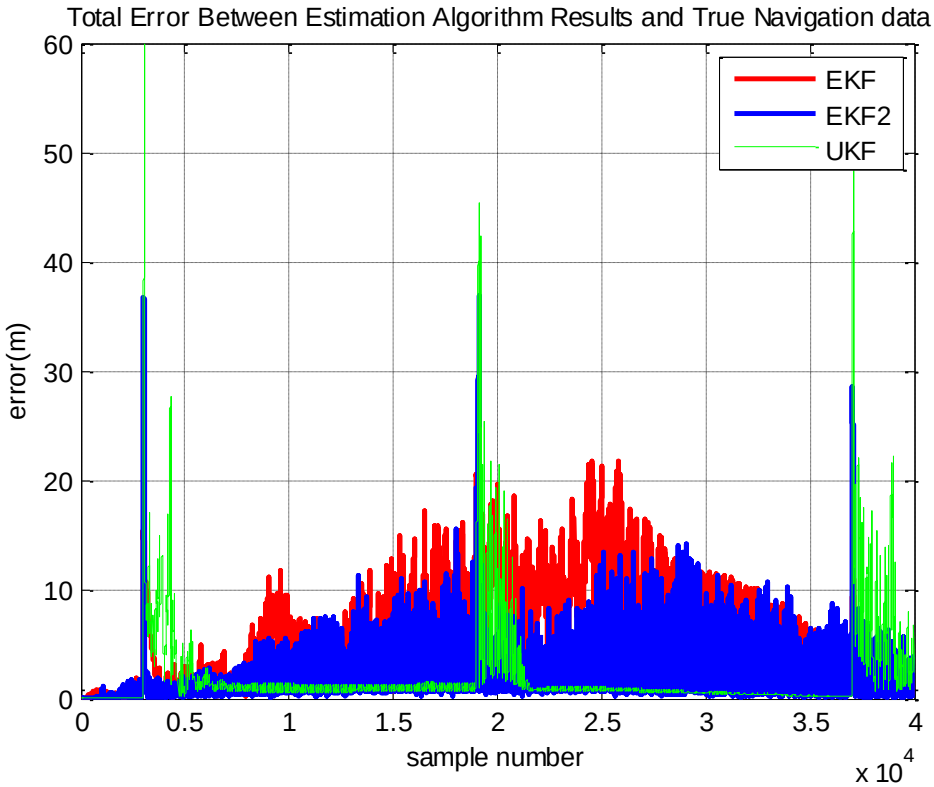

Figure 4.24 Total error between estimation algorithm results and true navigation data when GPS outlier standart deviation is 31.62 m.

Also, true navigation data and EKF and UKF results for three Cartesian coordinates are comparatively shown in Figure 4.25 and Figure 4.26 respectively. Figure 4.25 (d-f) and Figure 4.26 (d-f) also show the error between true navigation data and EKF and UKF results respectively when standart deviation of GPS outlier is 100 m.

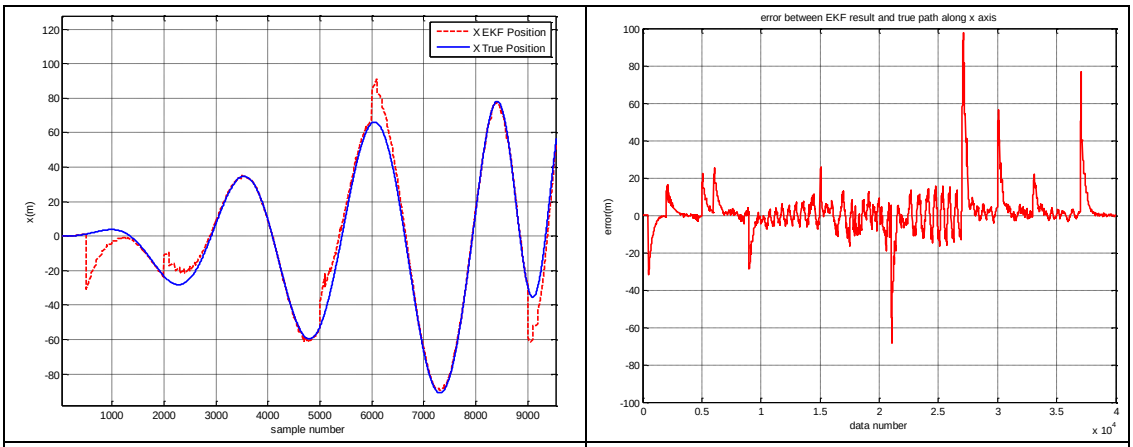

a.	d.

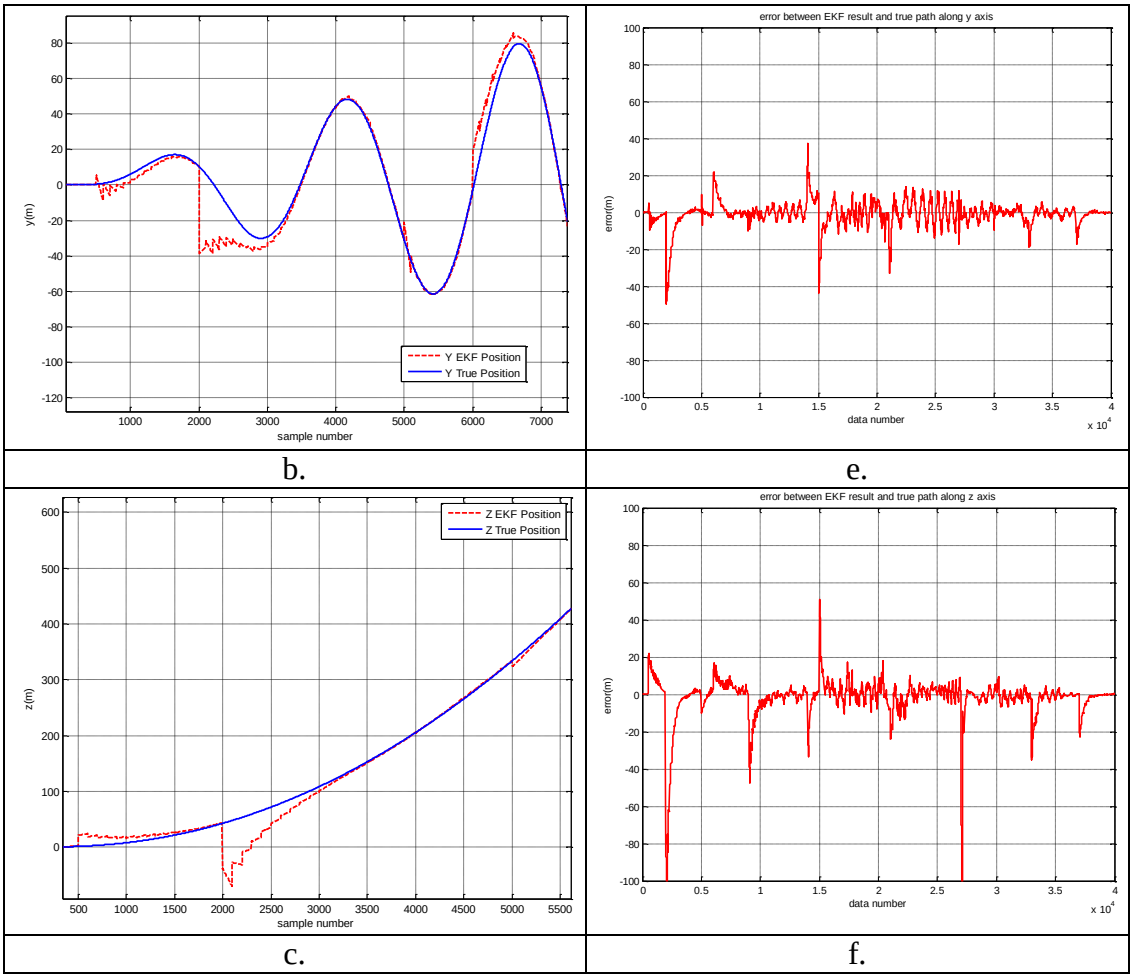

Figure 4.25 Comparison of true navigation data and EKF results in (a) x-axis, (b) y-axis, and (c) z-axis and error between EKF results and true navigation data for (d) x-axis, (e) y-axis, and (f) z-axis

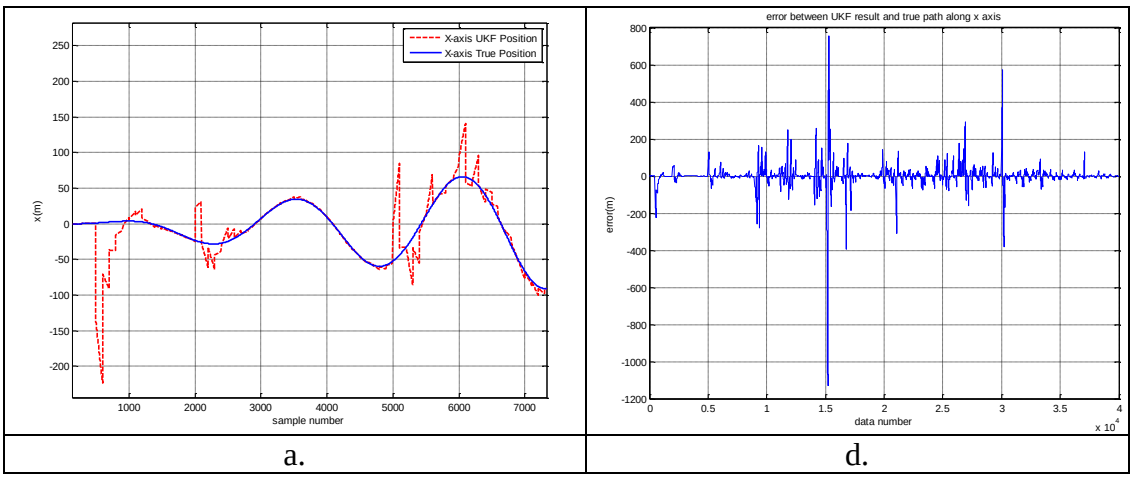

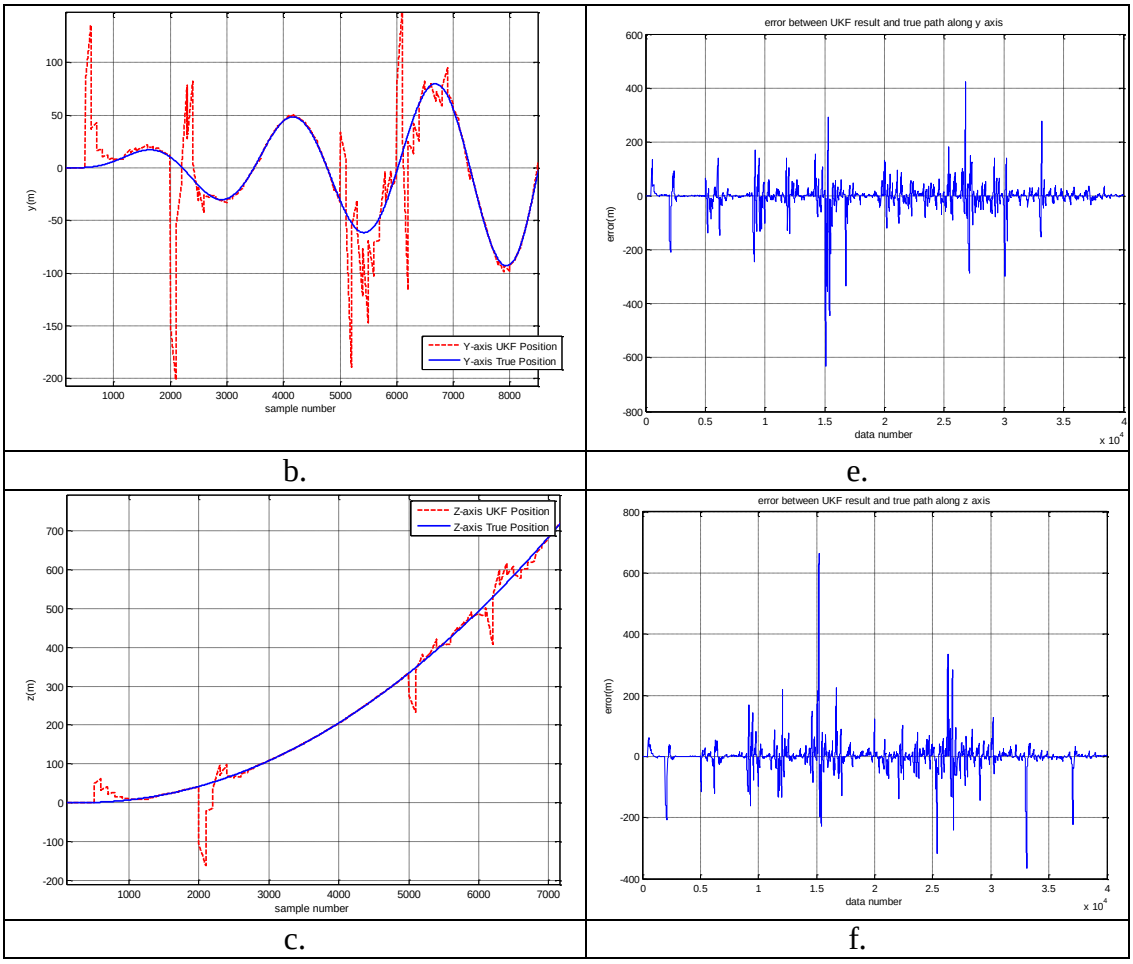

Figure 4.26 Comparison of true navigation data and UKF results in (a) x-axis, (b) y-axis, and (c) z-axis and error between UKF results and true navigation data for (d) x-axis, (e) y-axis, and (f) z-axis

Total error between estimation algorithm results and true navigation data ($\sqrt{\left((x_k - x_k^{true})^2 + \left(y_k - y_k^{true}\right)^2 + (z_k - z_k^{true})^2\right)}$) when standart deviation of GPS outlier is 100 m is shown in Figure 4.27.

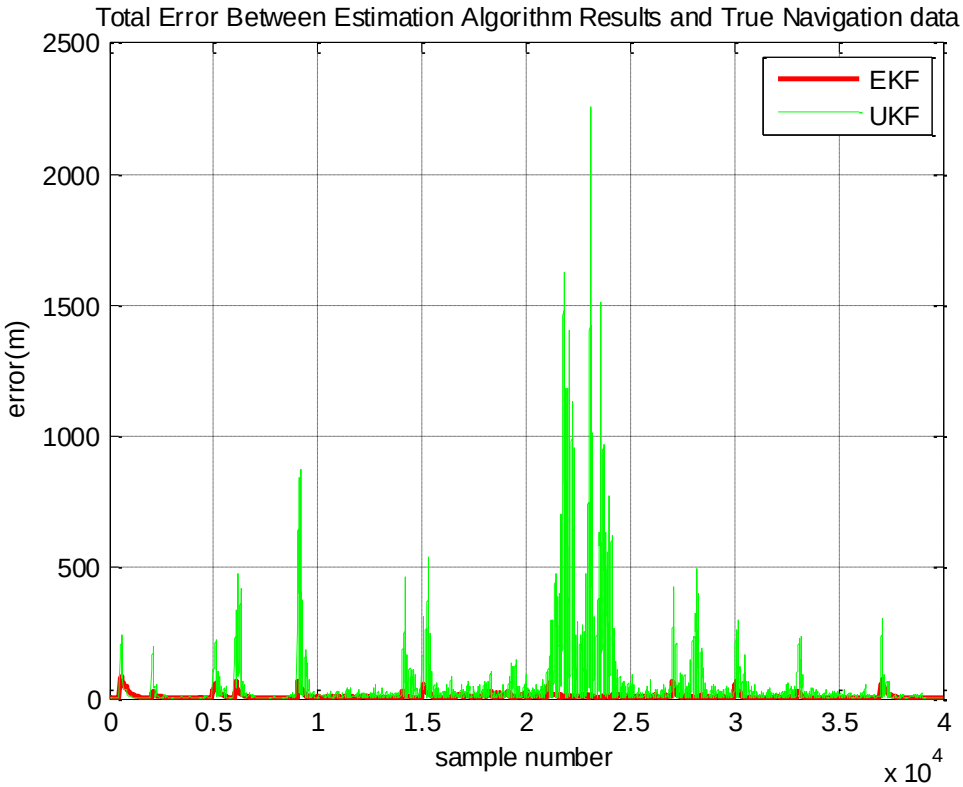

Figure 4.27 Total error between estimation algorithm results and true navigation data when GPS outlier standart deviation is 100 m.

Table 4.10 shows RMSE results for GPS outlier situation in terms of three Cartesian coordinates.

It is seen from Table 4.10 that once the observed GPS data is added with outliers which has 100 m standart deviation, the error of estimation of UKF algorithm is increasing. Moreover, UKF causes jumps and results poor robustness while it works with higher accuracy than EKF when outliers with 31.62 m standart deviation are added to observed GPS data.

Also, Table 4.10 shows that EKF2 is not robust to GPS outlier. It becomes diverged when standart deviation of outlier is increased. It is also obvious from Figure 4.21-4.23 and Figure 4.25-4.26 that the points where error increases are the outlier added points as expected. And the error level is increasing with the standart deviation of outlier added to GPS data.

Table 4.10 RMSE results for EKF, EKF2, and UKF

Algorithms	Time on GPS Outlier Data (seconds)	Standart Deviation of GPS Outlier(m)	RMSE Values (m)		
			x-axis	y-axis	z-axis
EKF	1.25, 5, 12.5, 15, 22.5, 35, 37.5, 52.5, 67.5, 75, 82.5, 92.5	100	10.9538	6.7415	11.2234
	7.5, 47.5, 92.5	31.62	4.9194	4.3392	4.5156
EKF2	1.25, 5, 12.5, 15, 22.5, 35, 37.5, 52.5, 67.5, 75, 82.5, 92.5	100	DIVERGED		
	7.5, 47.5, 92.5	31.62	4.4821	2.8029	3.0437
UKF	1.25, 5, 12.5, 15, 22.5, 35, 37.5, 52.5, 67.5, 75, 82.5, 92.5	100	59.715	48.6655	42.8829
	7.5, 47.5, 92.5	31.62	2.7390	2.8744	2.6812

All those experimental results for GPS outlier situation has proved that for nonlinear problems, EKF is a good solution, however, it is inappropriate for some nonlinear systems to calculate the Jacobian matrix and Taylor series linearization provides “first order” approximations (D. L. Hall 1992, Roth and Gustafsson 2011). In response to these problems, EKF2 which includes a second-order Taylor expansion of a nonlinear system can be used as an alternative to EKF (Bar-Shalom et. al. 2001). To overcome the limitations of EKF and EKF2, UKF is proposed which uses iterative weighted sampling to obtain the optimal solution instead of random sampling (Wan and Merwe 2000, Julier and Uhlmann 2003). But UKF is not robust enough, because data is affected by the factors that causes outliers in observation data (Liu et. al. 2014).

In order to handle the effect of outlier data, anti-outlier algorithms (Liu et. al. 2014, Zhao et. al. 2017) can be studied as a future work.

4.2 Case 2 Simulation Results

Generated path as true navigation data in Case 2 is shown in Figure 4.28.

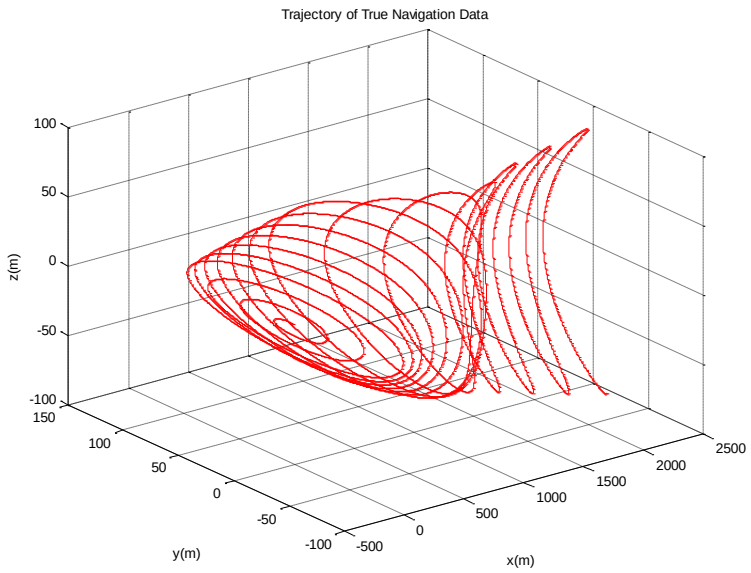

Figure 4.28 Trajectory of True navigation data in case 2

4.2.1 True navigation, standalone inertial and GPS results

In this section, true navigation, standalone inertial (INS) and GPS results based on Case 2 will be investigated comparatively.

3D flight trajectory of true navigation data in Figure 4.28 is split into its Cartesian coordinates as x, y, and z as seen in Figure 4.29.

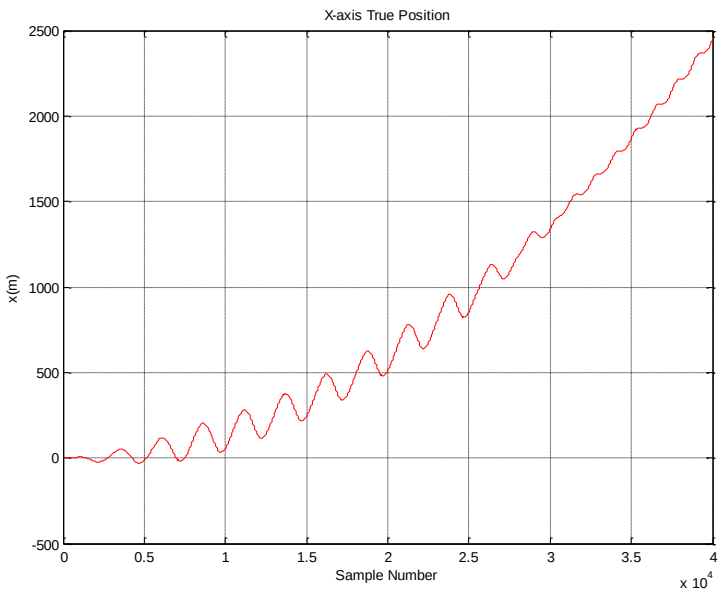
X-axis True Position
x(m)
2500
2000
1500
1000
500
0
-500
0
0.5
1
1.5
2
2.5
3
3.5
4
Sample Number
x 10^4

a.

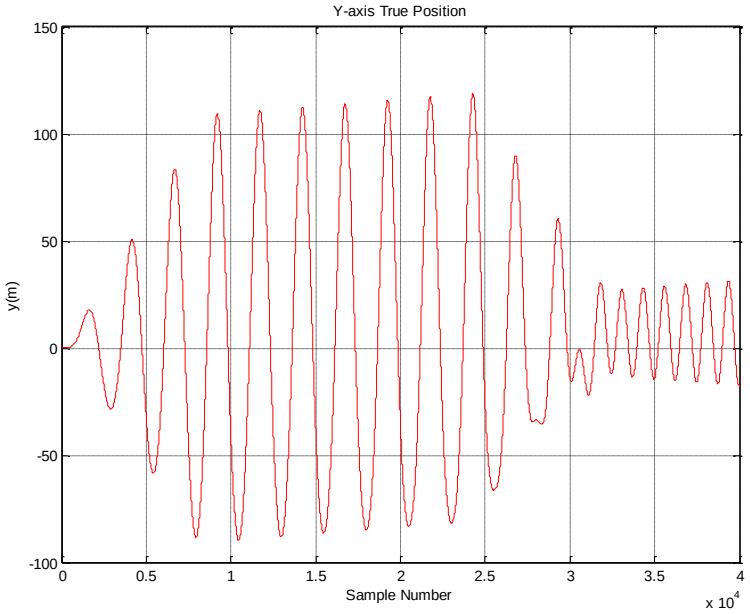
Y-axis True Position
y(m)
150
100
50
0
-50
-100
0
0.5
1
1.5
2
2.5
3
3.5
4
Sample Number
x 10^4

b.

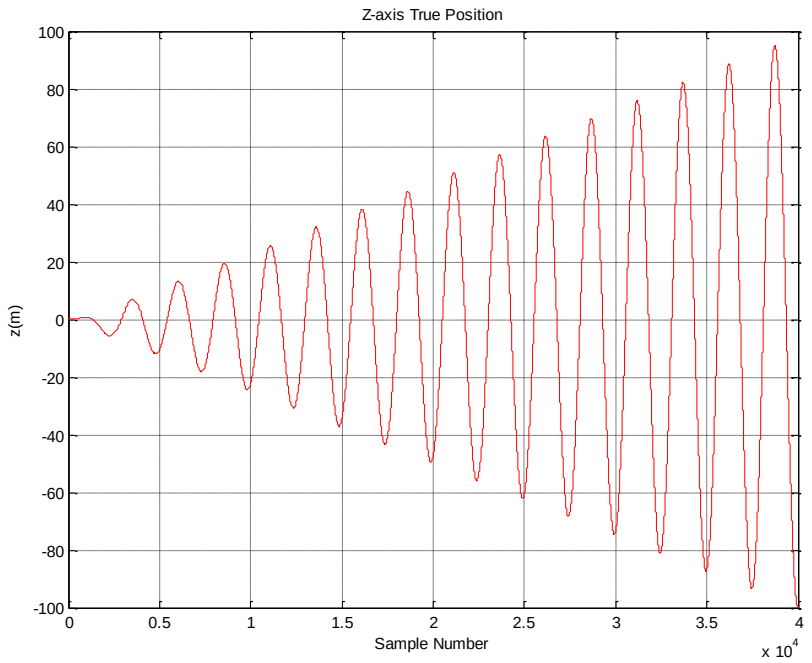

c.

Figure 4.29 Split coordinates of true navigation data into its Cartesian coordinates, (a) x-axis, (b) y-axis, and (c) z-axis for case 2

True navigation data is generated, then pathgen.m open source code generates GPS data as shown in Figure 4.30.

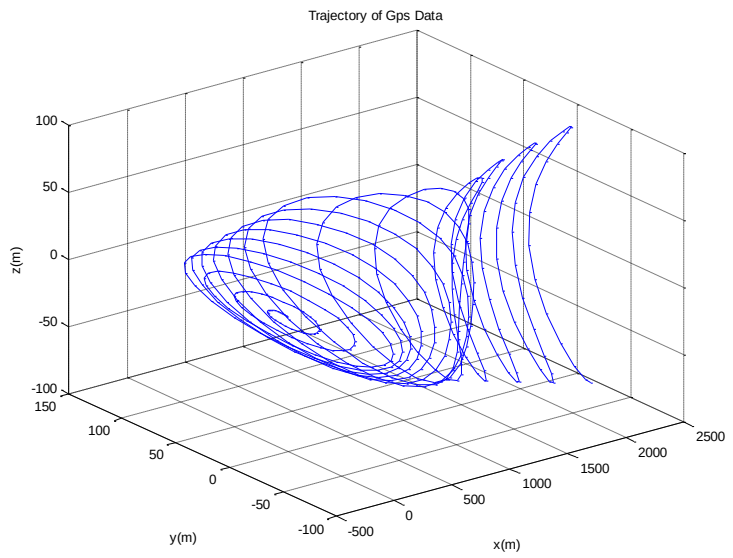

Figure 4.30 Trajectory of GPS data in case 2

3D flight trajectory of GPS data in Figure 4.26 is split into its Cartesian coordinates as x, y, and z as seen in Figure 4.31.

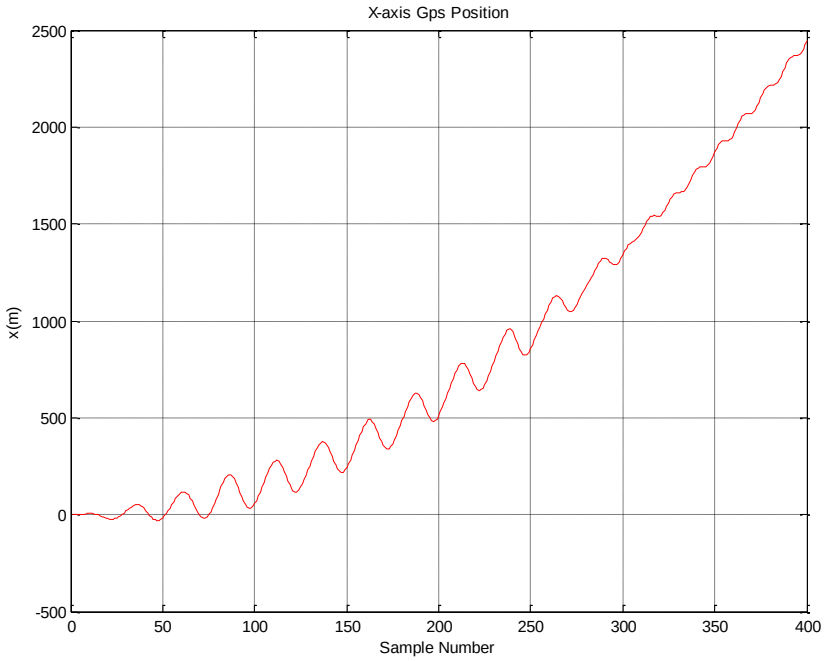

a.

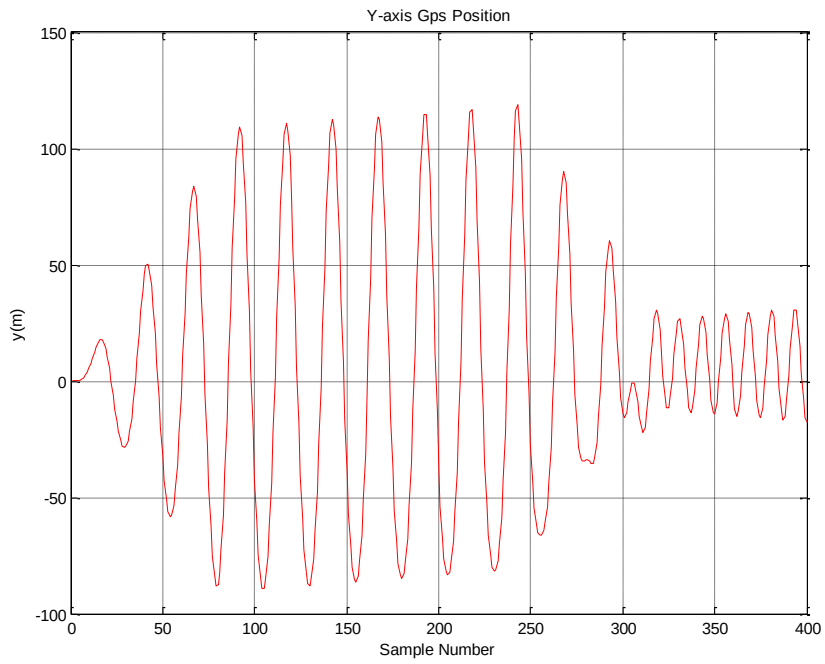

b.

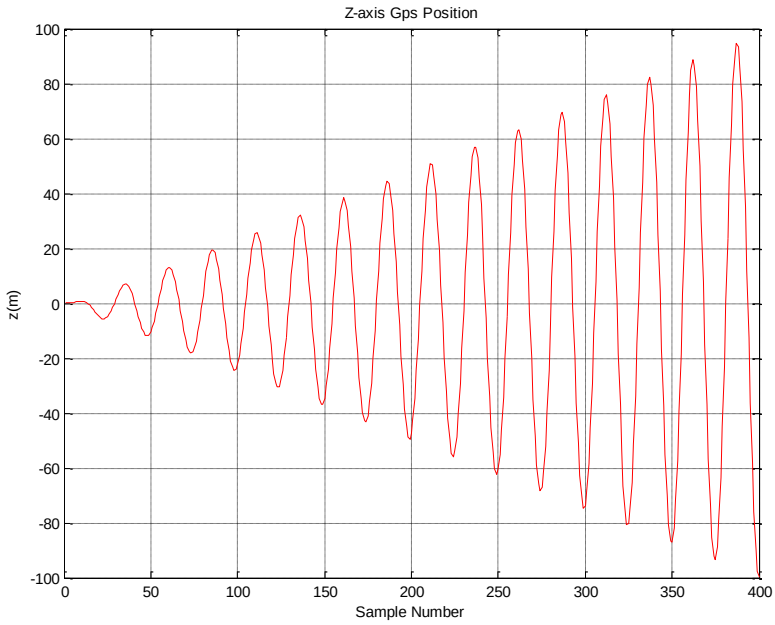

c.

Figure 4.31 Split coordinates of GPS data into its Cartesian coordinates, (a) x-axis, (b) y-axis, and (c) z-axis for case 2

True navigation data in Figure 4.29 and GPS data in Figure 4.31 are comparatively shown in Figure 4.32.

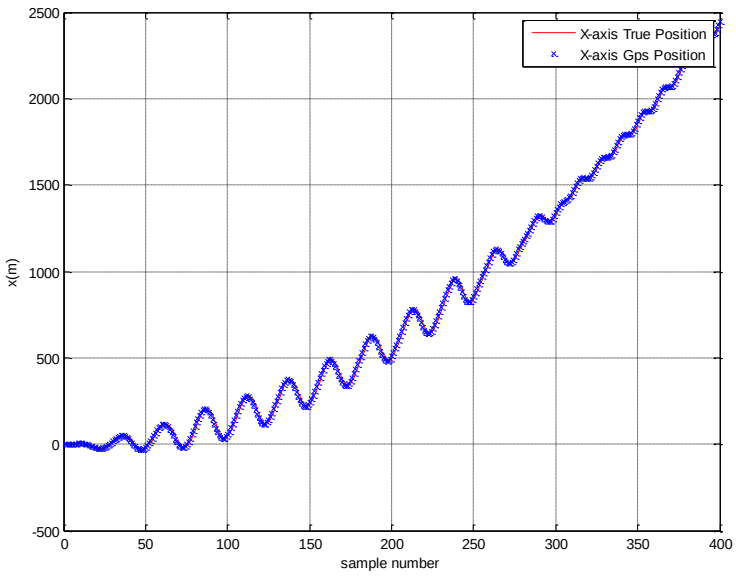

a.

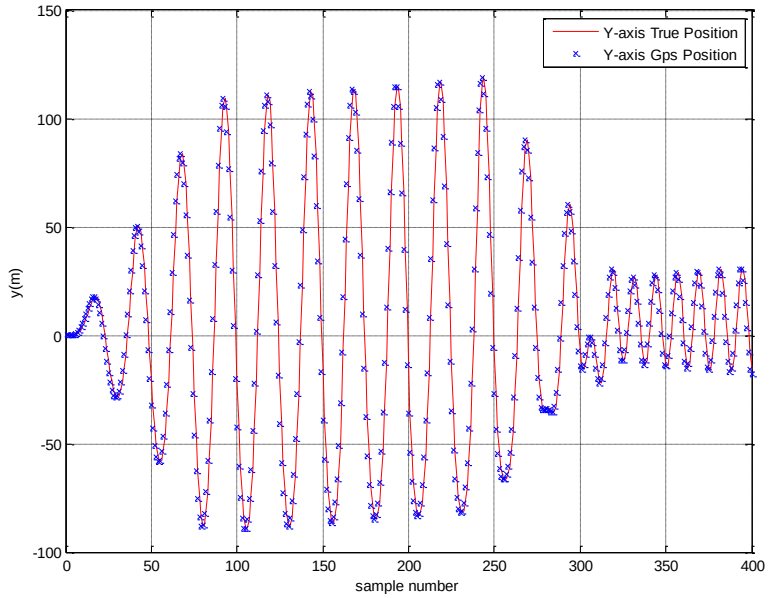

b.

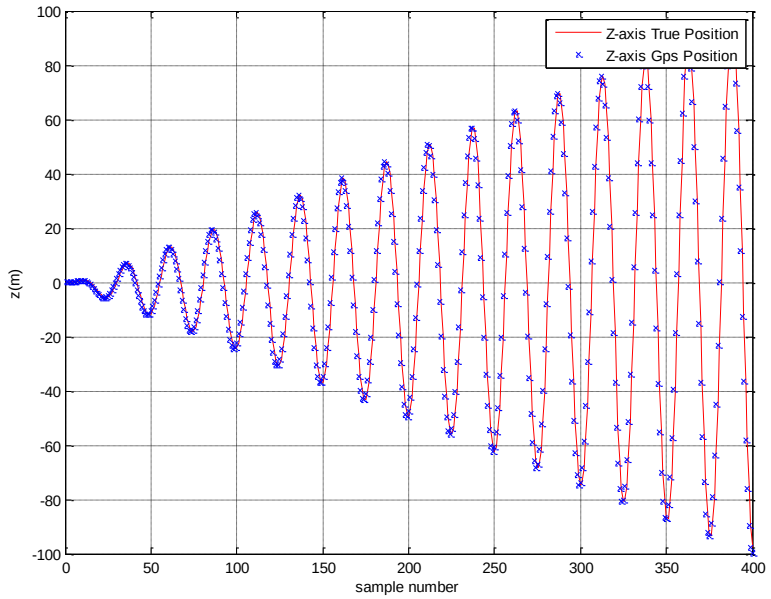

c.

Figure 4.32 Comparison of true navigation data and GPS data in (a) x-axis, (b) y-axis, and (c) z-axis for case 2

The position of the vehicle, obtained by double integration of the linear accelerations, is shown in Figure 4.33.

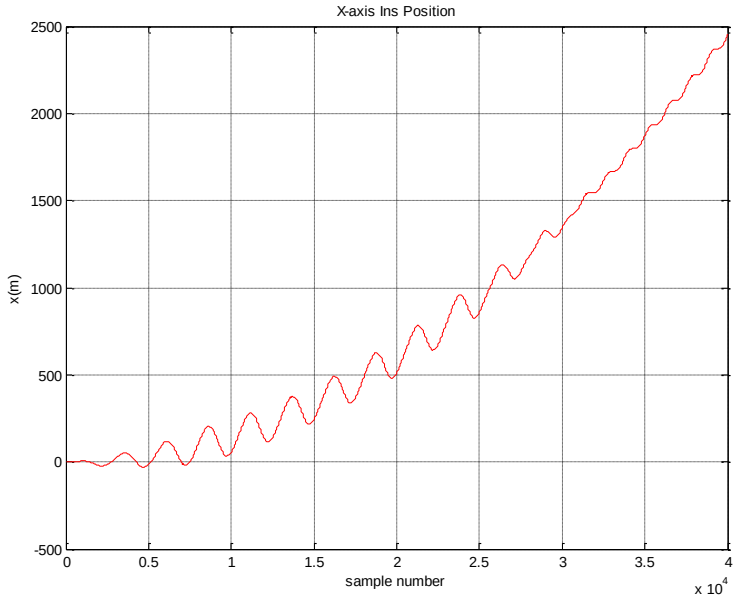
X-axis Ins Position
2500
2000
1500
1000
500
0
-500
x(m)
0
0.5
1
1.5
2
2.5
3
3.5
4
sample number
x 10^4

a.

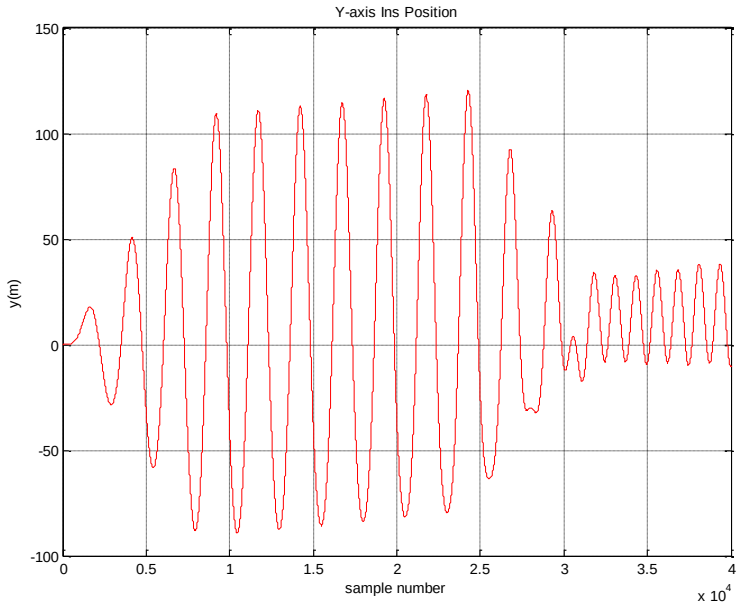
Y-axis Ins Position
150
100
50
0
-50
-100
y(m)
0
0.5
1
1.5
2
2.5
3
3.5
4
sample number
x 10^4

b.

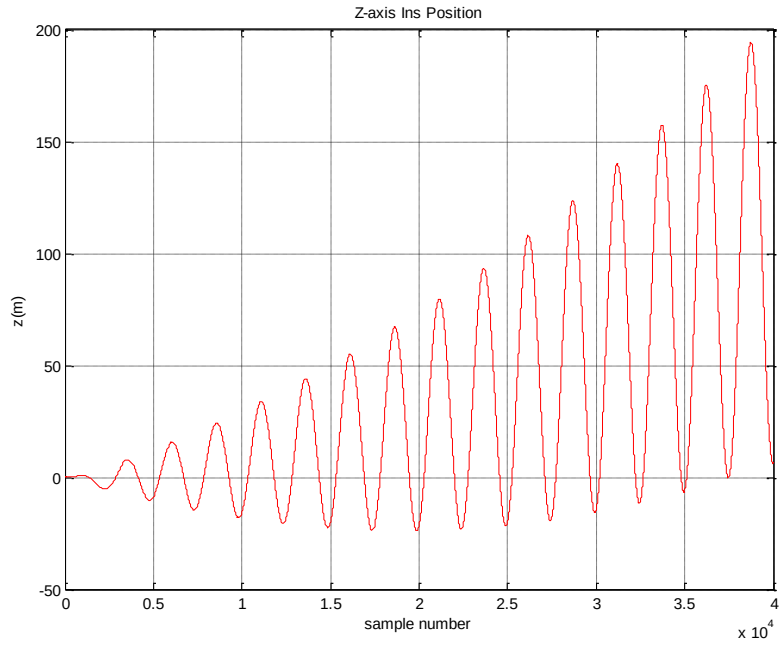

c.

Figure 4.33 Split coordinates of INS data into its Cartesian coordinates, (a) x-axis, (b) y-axis, and (c) z-axis for case 2

For Case 2, true navigation data in Figure 4.29 and INS data in Figure 4.33 are comparatively shown in Figure 4.34.

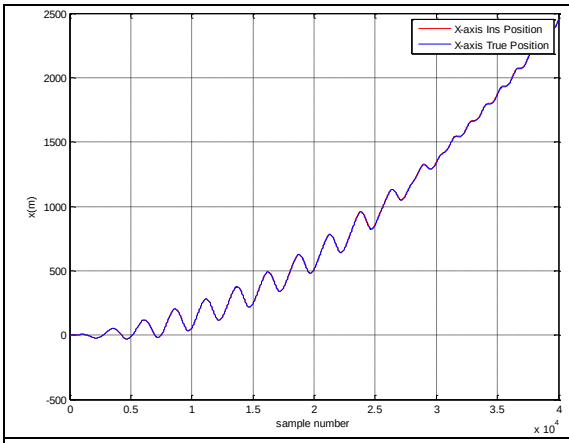

a.

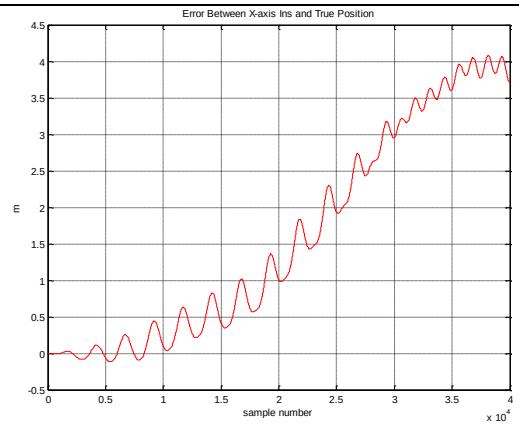

d.

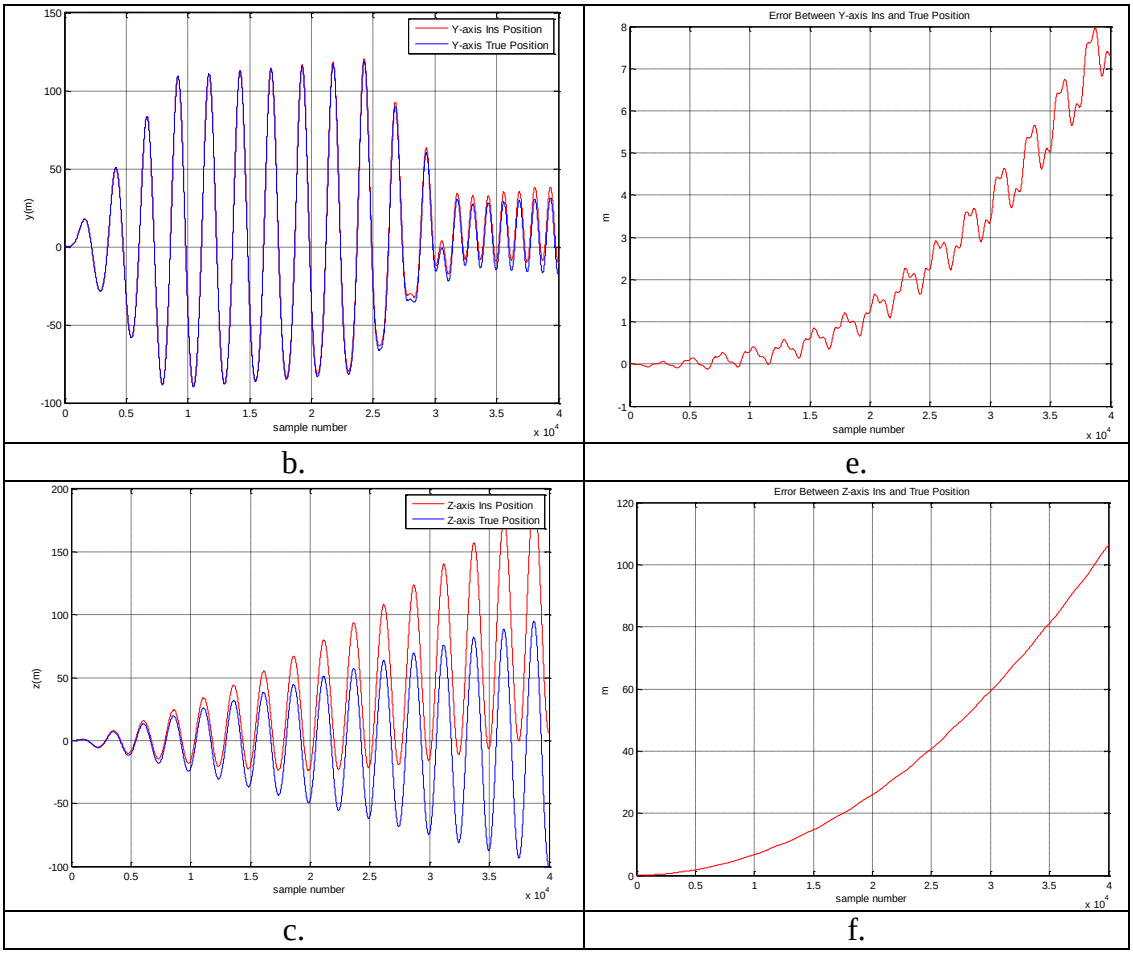

Figure 4.34 Comparison of true navigation data and INS data in (a) x-axis, (b) y-axis, and (c) z-axis, and errors for (d) x-axis, (e) y-axis, and (f) z-axis for case 2

4.2.2 EKF, EKF2 and UKF results for GPS available situation

In this section, EKF, EKF2 and UKF results will be investigated comparatively for Case 2.

True navigation data in Figure 4.29 and EKF results for three Cartesian coordinates are comparatively shown in Figure 4.35. Figure 4.35 (d-f) also show the zoomed versions of Figure 4.35 (a-c).

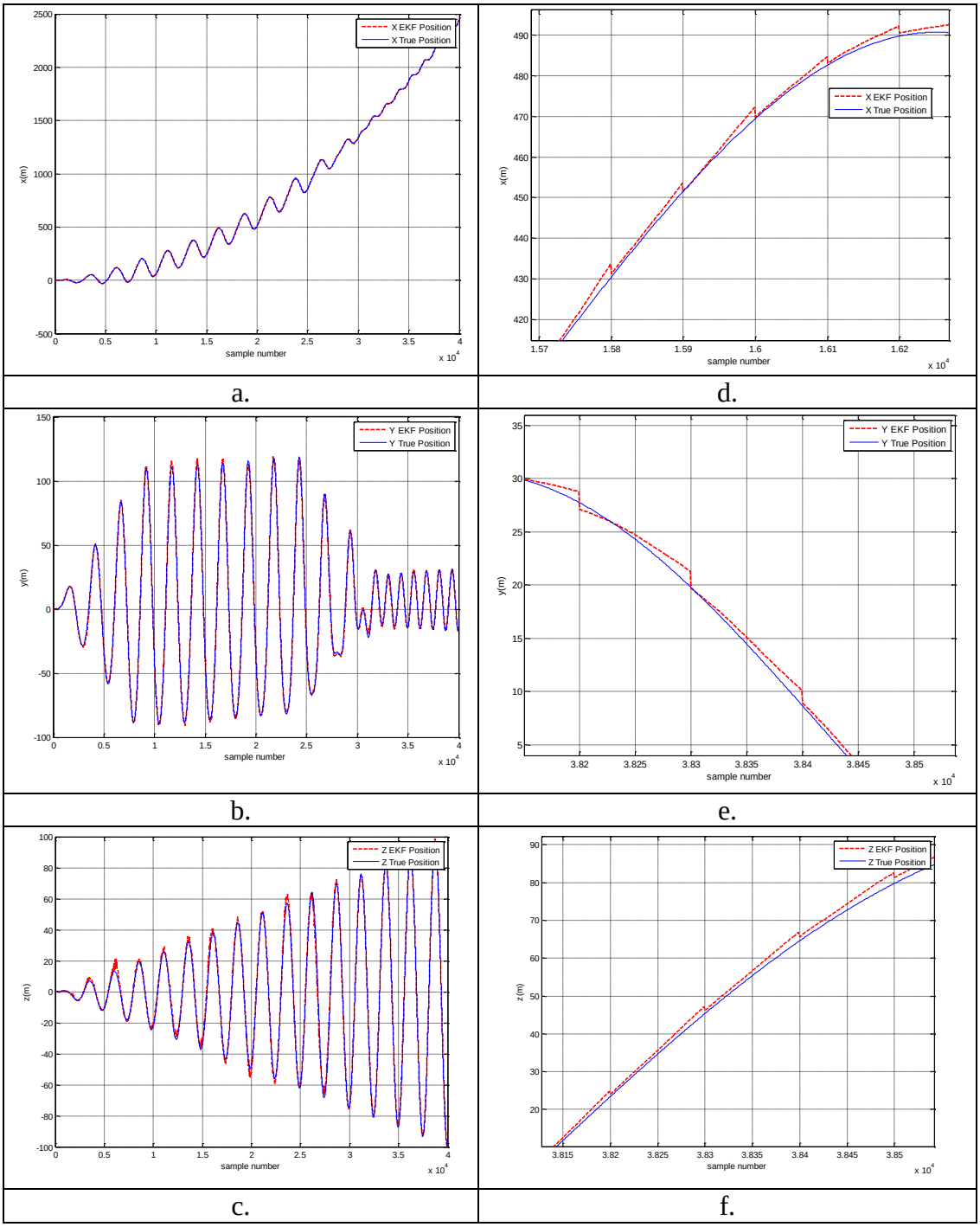

Figure 4.35 Comparison of true navigation data and EKF results in (a) x-axis, (b) y-axis, and (c) z-axis and zoomed versions for (d) x-axis, (e) y-axis, and (f) z-axis for case 2

Table 4.11 comparatively shows RMSE results for EKF in terms of three Cartesian coordinates.

Table 4.11 RMSE results for EKF in case 2

EKF	x-axis	y-axis	z-axis
RMSE (m)	1.783792865425624	1.643438614111940	2.175880787098736

True navigation data in Figure 4.29 and second order EKF results for three Cartesian coordinates are comparatively shown in Figure 4.36. Figure 4.36 (d-f) show the zoomed versions of Figure 4.36 (a-c).

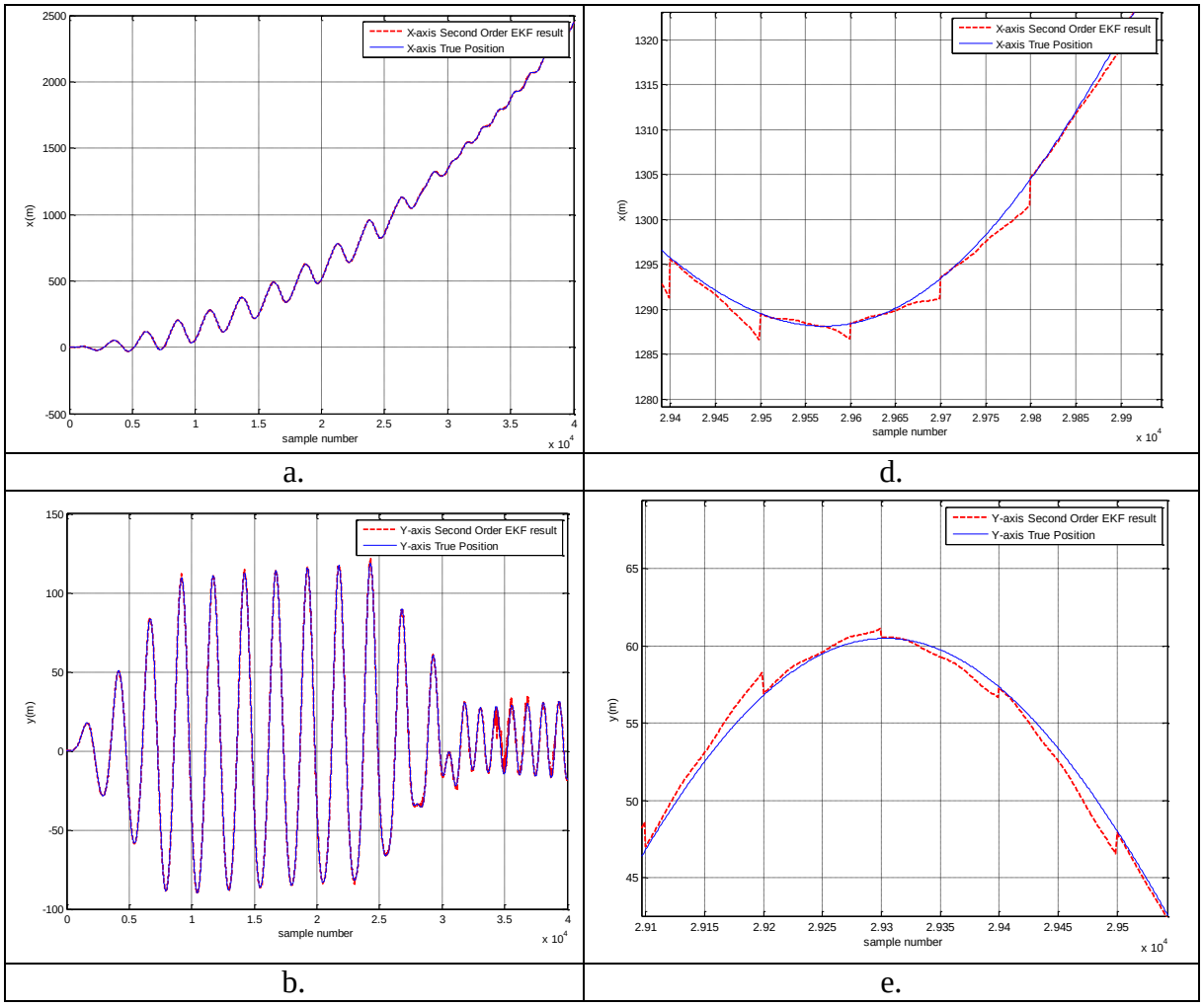

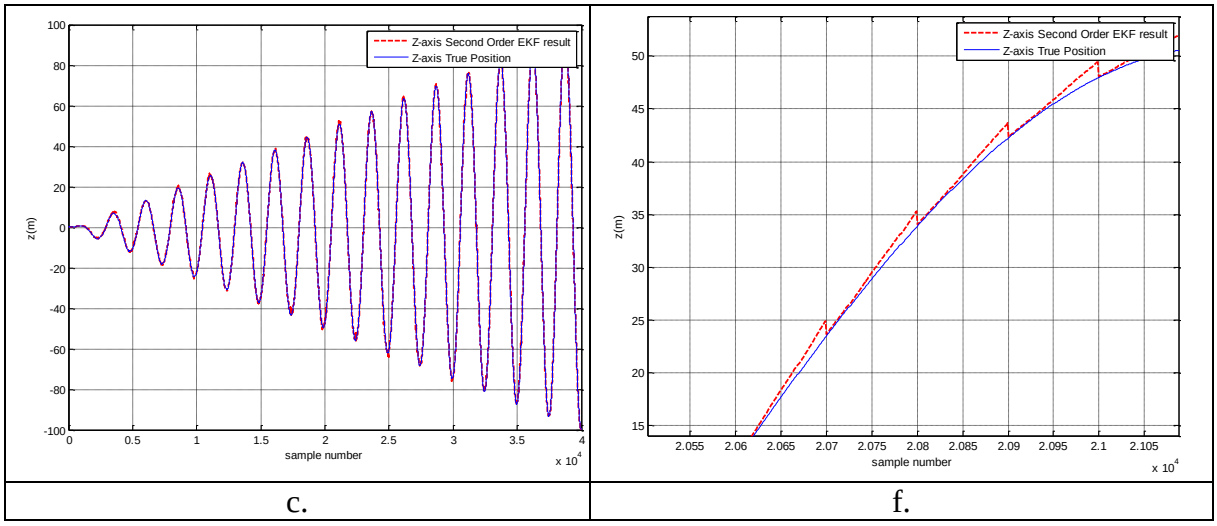

Figure 4.36 Comparison of true navigation data and second order EKF results in (a) x-axis, (b) y-axis, and (c) z-axis and zoomed versions for (d) x-axis, (e) y-axis, and (f) z-axis for case 2

Table 4.12 comparatively shows RMSE results for EKF2 in terms of three Cartesian coordinates.

Table 4.12 RMSE results for EKF2 in case 2

EKF2	x-axis	y-axis	z-axis
RMSE (m)	0.880142190264209	1.100674973751344	0.747460252829314

Finally, true navigation data in Figure 4.29 and UKF results for three Cartesian coordinates are comparatively shown in Figure 4.37. Figure 4.37 (d-f) show the zoomed versions of Figure 4.37 (a-c).

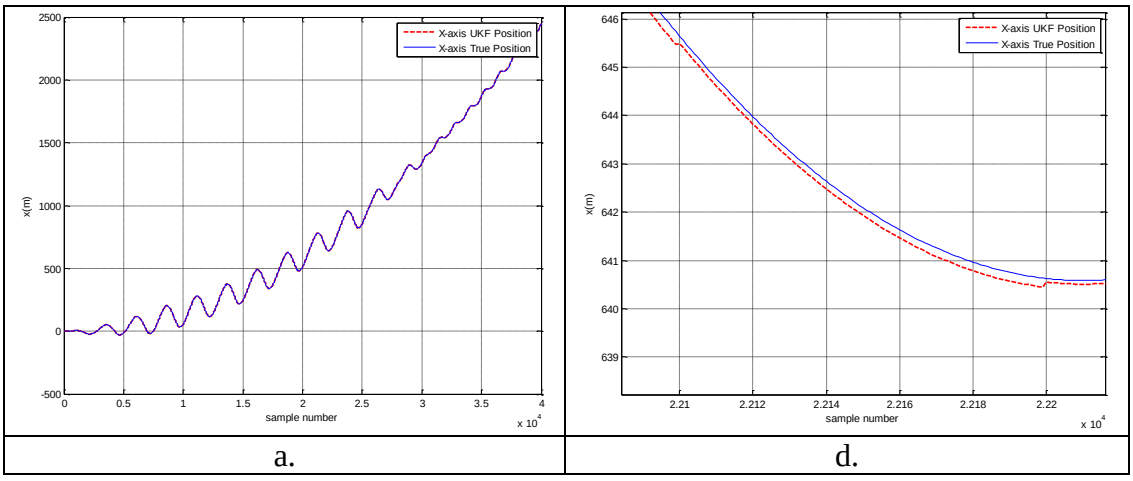

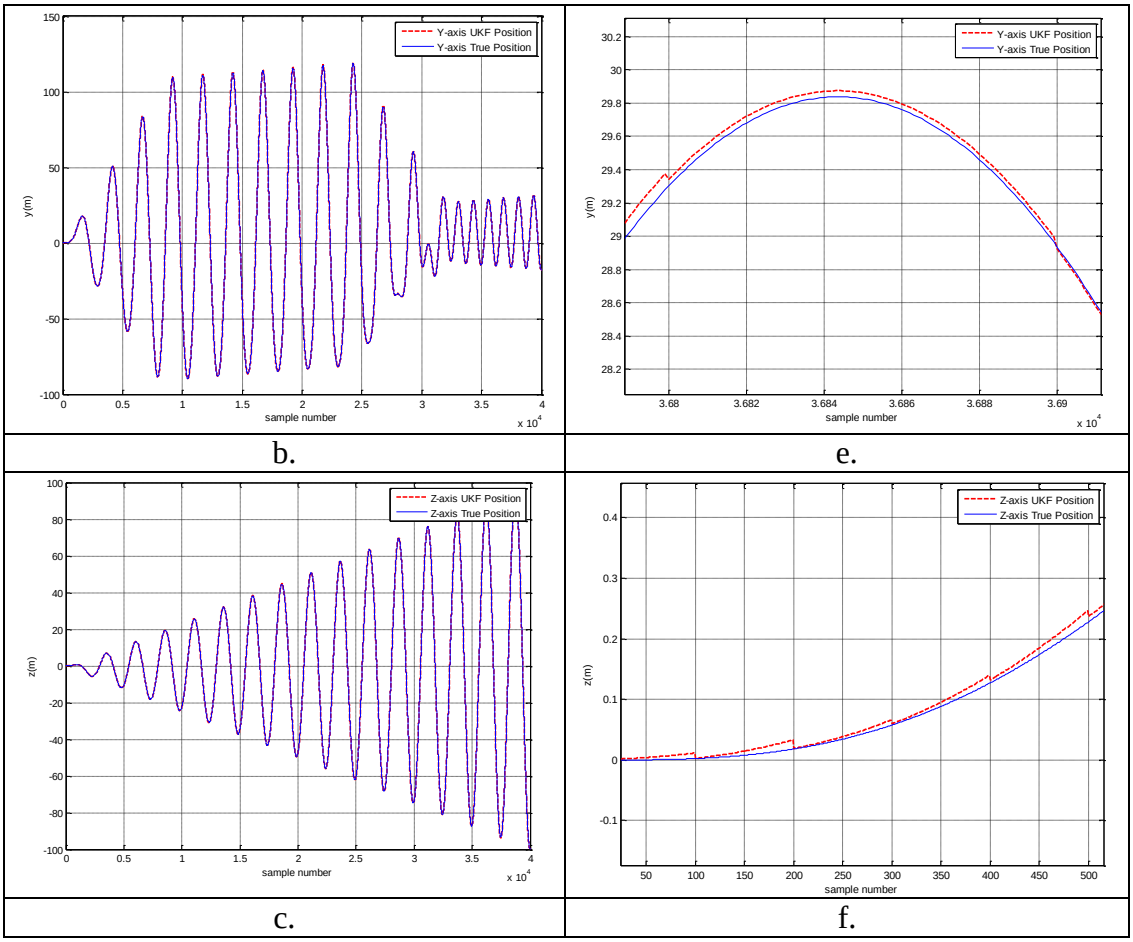

Figure 4.37 Comparison of true navigation data and UKF results in (a) x-axis, (b) y-axis, and (c) z-axis and zoomed versions for (d) x-axis, (e) y-axis, and (f) z-axis for case 2

Table 4.13 comparatively shows RMSE results for UKF in terms of three Cartesian coordinates.

Table 4.13 RMSE results for UKF

UKF	x-axis	y-axis	z-axis
RMSE (m)	0.164570237359815	0.149423545470660	0.103005322000962

Table 4.14 reveals that, UKF has better navigation performance than EKF and EKF2. Moreover, EKF2 introduces an increase in the performance according to standart EKF.

Table 4.14 Summary of experimental results

		RMSE Values (m)		
		x-axis	**y-axis**	**z-axis**
Case 1	**EKF**	5.0254	5.376024057975308	4.751929880242610
	EKF2	3.4533	3.6407	3.0736
	UKF	0.2532	0.2531	0.3432
Case 2	**EKF**	1.783792865425624	1.643438614111940	2.175880787098736
	EKF2	0.880142190264209	1.100674973751344	0.747460252829314
	UKF	0.164570237359815	0.149423545470660	0.103005322000962

Using trajectory of navigation data for Case 2, running times for each algorithm have also been recorded and compared as seen in Table 4.15.

Table 4.15 Running times for estimation algorithms

	Elapsed Time (seconds)
EKF	23.604751
EKF2	271.220739
UKF	105.488382

EKF and EKF2 take nearly 23 and 271 seconds respectively while UKF takes about 105 seconds. The reason why UKF takes significantly longer with respect to EKF to make estimation is that UKF has to handle all the sigma points. Also the Hessian matrices calculations in the EKF2 algorithm made EKF2 to take longer time than EKF.

In order to investigate the noise sensitivity, Table 4.16 shows the effect of IMU noise on each estimation algorithm comparatively.

Table 4.16 The effect of IMU noise on each algorithm

Algorithms	IMU Noise [σ_{acc}(m/s^2) and σ_{gyr}(rad/s)]	RMSE Values (m)		
		x-axis	y-axis	z-axis
EKF	0.01	1.7062542198517	1.76690804346385	1.999384368885994
	0.031	1.7837928654256	1.64343861411194	2.175880787098736
	0.1	2.0838156501866	2.28468812331752	2.537073301033487
	0.31	DIVERGED		
EKF2	0.1	0.9601124574127	1.1821611473265	0.76023845752956
	0.031	0.8801421902642	1.1006749737513	0.747460252829314
	0.1	DIVERGED		
UKF	0.1	0.1545388099668	0.1294239272868	0.998025511689463
	0.031	0.1645702373598	0.1494235454707	0.103005322000962
	0.1	0.1646569837589	0.1495286245701	0.103092764539015
	0.31	13.011169624082	12.163116172094	16.165773170343030
	1	DIVERGED		

According to Table 4.16, EKF is more sensitive to additive noise on the IMU measurements with respect to UKF. Hence, it can be noted that UKF is working with wide range of noise levels. Higher order EKFs ensure performance advantages when the measurement noise is small. Also, increasing the noise on IMU measurements forces the EKF2 to diverge quickly.

CHAPTER 5

CONCLUSION

GPS, satellite-based three-dimensional navigation system calculates the speed and position using GPS satellites. However, systems using only GPS can not succeed desired accuracy in some applications. In order to enhance accuracy of integrated navigation, INS has been utilized and thus, INS/GPS integrated systems overcome disadvantages of standalone GPS and INS for the purpose of developing an enhanced accurate integrated navigation solution. Estimation algorithms used in this thesis for INS/GPS integrated systems are EKF, EKF2, and UKF. Experimental results show that, UKF gives better performance in accuracy of INS/GPS integrated navigation system rather than EKF and EKF2 for GPS available situation.

In the light of that motivation, firstly fundamental information about INS has been presented, then, inertial sensors, their design technologies have been discussed particularly. Then, advantages and disadvantages of GPS has been presented. Estimation algorithms; EKF, EKF2 and UKF have been explained in detail with pseudo codes for each algorithm. INS/GPS integration architectures; loosely coupled, tightly coupled and ultra tightly coupled have been discussed with their benefits and drawbacks. State space model and the measurement model used in this thesis have been mentioned. Finally, the results obtained from the simulations have been presented and performances of the three algorithms have been compared by RMSE metric. Complexity and sensitivity to noise on the IMU measurements, effect of changing process noise covariance matrix for GPS available situation are examined. Also, GPS outage and GPS outlier situations are examined in terms of accuracy of EKF, EKF2 and UKF.

It is understood that UKF and EKF2 can be used instead of EKF to evolve the accuracy of the navigation systems. Moreover, EKF2 introduces an increase in the performance according to EKF. The reason why EKF2 is more successful than EKF is that linearization process by first order Taylor expansion causes second order errors in the mean and covariance of the state estimate while EKF2 uses second order Taylor expansion that it has second order correction terms in its equations. This results in better state estimate in EKF2 rather than EKF.

It is also concluded that UKF has better navigation performance than EKF and EKF2. Because, UKF uses sigma points from the Gaussian distribution obtained by UT. UT adjusts the spread of sigma points and controls the higher order estimation errors. Therefore, UKF is less sensitive to additive noise on the IMU measurements with respect to EKF. However, this fact causes the algorithm to have longer running time. EKF has the less running time according to the other estimation algorithms.

However, those conclusions are valid only for GPS available situation without any parameter changes and/or GPS interference (outage or outlier).

Effect of changing process noise covariance matrix ($\mathrm{Q_k}$) on EKF, EKF2, and UKF results for GPS available situation has also been examined. Increasing $\mathrm{Q_k}$ values in EKF and EKF2 decreases RMSE values since the gain increases. Nevertheless, it effects negatively after a while. It is also seen that UKF is still robust to too large Q_k values, but EKF2 is not as expected.

The effect of GPS outage on each algorithm has also been investigated. UKF has the best performance with respect to EKF and EKF2 when GPS signal is lost. Although the duration of GPS outage is extended, UKF still estimates the positions after a while with lower error than EKF. Also, RMSE values of EKF2 in longer GPS outage duration become higher than the other algorithms. As a result, EKF2 can not work good in harsh environment condition. That is, although EKF2 introduces an increase in the performance according to EKF without GPS interruption, it is not robust to GPS outages.

EKF2 is also not robust to GPS outlier situation since it diverges when the outlier standart deviation is increased.

In future, examination can be done by using different metrics rather than RMSE. Also, a tightly coupled integration method can be implemented as a future work to increase the performance of the INS/GPS integrated system.

REFERENCES

Abd Rabbou, M., El-Rabbany, A., Integration of GPS Precise Point Positioning and MEMS-Based INS Using Unscented Particle Filter, Sensors (Basel), Vol. 15, No. 4, pp. 7228-7245, 2015

Abdoli, A., Suratgar, A. A., Menhaj, M. B., Taghavi, S. H., "Neuro-Fuzzy Adaptive Kalman Filtering for INS/GPS Integration", 2016 4th International Conference on Control, Instrumentation, and Automation (ICCIA), Iran, pp. 87-92, 2016

Aftatah, M., Lahrech, A., Abounada, A., "Fusion of GPS/INS/Odometer Measurements for Landvehicle Navigation with GPS Outage", 2016 2nd International Conference on Cloud Computing Technologies and Applications (CloudTech), Marrakech, Morocco, pp. 48-55, 2016

Alban, S., Akos, D. M., Rock, S. M., "Performance Analysis And Architectures for INS-Aided GPS Tracking Loops", Proceedings of the 2003 National Technical Meeting of The Institute of Navigation, Anaheim, CA, pp. 611-622, 2003

Angrisano, A., "GNSS/INS Integration Methods", Universita' Degli Studi Di Napoli "Parthenope", Department of Science Applications, Ph.D. Thesis, 2010

Bar-Shalom, Y., Li, X., Kirubarajan, T., Estimation with Applications to Tracking and Navigation: Theory Algorithms and Software, John Wiley and Sons, Inc., New York, 2001

Bekir E., Introduction to Modern Navigation Systems, World Scientific Publishing Co. Pte. Ltd., Singapore, 2007

Bistrovs, V., Kluga, A., The Analysis of the UKF-Based Navigation Algorithm during GPS Outage, Elektronika IR Elektrotechnika, Vol.19, pp. 13-16, 2013

Ding, W., Wang, J., Almagbile, A., "Adaptive Filter Design for UAV Navigation with GPS/INS/Optic Flow Integration", 2010 International Conference on Electrical and Control Engineering (ICECE), Wuhan, pp. 4623-4626, 2010

Duong, B. P., Nguyen, V. H., “Development of a GPS/INS Integrated Navigation System for Model Aircraft”, 2014 14th International Conference on Control, Automation and Systems (ICCAS), Seoul, pp. 201-206, 2014

Graham, M. C., How, J. P, Gustafson, D. E., Robust State Estimation with Sparse Outliers, Journal of Guidance, Control and Dynamics, Vol. 38, No. 7, pp. 1229–1240, 2015

Grewal, M. S., Weill, L. R., Andrews, A. P., Global Positioning Systems, Inertial Navigation, and Integration, John Wiley and Sons, New York, 2001

Groves, P. D., Principles of GNSS, Inertial, and Multisensor Integrated Navigation Systems, Artech House, Boston, 2008

Hall, D. L. Mathmetical Technique in Multi-sensor Data Fusion. Artech House, Boston, London, 1992.

Hashlamon, I., Erbatur, K., An Improved Real-time Adaptive Kalman Filter with Recursive Noise Covariance Updating Rules, Turkish Journal of Electrical Engineering & Computer Sciences, Vol. 24, pp. 524-540, 2016

Haykin, S., Kalman Filtering and Neural Networks, John Wiley and Sons Inc, 2001

Jingsen, Z., Wenjie, Z., Bo, H., Yali, W., “Integrating Extreme Learning Machine with Kalman Filter to Bridge GPS Outages”, 2016 3rd International Conference on Information Science and Control Engineering, Beijing, China, pp. 420-424, 2016

Julier, S. J., Uhlmann, J. K., Unscented Filtering and Nonlinear Estimation, Proceedings of the IEEE, Vol. 92, Issue 3, pp. 401 – 422, 2004

Kaplan, E. D., Hegarty, C. J., Understanding GPS Principles and Applications, Artech House, Boston, 2006

Ko, N. Y., Choi, H. C., Lee, C., Moon, Y. S., “Navigation of Unmanned Surface Vehicle and Detection of GPS Abnormality by Fusing Multiple Sensor Measurements”, OCEANS 2016 MTS/IEEE Monterey, Monterey, CA, USA, pp. 1-5, 2016

Lijun, W., Huichang, Z., Xiaoniu, Y., “The Modeling and Simulation For GPS/INS Integrated Navigation System”, International Conference on Microwave and Millimeter Wave Technology (ICMMT 2008), Nanjing, pp. 1991-1994, 2008

Liu, W., Bian, H., Wang, R., Application of Anti-outlier UKF Algorithm in Integrated Navigation, Applied Mechanics and Materials, Vol. 641-642, pp. 1307-1311, 2014

Moreno, V. M., Pigazo, A., Kalman Filter Recent Advances and Applications, Intech, 2009

NATO RTO-SET-054/RTG-30 Panel, Basic Guide to Advanced Navigation, 2003

Open Source Inertial Navigation Toolkit, www.instk.org, Date of Access: 02.05.2016

Rhudy, M., Gu, Y., Gross, J., Gururajan, S., Napolitano, M. R., Sensitivity Analysis of Extended and Unscented Kalman Filters for Attitude Estimation, Journal of Aerospace Information Systems, Vol. 10, No. 3, pp. 131-143, 2013

Roth, M., Gustafsson, F., “An Efficient Implementation of the Second Order Extended Kalman Filter”, 2011 Proceedings of the 14th International Conference on Information Fusion (FUSION), Chicago, pp. 1 – 6, 2011

Sadeghi, B., Moshiri, B., “Second-order EKF and Unscented Kalman Filter Fusion for Tracking Maneuvering Targets”, 2007 IEEE International Conference on Information Reuse and Integration, Las Vegas, pp. 514-519, 2007

Shi, Z., Wu, Z., Liu, J., Fu, B., “Cubature Kalman Filter Based Attitude Estimation for Micro Aerial Vehicles”, 2016 8th International Conference on Intelligent Human-Machine Systems and Cybernetics, Hangzhou, China, pp. 121-125, 2016

Siddiqui, S. M., “Integrated Navigation and Self Alignment Using Square Root Unscented Kalman Filtering”, 10th International Bhurban Conference on Applied Sciences and Technology (IBCAST), Islamabad, pp. 73-76, 2013

Wan, E. A., Merwe, R., “The Unscented Kalman Filter for Nonlinear Estimation”, Proceedings of the IEEE Symposium (AS-SPCC), Lake Louise, Alberta, CA, 2000

Wu, T., Hung, J. Y., “State Estimation for a Tractor-trailer System Using Adaptive Unscented Kalman Filter”, SoutheastCon 2017, Charlotte, NC, USA, pp. 1-5, 2017

Yu, M. J., INS/GPS Integration System Using Adaptive Filter for Estimating Measurement Noise Variance, IEEE Transactions on Aerospace and Electronic Systems, Vol. 48, Issue 2, pp. 1786-1792, 2012

Zhao, J., Mili, L., Abdelhadi, A., “Robust Dynamic State Estimator to Outliers and Cyber Attacks”, IEEE Power Engineering Society General Meeting, pp. 1-5, 2017

Zhao, Y., Performance Evaluation of Cubature Kalman Filter in a GPS/IMU Tightly Coupled Navigation System, Signal Processing, Vol. 119, pp. 67-79, 2016

Zhang B., Chu, H., Sun, T., Jia H., Guo L., Zhang, Y., Error Prediction for SINS/GPS after GPS Outage Based on Hybrid KF-UKF, Mathematical Problems in Engineering, Vol. 2015, pp. 1-9, 2015

Zhou, J., Edwan, E., Knedlik, S., Loffeld, O., “Low-cost INS/GPS with Nonlinear Filtering Methods”, 2010 13th Conference on Information Fusion (FUSION), Edinburgh, pp. 1 – 8, 2010